UNIVERSITY of the
WESTERN CAPE

DEVELOPMENT OF AN APTAMER BASED LATERAL FLOW TEST STRIP FOR A DIABETES BIOMARKER

KOENA LEAH MOABELO

A thesis submitted in partial fulfilment of the requirements for the degree Magister Scientiae in the Department of Biotechnology, University of the Western Cape.

Supervisor: Prof. Abram Madiehe

Co-Supervisor: Prof. Mervin Meyer

August 2019

KEYWORDS

Aptamers

Biomarker

Colorimetric aptasensor

Diabetes

Dissociation constant

Gold nanoparticles

Lateral flow test strips

Point-of-care

Retinol binding protein 4 (RBP4)

Surface Plasmon Resonance

ABSTRACT

DEVELOPMENT OF AN APTAMER BASED LATERAL FLOW TEST STRIP FOR A DIABETES BIOMARKER

KL MOABELO

MSc. Thesis, Department of Biotechnology, University of the Western Cape

Diabetes mellitus is one of the major chronic diseases that poses a significant risk to human health globally. Current diagnostics for diabetes are based on blood glucose measurements, which can go unnoticed for years. As such, there is an urgent need for diagnosis of diabetes at the point-of-care (PoC), and in low-income settings. Recent developments in the field of nanotechnology, and the use of aptamers show great promise in developing sensitive and disease-specific assays. Aptamers have high specificity, selectivity, low molecular weight, nontoxicity, non-immunogenicity, and are easy to produce. The aim of the study was to characterize and identify dual aptamers for the development of an aptamer-based PoC diagnostic kit for diabetes.

Retinol binding protein 4 (RBP4) and its binding aptamers were identified through *in silico* approach. The secondary structures of the selected retinol binding aptamers (RBA) were predicted by M-fold and Quadruplex forming G-Rich Sequences mapper. Binding affinity of aptamers to the biomarker was characterized by Surface Plasmon Resonance(SPR), Electrophoretic mobility shift assay (EMSA) and Enzyme-Linked Aptamer Assay (ELAA) and the aptamer pairs were evaluated by sandwich-based SPR and ELAA. Gold nanoparticles (AuNPs) were synthesized using the Turkevich method, and characterized by UV-visible (UV-vis) spectrophotometry, Zetasizer and Transmission Electron Microscopy. One aptamer was conjugated to AuNPs and the conjugate was characterized by UV-Vis, Zetasizer, Qubit assay and gel electrophoresis. The apt-AuNPs were used in the preparation of the lateral flow test strips and a colorimetric aptasensor for the detection of RBP4.

RBP4 and four Retinol binding aptamers (RBA's) were selected for this study. The aptamers shared conserved motifs that might play an ancillary role in binding. A small stem loop in the nucleuotide sequence -TAGTAAGTGCAA- at 62-73 nts was present for all predicted structures. Furthermore, RBA-1 and RBA-3 shared a conserved motif of -GTTG- at base 44-47, whereas, RBA-1 and RBA-2 shared a motif of -AGGGG- at base 26-32. Kinetic studies

revealed that all selected aptamers showed binding to RBP4, with dissociation constants in the nanomolar (nM) and picomolar range and that RBA-2 and RBA-1 bound to RBP4 at different sites. The AuNPs had a hydrodynamic size of 14 nm, a polydispersity index of 0.216 and a zeta potential of -30.31 mV. RBA-2 was chosen as a capture probe hence it was conjugated to AuNPs. Apt-AuNPs showed efficient conjugation at 50 µM. The development of the lateral flow test strip was unsuccessful and this could be attributed to desorption of the protein on the nitrocellulose membrane or insufficient protein concentration used. However, a colorimetric aptasensor for the detection of RBP4 was successful with a detection limit of 45.32 nM.

This study demonstrated the feasibility of developing an aptamer based LFA for the detection of novel RBP4. Therefore, further optimizations on different types of membranes, buffers, pH and target concentrations are needed in order to obtain better resolutions and intensity on the test strips. Moreover, the study demonstrated the successful development of a simple yet effective colorimetric assay for RBP4 detection using one aptamer and AuNPs.

DECLARATION

I declare that *"Development of an aptamer based lateral flow test strip for a diabetes biomarker''* is my own work, that it has not been submitted for any degree or examination in any other university and that all the sources I have used or quoted have been indicated and acknowledged by complete references.

Name: Koena Leah Moabelo

Signature: 

Date signed: 26 August 2019

ACKNOWLEDGMENTS

- First and foremost, I would like to give thanks to God. It is by His Glory that I was given this opportunity to pursue my postgraduate studies. I would not be where I am if it was not for Him.

- A special thanks to my parents (Mrs Mmatlou and Mr Mmaphuti Moabelo) for allowing me to continue with my studies. Your support is what kept me motivated and your love is highly appreciated. To my aunts (Miss Tlou Boloko, Miss Nare Boloko and Mrs Mmagauta Netshilindi) and uncle (Mr Ben Netshilidi), I sincerely thank you, for always being my pillars of strength. To the children at home (Seemole and Phuti Moabelo, Mmakgabo, Phuti, Molemo and Neo Boloko), thank you for motivating me to take this path; it was indeed created to inspire you to reach greater heights.

- My deepest appreciation to my supervisors, Prof. Abram Madiehe and Prof. Mervin Meyer; thank you for your support, guidance and assistance throughout the years. Your commitment to your students and research is indeed extraordinary.

- A special appreciation to my friend, a mom away from home and a colleague, Dr. Nicole Sibuyi, for always encouraging me to excel and the advices you have given me. Having you in my life has been a blessing in disguise.

- To Prof. Onani, your praises assured me that I was indeed in the correct place and doing the work that was appreciated. You indeed restored my self-confidence and inspired me to work even harder than before and for that, I thank you.

- To Mr Riziki Martins and Miss Lauren Swartz, thank you for your dedication in helping me with my lab work. Your efforts are highly appreciated. I have learnt a lot from both of you.

- Much appreciation to Dr. Dorcas Wusu, your prayers gave me strength and brought me closer to the Lord when I felt like losing hope.

- Thanks to the DST/Mintek Nanotechnology Innovation Centre and National Research Foundation for granting me with financial support.

- Not forgetting my wonderful colleagues who became my friends (Miss Phumuzile Dube, Miss Keletso Modise, Miss Philisile Molefe, Miss Yonela Ngugeni, Miss Taahirah Boltman and Miss Shakeela Lucas), thank you for the assistance, kindness and motivation. My years would not be complete without you.

- I would like to extend my appreciation to Prof. Ciara O'Sullivan and her team at Universitat Rovira i Virgili (Interfibio group), for their assistance and allowing me to use their equipment's. I'm grateful to Dr. Marketa Svobodová, Dr. Miriam Jauset-Rubio and Dr. Teresa Mairal Lerga because; none of this would be possible without you.

- To my two best friends, Mr Rendani Musoliwa and Mr Mpho Muthevhuli, thank you for being wonderful friends.

- Last, but not least, I would like to thank my brothers (Dr. Neo Netshilindi and Mr Kgabo Boloko) and my sister (Mrs Yvonne Boloko) for their endless support and love. You have really set out a good example, and I intend to continue to make our parents proud.

TABLE OF CONTENT

LIST OF ABBREVIATION

β-cells	Beta cells
λ_{max}	Absorption maximum
ζ-potential	Zeta potential
χ^2	Chi^2
2DGE	Two-dimensional electrophoresis
a2MG	Alpha-2-macroglobulin
ADA	American diabetes association
Apt	Aptamer
AuNPs	Gold nanoparticles
BLI	Bio-layer interferometry
CE-SELEX	Capillary electrophoresis based SELEX
CRP	C-reactive protein
DM	Diabetes mellitus
DNA	Deoxyribonucleic acid
EDX	Energy dispersive x-ray spectroscopy
ELAA	Enzyme linked aptamer assay
ELISA	Enzyme linked immunosorbent assay
FPG	Fasting plasma glucose

FTIR	Fourier-transform infrared spectroscopy
GO-SELEX	Graphene oxide SELEX
Hb	Haemoglobin
HPR	Horseradish peroxidase
IDF	International Diabetes Federation
K_D	Dissociation constant
LFA	Lateral flow assays
MAbs	Monoclonal antibodies
MRE	Molecular recognition element
MS	Mass Spectrometry
MST	Microscale Thermophoresis
Mv	Millivolts
NP	Nanoparticles
Nt	Nucleotide
OGT	Oral glucose tolerance
PCR	Polymerase chain reaction
PDI	Polydispersity index
PoC	Point-of-care
QGRS	Quadruplex forming G-Rich Sequences

RBA	Retinol binding aptamer
RBP4	Retinol binding protein 4
RFG	Random plasma glucose
RU	Resonance Unit
SELEX	Systematic Evolution of Ligands by Exponential Enrichment
SPR	Surface Plasmon Resonance
T1DM	Type 1 diabetes mellitus
T2DM	Type 2 diabetes mellitus
TEM	Transmission electron microscopy
UV-Vis	Ultraviolet-visible
WHO	World Health Organization

LIST OF FIGURES

LIST OF TABLES

CHAPTER 1: LITERATURE REVIEW

1.1 Introduction

Diabetes Mellitus (DM) is one of the major chronic diseases that pose a significant risk to human health (Xiao *et al*., 2014). If it is poorly managed or undiagnosed, it can lead to a state of persistent hyperglycaemia that may results in complications such as retinopathy, neuropathy, blindness and cardiovascular diseases (World Health Organization (WHO), 2016). As such, patients with diabetes often have a reduced life expectancy and poor quality of life. Difficulties in treating this disease in its advanced stages intensely recommend preventative measures through quick and reliable diagnostics (Sharma *et al*., 2015). Consequently, a particular focus on early detection will increase the treatment efficiency and encourages patients to make lifestyle modification; hence, increasing the survival rate of the patient (DiMatteo *et al*., 2002; Willet and Liebel, 2002).

Diabetes requires frequent glucose measuring and most commercially available diagnostic tests for diabetes are invasive, painful and may cause discomfort and discourage patients to go for regular check-ups. This often results in diabetes progression, eventually leading to irreversible complications; thus, contributing to high mortality rates (Panchbhai, 2012; Panda *et al*., 2012). In recent years, proteomic analysis of plasma and serum for the identification and characterization of differentially expressed biomarkers have shown potential for diagnosis of various communicable and non-communicable diseases (such as diabetes, cancer and etc.). However, the technique is labour intensive and invasive (Al-Tarawneh *et al*., 2011).

In addition, proper diagnosis and early detection of diabetes and its associated diseases in an environment that lacks resources has proven to be a challenge due to lack of access to well-equipped clinical laboratories and requires a high level of technical competence (Quesada-Gonza´lez and Merkoçi, 2017). Their comparative long assay time and separation time has also made it impossible for these diagnostics to be applied in point-of-care (PoC) detection (Sharma *et al*., 2015). Thus, developing a diagnostic kit for diabetes and its associated diseases which is cost effective and can be easily implemented, remains an important global health goal. To achieve this goal, one promising approach is to detect disease biomarkers from accessible body fluids with PoC devices that are cost effective, non-invasive and/or do not require trained medical personnel (Kumar *et al*., 2018). This put forth the development of

PoC devices systems as a potential diagnostic tool that may potentially improve patient care in real-time and through remote health monitoring.

An example of a PoC device is a biosensor, which is defined as an analytical device, that is used for the detection of an analyte that combines a biological component with a physicochemical detector (Florinel-Gabriel, 2012; Newmand and Setford, 2006). Recently, the use of biosensors in diagnostics have gained momentum because of their good sensitivity and selectivity, as well as rapid and easy operation (Srinivasan and Tung, 2016). Hence, various biosensors using different transducers have been reported as effective in detecting and identifying disease biomarkers. To date, research in this area is rapidly growing and a massive number of technologies have been developed to diagnose diseases, toxins, pathogens and viruses (Morales-Narvaez, 2015; Ngom *et al*., 2010; Shukla *et al*., 2014). Most of these biosensors rely on the interaction between antibody and an analyte. However, antibodies are presented with disadvantages such as high cost, instability, poor sensitivity, or and limitation of targets kinds (Mao *et al*., 2009).

The use of aptamers in the field of biotechnology has emerged as a solution to many challenges met in signal transduction processes for a wide range of smaller molecule (Liu *et al*., 2009). Aptamers have been preferred because they have the following advantages: high specificity, low molecular weight, easy and reproducible production as compared to antibodies (Fang *et al*., 2003). Aptamers present a more favourable and desirable molecular recognition element (MRE) and have been employed in the development of biosensors for diagnosis purposes. However, similar to antibody-based biosensors, single aptamer based biosensors have also suffered from weak sensitivities. Therefore, they cannot be applied in the field and most of them do not make it to the commercialization stage. To overcome such challenges, sandwich-type biosensors, which uses a pair of aptamers or aptamer/antibody complex, have been developed (Guo *et al*., 2012; Pultar *et al*., 2009). By using dual aptamers, biosensors that have poor sensitivity can be recalled and repurposed. Therefore, this study will focus on developing a lateral flow detection device that is versatile, cost-effective, rapid, portable and easy for use at PoC for the detection of a diabetes biomarker.

1.2 Diabetes mellitus

Diabetes mellitus, simply referred to as diabetes, is a group of diseases characterized by high glucose levels, due to defects in insulin production, the body's inability to respond properly to insulin, or both (Shoback, 2011). The American Diabetes Association (ADA) have described diabetes as a metabolic disorder of multiple aetiology categorized by chronic hyperglycaemia with disturbances of carbohydrate, fat and protein metabolism (ADA, 2009). It is associated with reduced life expectancy and morbidity due to related complications such as microvascular and macrovascular complications that diminishes the quality of life (Aring *et al*., 2005). Diabetic patients may present characteristics symptoms, such as constant thirst, polyuria, blurred vision and weight loss. These symptoms are not severe or may not all be present. As such, patients with diabetes may leave up to 7 years or more without the knowledge of having the disease, thereby restricting its early diagnosis (Vaishya *et al*., 2018).

Under physiological conditions, after a meal, carbohydrates are broken down into glucose molecules in the gut and the amount of glucose in the bloodstream increases. The pancreatic beta-cells (β-cells) in the pancreases detect this increased amount of glucose and release insulin into the bloodstream (Brerenton *et al*., 2016). The insulin lowers the blood glucose levels by increasing glucose uptake in the muscles and adipose tissue through the stimulation of glycolysis and glycogenesis (Sundstena and Ortsäterb, 2009). As insulin works on the body, the amount of glucose eventually returns to normal or same level as before taking a meal (as outlined in **Figure 1.1**). The release of insulin stimulate an enzyme called glycogen synthase in the liver, which convert glucose to glycogen, that is then stored in the liver and used in the future when blood glucose levels are too low (Han *et al*., 2016).

However, changes in insulin production and secretion can negatively affect blood glucose levels. A decrease in insulin production will inhibit uptake by the muscles and adipose tissues, resulting in hyperglycaemia. The same effect can be triggered by the body's inability to respond to insulin action and ultimately lead to a build-up of glucose in the blood (Wilcox, 2005). Initially, due to increased blood glucose levels, the patient enters a pre-diabetic stage which is defined as a period where glucose levels are higher than normal but not high enough to be diagnosed as diabetes (Coppari, 2017; Wilcox, 2005). At this stage, the pre-diabetic patient is advised to make some lifestyle modifications through physical activity and eating a healthy balanced diet in order to prevent developing diabetes later in life. However, if no action is taken and the glucose levels are not kept at a normal standard, they will continue to

increase to a level where a person is diagnosed as diabetic (Sundstena and Ortsäterb, 2009). This stage is often followed by severe complications and may in the long run lead to death.

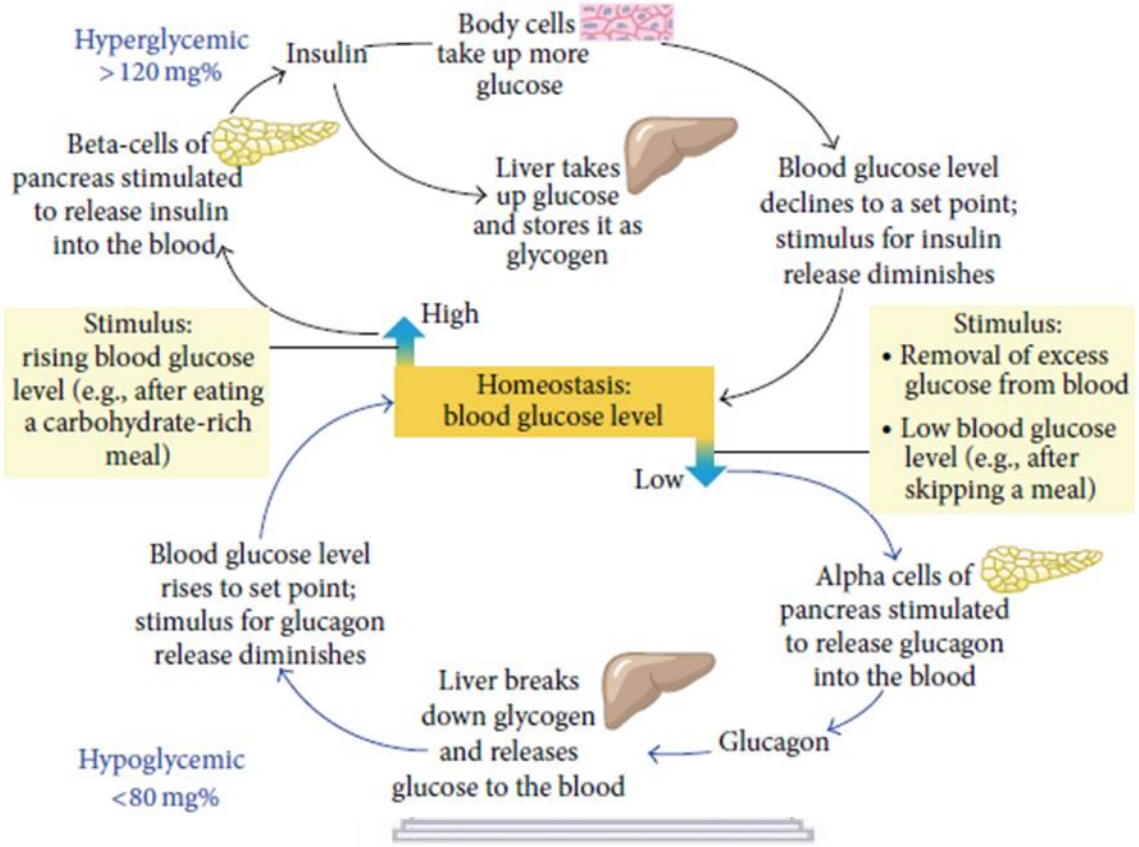

Figure 1.1: **Schematic representation of the glucose-lowering effects of insulin in different organs (Lowe, 2005).**

1.2.1 Prevalence and risk factors of DM

DM have reached an epidemic proportion and it is presumed that it will be one of the top 7 leading causes of death by 2030 (WHO), 2016). As shown in **Figure 1.2**, about 425 million people are diagnosed with diabetes worldwide, and the number is expected to rise to 629 million by 2045 (International Diabetes Federation (IDF), 2018). Approximately 50% of diabetes cases are undiagnosed, with the majority of these occurring in low-income and middle-income countries (IDF, 2017).

In Africa, the proportion of undiagnosed diabetes is 69.2% and approximately 77% of deaths occurred due to diabetes in individuals younger than 60 years in 2017 (IDF, 2017). South Africa (SA) is not an exception to the above statement as there were about 1 million new cases of diabetes reported in 2017 (IDF, 2018). The latest population estimates for South

Africa indicate that about 3.85 million South Africans between 21 and 79 may have diabetes. Furthermore, reports show that about 6% of the South African population suffer from T2DM while many more remain undiagnosed and are at a higher risk of developing harmful and costly complications. In 2009, more than 73 000 disability-adjusted life years were attributable to T2DM and its associated diseases; and the number of diabetes-related amputations and cases of blindness was estimated at approximately 2 000 and 8 000, respectively (Bertram *et al.*, 2013; Cabrera Escobar *et al.*, 2013).

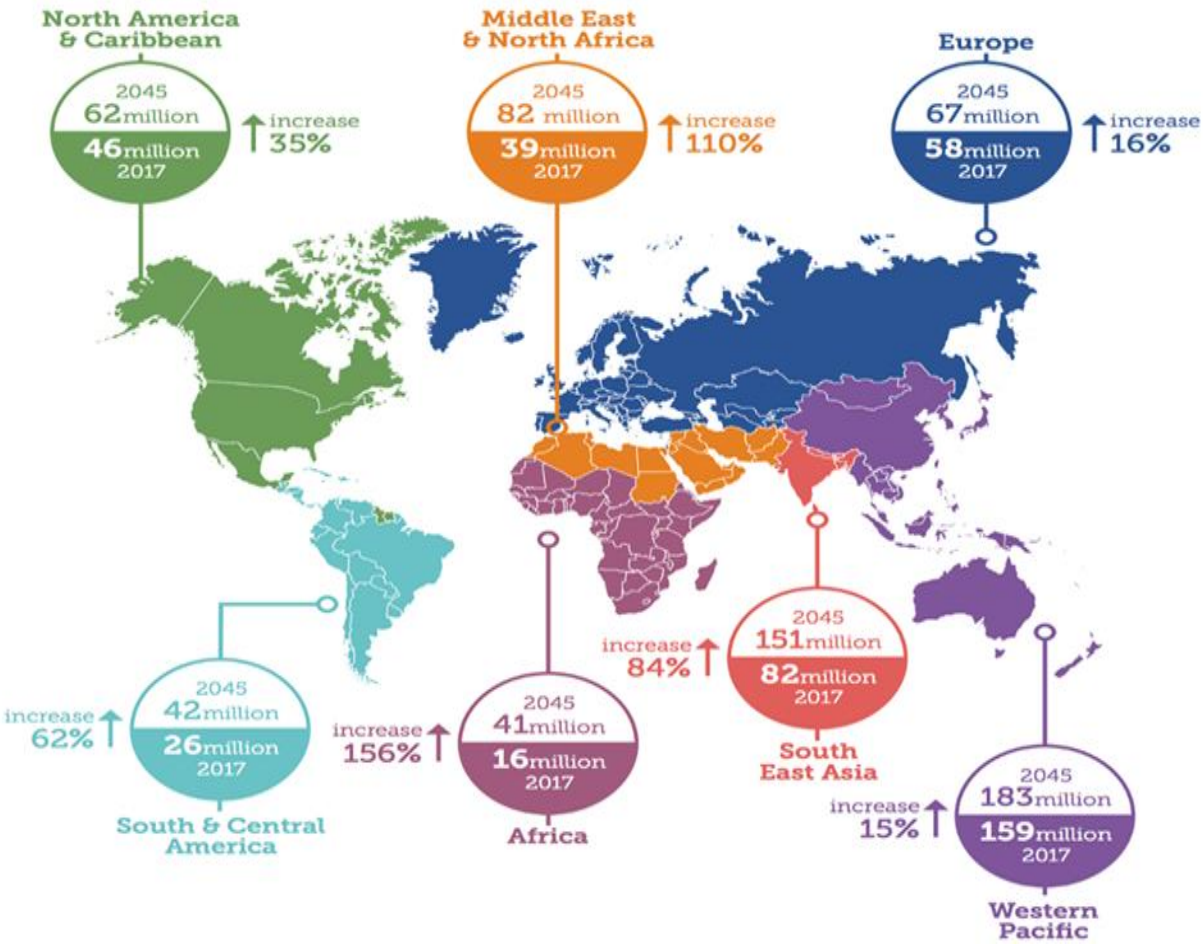

Figure 1.2: **Diabetes prevalence rate worldwide in 2017, the estimated percentage increase from 2017 to 2015 and the prevalence for 2045 (IDF, 2017).**

Several factors such as the ageing population, economic transition and urbanisation associated with nutrition transition and obesity have significantly contributed to the increased diabetes prevalence (Kengen *et al*., 2013; Peer *et al*., 2013; Vorster *et al*., 2005). Over the years, several studies have also reported on the link between obesity and T2DM (Abel *et al*., 2001; Riaz, 2015; Yang *et al*., 2005) and the studies revealed that about 87% of diabetes cases in SA were attributed to obesity in 2000 (Jourtbet *et al*., 2007). In 2015, the global burden of disease study estimated that high body mass index and hyperglycaemia, ranked as the second and third leading risk factors, respectively, for early death and disability in SA (Fleming *et al*., 2014). The figures mentioned above clearly confirm that diabetes is a major health threat in SA and around the world; hence, it requires an urgent responsiveness through proper treatment and early detection.

Apart from factors listed above, genetic factors have also played a role in the development of diabetes. More interestingly, the prevalence of diabetes in SA differs for each ethnic group (as shown in **Table 1.1**). The Indian population has the highest prevalence of 11 - 13%, while the White population has the lowest prevalence of 4% (Otternman, 2012). These figures corroborate with studies conducted in multi-ethnic populations of other countries, which have showed that individuals of certain ethnicities are more susceptible to develop T2DM in their life time (Unnikrishnan *et al*., 2017)

Table 1.1: The prevalence of diabetes for South African ethnic groups (Otternman, 2012).

Ethnicity/Race	Prevalence
Indian population	11 - 13%
Coloured population	8 - 10%
Black population	5 - 8%
White population	4%

1.2.2 Classification of DM

Generally, there are two main categories of DM: type 1 diabetes mellitus (T1DM) and T2DM. T1DM is caused β-cell dysfunction whereas T2DM is characterized by the body's resistance to insulin action and a decrease in pancreatic β-cell mass (Graham *et al*., 2006; Kaku, 2010). A third form of diabetes, called Gestational DM (GDM), that develops during pregnancy also exist. However, the glucose levels return to normal after childbirth. Other specific types of diabetes may also develop due to other causes, e.g. monogenic diabetes syndromes, diseases of the exocrine pancreas, and drug- or chemical-induced diabetes (ADA, 2018).

a) Type 1 diabetes mellitus

T1DM is defined as an autoimmune disease which is characterised by β-cell destruction caused by an autoimmune process that may leads to insulin deficiency (Lowe *et al*., 2017). Genetic and environmental factors are known to play a vital role in the pathophysiological mechanisms of this disease (Insel *et al*., 2015). In previous years, it was known as insulin-dependent or juvenile-onset diabetes (Ooi and Loke, 2012; Pociot and Lernmark 2016). It was given the term "juvenile-onset" as it was normally diagnosed in children and young adults (Miller *et al*., 2009); however, this condition can now develop at any age (Covantev *et al*., 2016). It has also been referred to as insulin-dependent diabetes because T1DM patients takes insulin on their daily basis in order to control the glucose levels.

b) Type 2 diabetes mellitus

T2DM is defined as a heterogeneous group of metabolic diseases (Wilcox, 2005) which are characterized by hyperglycaemia resulting from defects in insulin secretion, insulin action, or both (Berlanga-Acosta, 2013; Pociot and Lermark, 2016; Miller *et al*., 2009). The relative contribution of these two pathophysiological mechanisms for the development of T2DM vary between individuals and may also differ between ethnic groups (Unnikrishnan *et al*., 2017). This is attributed by the fact that T2DM is defined as a polygenic disorder composed of subtypes whereby genetic susceptibility is strongly associated with environmental factors (Groop and Pociot, 2013; Riaz, 2009). In addition, there may be other hormonal systems that predispose individuals to the development of chronic hyperglycaemia; however, these hormonal changes are not yet well characterized (Unnikrishnan *et al*., 2017). T2DM usually

occurs in adulthood and develops more with age, and sometimes it is also observed in children and some adolescents having obesity (Riaz, 2015).

c) Gestational diabetes

GDM is a third form of diabetes that occurs during pregnancy, when a woman with no previous history of diabetes develops high blood glucose levels. It is usually recognized during the third trimester of a woman's pregnancy (Dinneen, 2006). During pregnancy, the insulin physiology gets altered by hormonal changes (Lowe and Karban, 2014). These hormones work by modulating insulin action, and making it resistant which results in high blood glucose levels (Kapustin, 2008). After childbirth, blood glucose levels usually return to a normal level; however, some women who have had GDM, have an increased risk of developing T2DM later in life (Järvelä *et al*., 2006).

1.2.3 Complications of DM

Complications can affect different parts of the body and manifest in various ways in individuals. Complications of diabetes are classified as either acute or chronic complications (Riaz, 2009).

Acute complications may be less severe in people with a manageable blood glucose levels (Nathan *et al*., 2005). The acute complications of T2DM may include hypoglycaemia, hyperglycaemia and diabetic coma (Cypress, 2001). These complications develop over a short period of time; however, they can be prevented (Coppari, 2017). It is also possible to reverse the complications when a patient follows a healthy lifestyle with proper consultations and medications (Codera and Adam, 2016).

Chronic complications of DM includes progressive development of the specific retinopathy with potential blindness, nephropathy that may lead to renal failure and/or neuropathy with risk of foot ulcers that may lead to foot amputation (ADA, 2009). DM may also impair salivary gland functions, which leads to a reduction in the salivary flow and changes in saliva's composition (Aravindha Babu *et al*., 2014). These complications are not irreversible, and often, patients are at an increased risk of developing cardiovascular, peripheral vascular and cerebrovascular diseases in their life time (Arguedas *et al*., 2013; Desphande *et al*., 2008).

Risk factors such as age, type of diabetes, gender and genetic factors plays a determination role on the type of complications a diabetic patient may develop over the years (Wu *et al*., 2014). Nonetheless, the exact pathogenetic mechanisms causing the diabetic complications are still unclear and remains an interesting field that still need to be explored in the quest to better understanding of this disease. Interestingly, an independent study by Porta (2016) reported that some genes provide protection against diabetic complications, which is evident in a subtype of long-term T1DM survivors without complications. This could explain why some patients with diabetes are not susceptible to developing complications.

1.2.4 Standard diagnostic methods for diabetes and their limitations

Existing methods for diagnosis of diabetes generally use blood to detect glucose levels making them invasive and when found it is usually too late (Malamud, 2011). Commercially available diagnostic kits methods such as Fasting Plasma Glucose (FPG), Oral Glucose Tolerance Test (OGTT), Haemoglobin A1C (HbA1C) and Random Plasma Glucose test (RPG) are used as the golden standard for diagnosis of diabetes. The diagnosis of diabetes is based on the ADA criteria: FPG of ≥ 126 mg/dL (7.0 mmol/L), 2-h post-prandial plasma glucose of ≥ 200 mg/dL (11.1 mmol/L) during OGTT, HbA1c of ≥ 6.5% (47.5 mmol/L) and RPG of ≥ 200 mg/dL (11.1 mmol/L). (ADA, 2014). However, all of these tests requires further confirmatory test. Hence, it is recommended that the same test be repeated or a different test be performed. Usually, if two different tests are both above the diagnostic threshold, then a person is considered to be diabetic. Nevertheless, if a patient has conflicting or varying results from two different tests, then the test result that is above the diagnostic cut-off point should be repeated (ADA, 2018).

The FPG test is mostly the most preferred test because it is convenient and cheap; however, it may miss some diabetes or prediabetes that can be found with the OGTT (Melmed *et al*., 2000). The OGTT is more sensitive than the FPG test for diagnosing prediabetes, but it is less convenient to administer. Moreover, the OGTT measures blood glucose at a single point time. The FPG test is mostly reliable when done in the morning; therefore, it is not convenient for patient or health care provider as it requires fasting and scheduling a morning appointment or return visits to the hospital/clinic, which could be costly and tiring.

Other diagnostics methods such as RPG measures blood glucose levels without taking into account the last meal of the patient. This test, along with an assessment of symptoms, is used

to diagnose diabetes but not prediabetes and a second confirmation test is also required (ADA, 2018). The HbA1C test measure the amount of glucose attached to Hb and has shown to have more advantages over other tests; moreover, it does not require fasting prior to taking the test (Cowie *et al*., 2010). However, it is less sensitive and not accurate in people with anaemia (ADA, 2018). Furthermore, the test is not suitable for people of different ethnicities such as people in Africa, Mediterranean or Southeast Asian descent (Herman, 2016; Ziemer *et al*., 2010). Thus, a health care professional may need to order a different type of HbA1C test which may be costly. Therefore, this highlights the urgent need to develop diagnostic devices that are suitable in a poor resource settings and that can compete on a global scale. These devices should also be able to detect diabetes at its early stages.

1.2.5 Biomarker discovery as an alternative

A biomarker is a biological molecule found in body fluids or tissues that can be seen as an indicator of a normal or abnormal processes or diseases (Strimbu and Tavel, 2010). Since the beginning of high-throughput OMICS technologies which are capable of inclusive analysis of genes, transcripts, proteins and other biological molecules, biomedical scientists have successfully identified molecular biomarkers associated with various diseases processes (McDermot *et al*., 2013). This discovery has played a significant role in disease diagnosis and treatment and has created a surge among biomedical researchers. Many diseases associated biomarkers have been studied, and current research is focusing on various areas which includes risk assessment, screening differential diagnosis, determination of prognosis, prediction of response to treatment and monitoring of progression of various diseases (Chen *et al*., 2018; Henry and Hayes, 2012; Mason *et al*., 2013). Thus, an emphasis on biomarker discovery within multiple areas of research has become a high priority.

Recently, proteome analysis of plasma and serum for the identification and characterization of T2DM protein biomarker has sparked a great interest. Certain biomarkers were found to be either upregulated or downregulated during the development of T2DM. Most of these proteins have been successfully analysed using mass spectrometry (MS) or protein microarrays (Backus *et al*, 2016; Thebani *et al*, 2016). Using MS, approximately 487 salivary proteins which were differentially expressed between three stages of T2DM were identified. Out of the 487 proteins/peptides, 65 potential biomarkers showed higher expression in three stages of T2DM. Western blot confirmed expression of selected 5 salivary biomarkers namely: alpha-2-macroglobulin (a2MG), alpha-1-antitrypsin, cystatin C, transthyretin and

alpha-amylase. One of these 5 biomarkers, a2MG, showed increased levels in its expression with severity of T2DM based on previous diabetic diagnosis (Rao *et al*., 2009).

Other studies have incorporated the use of two-dimensional electrophoresis (2DGE) and MS to profile proteins associated with diabetes. 2DGE coupled with matrix-assisted laser desorption/ionization time of flight mass spectrometry (MALDI-TOF/MS) was used to compare the salivary proteomes between T1DM and non-diabetic patients, 6 proteins out of 17 differentially expressed spots in the 2DGE were identified. It was noted that alpha-amylase was the most predominant protein affected in diabetic patients (Hirtz *et al*., 2006). Analysis of plasma proteome of T2DM patients with nephropathy through proteomics identified 34 proteins spots differentially expressed. The unique proteins spots (31 in total) were associated with the metabolic (5'-AMP-activated protein kinase) and growth regulatory (LIM homeobox protein 6) processes. Moreover, the quantitative proteomic approach also identified several documented T2DM plasma biomarkers such as apolipoprotein A-I and ficolin. Interestingly, the study further reported on several putative T2DM biomarkers including calpain-7 and choline/ethanolamine kinase which have not been reported before. These proteins may be associated with the progression and development of T2DM and requires further analysis (Hung *et al*., 2011)

1.2.6 Protein biomarkers for early detection of T2DM

It is well documented that the development of T2DM occurs very slowly, going through periods of increased insulin secretion, insulin resistance, impaired glucose tolerance and β-cell dysfunction (ADA, 2009; Srinivasan *et al*., 2018). Thus, the current most acceptable diagnostics biomarkers for diabetes are based on high blood glucose levels and HbA1c. However, by the time these markers are elevated, it is usually too late and diabetes may have already progressed to severe complications. This serves as an indicator that improved detection techniques and/or putative biomarkers that can detect diabetes earlier are urgently needed across the entire spectrum of diabetes initiation and progression. Protein biomarkers that are present in the early stage of diabetes may provide insights on the pathophysiology of this disease. Furthermore, they may also help in the identification of high risk individuals even before the prediabetes stage, when the β-cells are still intact, in order to put effective measures in place which could ultimately help to prevent progression of this disease (Vaishya *et al*., 2018). As such, several hypothesis-based nonglycemic biomarkers have been assessed as risk factors indicators for diabetes (Kolberg *et al*., 2009; Wu *et al*., 2011).

Previous studies have demonstrated that various forms of apolipoproteins are present in patients with T2DM. For example, serum levels of apolipoproteins such as Apo A1 and Apo B levels are significantly increased in individuals with prediabetes and T2DM (Onat *et al*., 2010; Sasongko *et al*., 2011; Zheng *et al*., 2016). Proteins associated with diabetic macular oedema. These include pigment epithelium derived factor, ApoA-4, ApoA-1, thyroid hormone receptor interactor protein 11 (Trip-11), and vitamin D binding protein and only ApoH was present in non-diabetic controls (Nakanishi *et al*., 2002).

a2MG is an inhibitor of proteinase enzyme in blood and tissues, and was identified as a potential protein biomarker for T2DM (Borth, 1992). This protein acts as a binding protein for numerous cytokines and growth factors; and also acts as leptin protein in human plasma. In a recent study, plasma a2MG levels were reported to be high in diabetic patients, especially those with diabetes complications (Chung *et al*., 2016). a2MG levels were also elevated in human saliva of patients with diabetes; thus, indicating its potential use to non-invasively diagnose T2DM (Rao *et al*., 2009).

Another protein that has been associated with T2DM is the c-reactive protein (CRP). CRP is an acute phase protein, and a strong biomarker of inflammation in the progression of various diseases including diabetes. Genetic variation of this protein levels expression and its association with T2DM have been studied (Yudkin *et al*., 2004; Xu *et al*., 2007). It was found that the levels of CPR levels rise up to 1000 fold in diabetic patients as compared to CPR levels in non-diabetic individuals. Significant association of CRP, fibrinogen and plasminogen activator inhibitor-1 have been studied (Festa *et al*., 2002).

Multiple biomarkers for early detection of T2DM which included adipokines secreted proteins such as leptin (pro-inflammatory effect) and adiponectin (anti-inflammatory effect) were previously investigated (Umeno *et al*., 2015). The study demonstrated that leptin and adiponectin correlated well with insulin levels; thus, indicating their potential use as early biomarkers of T2DM. Other adipokines such as vasftin and resistin have also been shown to be upregulated in T2DM (Li *et al*., 2006; Stofkov, 2010). Studies have reported that the pro-diabetic effects of the resistin are attributed to inhibition of insulin signalling and a pro-inflammatory mechanism, that culminates in β-cell loss; whereas, vasftin has been shown to exhibit glucose-lowering and insulin sensitizing effects (Dunmore and Brown, 2013; Stofkova, 2010; Srinivasan *et al*.,2018).

1.2.7 Retinol Binding Protein 4 as the biomarker for T2DM

Retinol binding protein 4 (RBP4) is an adipokines secreted protein. It has a molecular weight of 21 kDa and belongs to the lipocalin family. Its function is to transport retinol from the liver to the peripheral tissues. In plasma, the RBP-retinol complex interacts with transthyretin, which prevents its loss by filtration through the kidney glomeruli (Newcomer and Ong, 2000).

Kahn and his group were the first researchers to discover the role of RBP4 in obesity and insulin resistance. Their research demonstrated that mice with an adipose-specific knockout GLUT4 developed an insulin resistance in muscles and liver (Abel *et al.*, 2001). In 2005, Yang and co-workers demonstrated that the expression of serum RBP4 was higher in insulin-resistant mice and humans with obesity and T2DM. The overexpression of RBP4 in wild-type mice causes insulin resistance while genetic depletion of RBP4 improves insulin sensitivity, suggesting that the depleting level of RBP4 could be a useful tool in the treatment of T2DM; whereas, increased levels of RBP4 could serve as a biomarker for diagnosis of T2DM (Yang *et al*., 2005). Proteomic analysis to assess the association of plasma proteins with the risk of developing T2DM has shown that RBP4 is independently associated with the risk of developing T2DM (Sun *et al*., 2014).

Since its discovery, various studies have been carried out with a goal to show a link between RBP4 and T2DM in human (Graham *et al*., 2006; Takebayashi *et al*., 2007). A study conducted by Graham *et al.* (2006) observed that the magnitude of increase in serum RBP4 correlates with insulin resistance among humans with obesity, impaired glucose tolerance, or T2DM, and among non-obese and nondiabetic subjects with strong family histories of T2DM. Furthermore, another study revealed that RBP4 levels increased in blood circulation by 104.8 ± 76.8 nanogram per mL (ng/mL) in obese and insulin resistance resistant patients when compared to control individuals, 87.9 ±38 ng/mL (Commucci *et al*., 2014). These findings were similar to finding of Takebayashi *et al*. (2007), whereby the study revealed that RBP4 was associated with certain biomarkers related to insulin resistance or diabetic complications. These studies contributed to the novelty of RBP4 as a potential biomarker for diagnosing diabetes.

1.3 Aptamers

The name aptamer comes from two words, “aptus” which is a Latin word for “to fit”, and “meros” which is a Greek word for “part” or “region” (Ellington and Szostak, 1990; Tuerk and Gold, 1993). Aptamers can be described as short single-stranded deoxyribonucleic acids (DNA) or ribonucleic acids that bind with high affinity and specificity to their target molecule; they do so by folding into unique three-dimensional shapes (Ellington and Szostak 1990; Berg *et al*., 2016). They bind to their target through intermolecular interactions such as van der Waals forces, hydrogen bonding, electrostatic interactions between charged groups, and Pi-Pi stacking of “flat-structured” aromatic moieties (Hermann and Patel, 2000; Keefe *et al*., 2010). They contain functional moieties that fold into different secondary structures, such as hairpin, stem, loops or bulge, G-quadruplex and pseudoknots (**Figure 1.3**), which have a significant impact on the conformational stability and target binding affinity of the aptamer (Kaur and Yung, 2012; Piganeau and Schroeder, 2003)

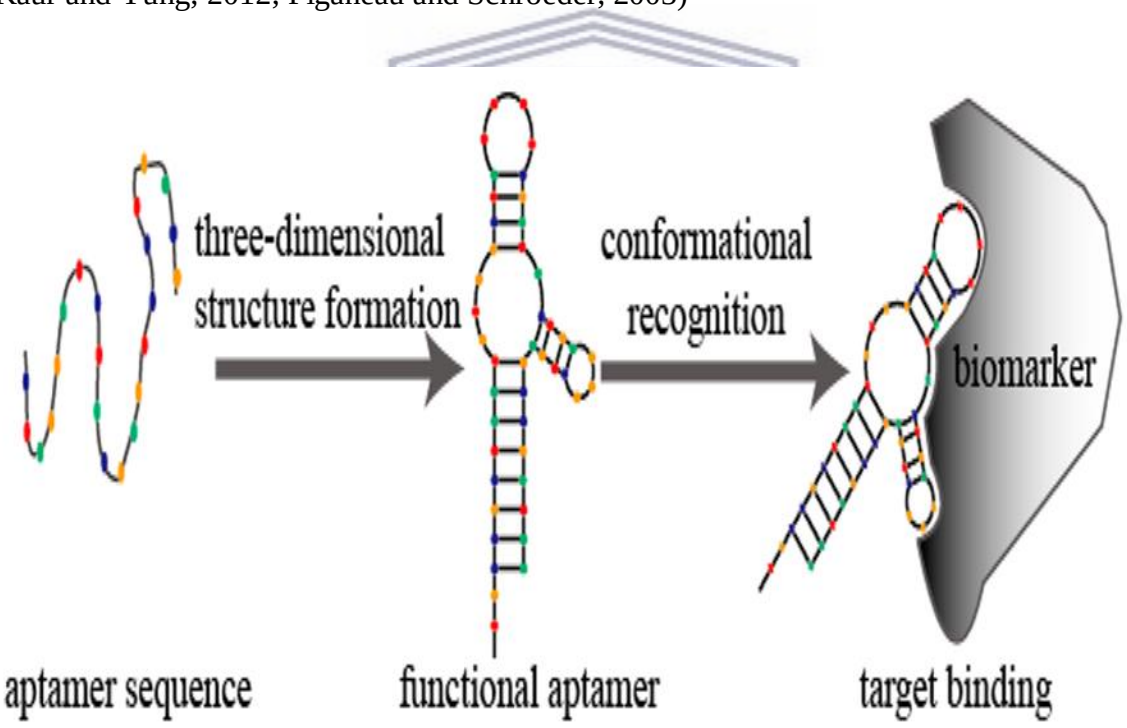

Figure 1.3: **Schematic representation of aptamer-target binding.** Aptamers fold into 3-D nucleic acids structures that bind to the target molecules via a high affinity lock and key mechanism (Sun and Su, 2015).

1.3.1 The selection of aptamers

Aptamers are selected from a set of a random oligonucleotide library and synthesized in vitro through a method called Systematic Evolution of Ligands by Exponential Enrichment (SELEX) (Sypabekova *et al.*, 2017; Tolle, *et al.*, 2014; Zhang *et al.*, 2017). A systematic schematic overview of the SELEX process is shown in **Figure 1.4**. The SELEX process generally starts with the generation of a randomized nucleic acid (DNA) library, normally consisting of about 1013 - 1015 different sequences (James, 2000). The DNA library is incubated directly with the target molecule, which is immobilized on a matrix material or is free in solution. Following incubation, the bound complexes are separated from the unbound oligonucleotides through numerous washing steps. Target-bound oligonucleotides are eluted and amplified using polymerase chain reaction (PCR) or reverse transcription PCR amplification (Stoltenburg *et al*., 2007). The enriched pool of selected oligonucleotides is then used in the next round of SELEX round (Sypabekova *et al*., 2017). The enriched aptamers are then sequenced, and the sequence is analysed using various bioinformatics tools in order to identify consensus motifs – the region playing the central role in the specificity of the target binding (Hoinka *et al*., 2012). The selected sequences are characterized using various methods such as Surface Plasmon Resonance (SPR), Microscale Thermophoresis (MST), and Bio-layer interferometry (BLI) system and etc. (Entzian and Schubert, 2016; Stoltenburg *et al*., 2016).

Usually, it takes about 8 - 15 rounds of SELEX to select aptamer candidates with the highest binding affinity for the target (Marshall and Ellington, 2000). Hence, this iterative process is more laborious and takes about few weeks or up to a month and sometimes it may be ineffective or longer to optimize as there is no standardized protocol. Therefore, optimization of the SELEX conditions is a very crucial step that is dynamic throughout the selection procedure (Darmostuk *et al*., 2015).

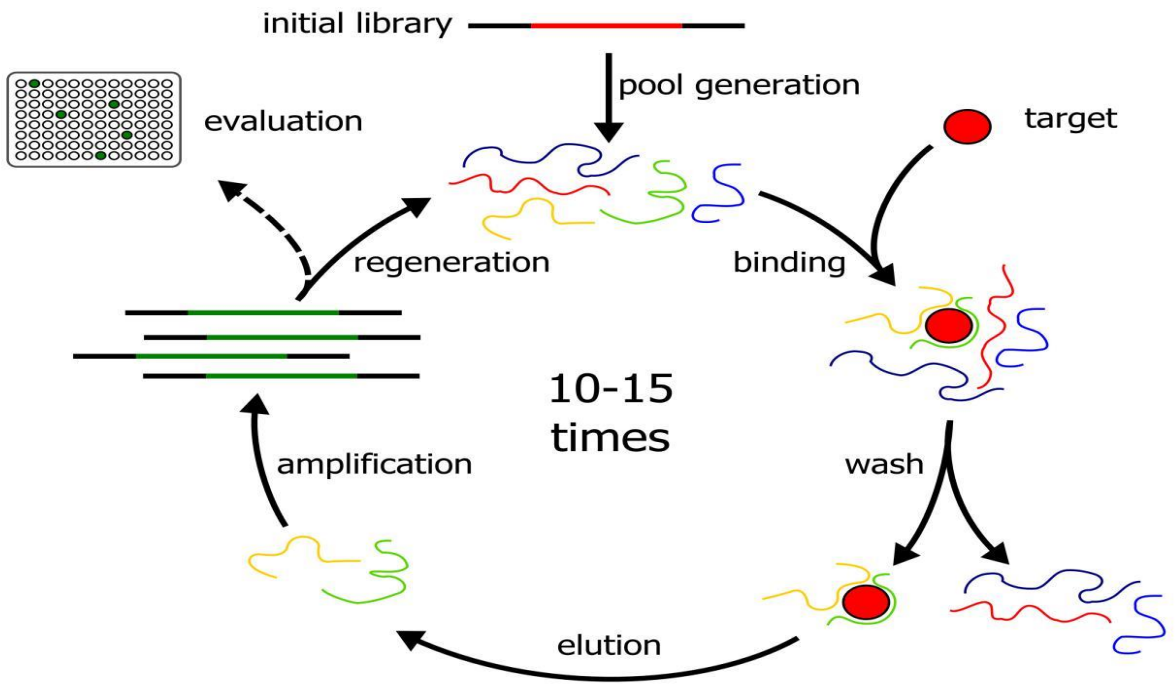

Figure 1.4: Overview of the SELEX process. A conventional SELEX procedure involves binding a random nucleic acid library to the target molecule, separating the bound and unbound nucleic acids, and amplifying the bound nucleic acid by PCR for use in the next round of selection. After several rounds of selection, the aptamers are then cloned and sequenced (Schütze *et al*., 2011).

1.3.2 Types of SELEX protocols

The SELEX procedure was first reported in 1990 by two laboratories of Ellington and Szostak (1990) and Tuerk and Gold (1990). Since then, numerous modifications have been applied and new strategies of selection have been developed (**Table 1.2**). This has been possible due to new developments in chemical synthesis, advanced technical equipment's and the availability of analysis methods to improve the properties of aptamers and the efficiency of their development (Blind and Blank, 2015).

Table 1.2: Various types of SELEX procedures, their advantages and aptamer targets.

Type of SELEX	Advantages	Aptamer target	Ref.
Counter SELEX	Incorporates similar target molecules during incubation	LNCap cells, Aflatoxin B1	Almasi *et al*., 2016; Setlem *et al*., 2016
Affinity-based chromatography SELEX	Selection against smaller molecules and proteins Selection based on affinity chromatography; whereby, the target molecule is immobilized on the beads	β-conglutin, Ractopamine	Nadal *et al*., 2012; Duan *et al*., 2017
Cell-SELEX	Selection against a whole mammalian or pathogenic cells Selection is performed against unknown cell surface components	Ramo cells, PC-3 cells, SK-BR-3, *Escherichia coli O157:H7*, Listeria monocytogenes	Chen *et al*., 2007; Duan *et al*., 2013; Lee *et al*., 2012; Wang 2014; Wang *et al*., 2009
Capillary electrophoresis based SELEX	The number of round of selection is reduced It does not involve any amplification step	IgE and neuropeptide Y, human immunodeficiency virus reverse transcriptase (HIV-1 RT), anthrax protective antigen	Cella *et al*., 2010; Mendonsa and Bowser, 2004; Mosing *et al*., 2005.
FluMag SELEX	Use of fluorescent labels for DNA quantification and use of magnetic beads for target immobilization Use of very small amounts of target for the aptamer selection, rapid and efficient separation of bound and unbound molecules and stringent washing steps For targets with varying properties and size	Streptavidin, RBP4	Stoltenburg *et al*., 2005; Lee *et al*., 2008
MonoLEX	Involves a one-cycle process Does not require any special equipment	Vaccinia virus. α-Bungarotoxin	Lauridsen *et al*., 2012; Nitsche *et al*., 2009

1.3.3 Advantages of aptamers over antibodies

Aptamers-based biosensing strategies strategy have emerged as a powerful tool in the field of diagnostics because they have shown to have more advantages over antibodies (**Table 1.3**). One of the most significant advantage is that aptamers bind to their target molecules with a high specificity and selectivity (Geiger *et al*., 1996; Jenison *et al*., 1994). Furthermore, aptamers can be chemically synthesized and can be easily modified to improve stability and the attachment of reporter molecules for various applications (Pendergrast *et al*., 2005). Aptamers have greater affinity, preferably in nanomolar (nM) to picomolar (pM) range (Chen and Yang, 2015) which is not affected by labelling (Sypabekova *et al*., 2017). They are also relatively small in size, giving them an advantage to penetrate tissues and are more easily internalized by target cells; improving their therapeutic value (Xiang *et al*., 2015).

In addition, aptamers are stable over a wide range of temperature and buffer conditions and are resistant to harsh physical or chemical denaturation without any significant loss of activity. As already stated above, aptamers can be generated from a wide range of molecules such as ions, small molecules, neurotransmitters, organic pollutants, drugs, proteins, peptides, and complex cells or tissues (Daniels *et al*., 2003; Li *et al*., 1996; Mallikaratchy *et al*., 2007; Mendonsa and Bowser 2004).

Aptamers offers higher flexibility and can adapt to different assay formats (Jauset Rubio, *et al*., 2017; Kim, *et al*., 2014). The affinity of aptamers can be improved by making longer dimeric or multivalent aptamer (Dhiman *et al*., 2017). These characteristics make aptamers good candidate molecules for the development of sensitive and selective sensor elements for diagnostic purposes, biomarker discovery and drug delivery systems for diagnosis and therapeutic purposes (Sharma *et al*., 2016; Zhou and Rossi, 2017).

Table 1.3: **Comparison of aptamers with antibodies (Chen and Yang, 2015).**

Feature	Antibody	Aptamer
Selection	Limited to physiologic conditions by animal immunization	In vivo and in vitro selection under a variety of conditions
Immobilization	Difficult through protein A/G	Easy through various orientation
Production	Time consuming and costly	Efficient with chemical synthesis at low cost
Affinity	In a low nM to pM range	In a low nM to pM range
Modification	Difficult and expensive	Easy to modify with other active groups in large scale and cheap
Reusability	Poor reusability	Good reusability
Shelf life	Short shelf life and requires a continuous cold storage	Long shelf life and does not require special storage conditions
In vivo application	High immunogenicity and low bioavailability due to a large size	Low immunogenicity and high bioavailability due to a small size

1.3.4 Application of aptamers in PoC diagnostic platforms

The development of PoC testing devices has attracted a wide attention in the field of diagnostics by enhancing the speed and accuracy of diagnosis. It is evident that PoC testing have become the preferred choice of diagnosis due to the reduction in turnaround time and cost (Gopinath *et al*., 2016; Nara *et al*., 2010); therefore, helping the patient to make informed decisions and to start early treatment (Dhiman, *et al*., 2017).

Moreover, the use of PoC technologies has transformed the healthcare of patients since they are simple to use, meaning that even without a medical background, people are able to use the devices and interpret the results (Song *et al*., 2014; Uludag *et al*., 2016; Yu *et al*., 2013; Zapatero Rodriguez and O'Kennedy, 2017). These devices are available for everyone regardless of where they are and also offer immediate results which will resolve issues that most patients experience during routine check-ups. They also eliminate having to travel to the hospital for follow up results, which can be costly and time consuming due to traffic (Lencova *et al*., 2010).

In addition, other factors that are of great significance for PoC devices is the affordability, robustness, and specificity of the test (Sajid *et al*., 2014). All this these above-mentioned

factors are in line with the WHO guidelines for the development of PoC tests (Carvalhal *et al*., 2010) and a device that fills these requirements is called a biosensor. A biosensor is a device that uses a biological entity to detect an analyte. In this case, a transducer will then give a detection signal in a form of an electrical signal that can be quantifiably measured using an appropriate readout (Luong *et al*., 2008; Srinivasan and Tung; 2015). Therefore, biosensors hold a great promise to detect changes in the disease state of an individual within minutes. For an example, one can analyse blood sugar levels or one can determine HIV status within a few minutes using a few drops of blood (Hyle *et al*., 2014; Molesworth *et al*., 2010). Similarly, on-site contamination of water (H_2O) with microbes or metal ions can easily be detected. Moreover, PoC biosensors can be used to rule out the possibility of a disease, perform confirmatory diagnostics or monitor treatment levels (Bhalla *et al*., 2016).

However, in order to develop a highly sensitive and specific assay, a suitable MRE that has high affinity must first be developed. In an attempt to find an alternative non-invasive diagnostic tool for diabetes, development of an RBP4 immunocolloidal gold fast test strip using high-sensitive monoclonal antibodies (mAbs) generated by DNA immunization was reported. Their strip, when compared with other commercially available RBP4 ELISA kits, provided faster results and was more convenient to use. However, producing mAbs that have high affinity to different epitopes remained a major stumbling block in the beginning. In addition, the production of antibodies was time consuming, costly and it is also challenging to generate specific monoclonal antibodies against non-immunogenic molecules (Bian *et al*., 2010).

To overcome such challenges, aptamers are promising MRE to use as biosensing tools since they can be selected and used under pre-defined conditions (Sypabekova *et al*., 2017). In an attempt to develop aptamers that could be used in the diagnosis of diabetes, an aptamer-based SPR biosensor to detect the level of RBP4 in serum samples was developed. The approach was more sensitive than ELISA and could be used for the detection of RBP4 in clinical applications, such as in early diagnosis of pre-diabetes (Lee *et al*. 2008). With recent advancement in technology and selection procedures, a microfluidic SELEX chip to continuously and automatically perform multiple rounds of SELEX to screen specific aptamers for HbA1c and Hb with high specificity and affinity was developed (Lin *et al*.,015). Thereafter, an integrated microfluidic system using aptamer-based testing was developed to measure HbA1c levels in blood samples. They later went on to develop an on-chip aptamer-

based sandwich assay for the detection of HbA1c via magnetic beads. This automatic HbA1c measuring system reduced reagent consumption by 75% and reduced analysis time to 30 min. However, to-date, there are no commercially available diabetes biosensors that are non-invasive and also utilizes aptamers.

1.4 Lateral flow assay

Lateral flow assays (LFAs) are described as a paper-based platform for the detection and quantification of an analyte in a complex mixture; the sample is placed on a testing device and the results are displayed over a short period of time, usually within 5-30 min (Koczula and Gallotta, 2016). LFAs have gained great popularity and demand because of their convenience, ease of use, low cost, rapid detection, accuracy and have a disposable format and adaptability to use at the PoC (Jauset-Rubio *et al*., 2017; Hu *et al*., 2014) and a well-known example is the pregnancy test which was first commercialized in 1990. Since then, this area of research has seen a massive growth and recent advances have included analytical readers to improve sensitivity (e.g. glucose reader). Another outstanding advantage of LFAs is the ability to test a wide range of biological molecules such as blood, urine, sweat, saliva and plasma (Assadollahi *et al*., 2009; Jauset-Rubio *et al*., 2017). Hence, the above-mentioned qualities have put forth PoC devices as a primary strategy for providing qualitative and semi-quantitative disease monitoring (Wright, 2011).

A LFA is based on affinity interactions, where a visible line is formed on a test strip when an analyte is present. It is assembled with the sample pad, conjugate pad, nitrocellulose membrane and an absorbent pad on a plastic backing pad, which gives it support (**Figure 1.5**). The sample pad transports the liquid sample to other components of the lateral flow strip in a smooth, continuous and homogenous manner (Sajid *et al*., 2014). Labelled bio-recognition molecules are dispensed on the conjugation pad, and activated when they come into contact with the liquid samples. Upon their activation, a control line will appear on the nitrocellulose membrane whereas a test line is only visualized if the test is positive (Malathi *et al*, 2014). Thus, a nitrocellulose membrane plays a role in determining the sensitivity of the lateral flow (LF) and also provide an optimal and stable binding of capture probes. Finally, the absorbent pad provides the capillary based driving force, which maintains the flow rate of the liquid sample over the membrane and prevents back flow (Millipore, 2009; Sajid *et al*., 2014).

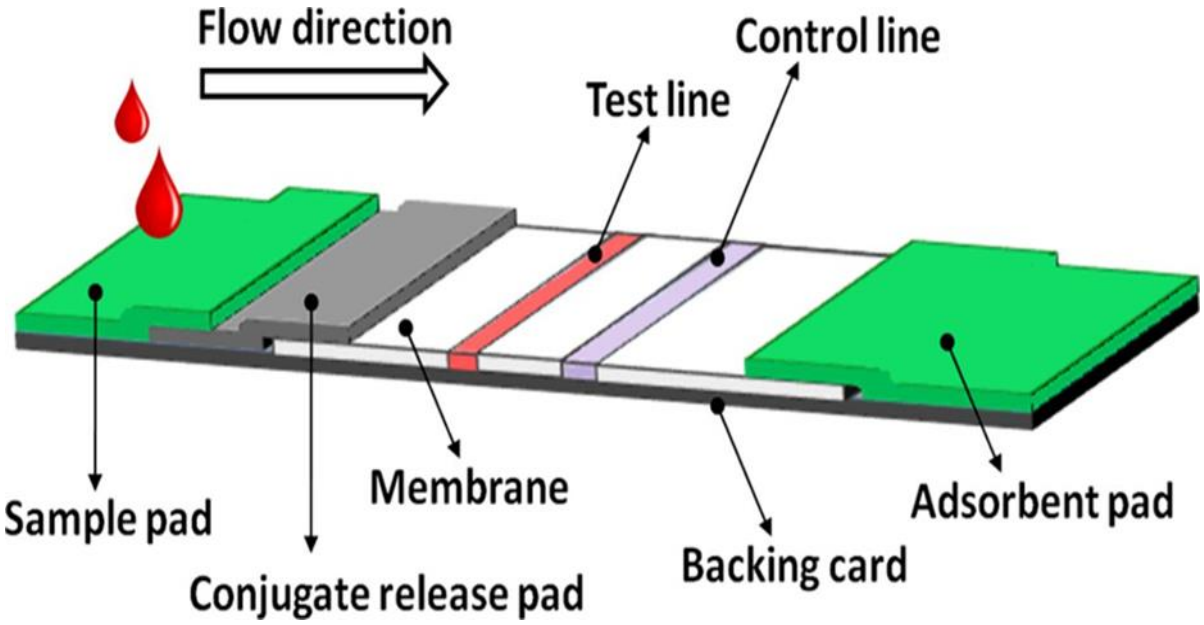

Figure 1.5: A typical lateral flow biosensor. A lateral flow strip is commonly composed of a conjugate pad, membrane and absorbent pad. On the membrane lies the test line and the control line, which changes its colour to show presence or absence of target in the sample or analyte (Koczula and Gallotta, 2016).

1.4.1 Different types of LF format

Numerous LF formats using aptamers have been reported over the years and some of them are highlighted in **Table 1.4**. The majority of these LFAs are either sandwich assays or competitive assays. A sandwich assay is the most preferred assay for larger molecules and in the presence of two aptamers that bind to the same target at different epitopes. An example of a sandwich format is a well-known commercialized insulin assay for diagnosis of diabetes. Whereas, a competitive format allows detection of low molecular weight or for target with a single specific epitope. Typical examples of this format are the more specialised tests for drugs and toxins (Chen and Yang, 2015).

Each format has advantages and disadvantages depending on the analyte, the antibody, sample matrix and the concentration range of interest. Generally, non-competitive immunoassay has a lower limit of detection (analytical sensitivity) over the competitive format. This is typically picogram/mL (parts per trillion) for non-competitive compared to ng/mL (parts per billion) for the competitive format. In situations where significantly high analyte concentrations might be encountered, non-competitive formats can suffer from the high-dose hook effect which can yield to false results. On the other hands, the competitive format does not have a high-dose hook effect (Rey *et al.*, 2017).

Table 1.4: Lateral flow assays using aptamers (Jauset-Rubio *et al*., 2017).

Target	LOD	Format	Test line	Control line	Bio conjugate	Ref.
Aflatoxin B-1	0.32	Competitive assay	SA	Anti-Cy5 antibody	_	Shim *et al*., 2014
ATP	0.5 µM	Sandwich assay	SA-biotin-split aptamer 2	SA-biotin DNA probe	AuNPs split aptamer 1	Zhu *et al*., 2016
***E. coli* 0157;H7**	10 CFU/Ml	Strand displacement	SA-biotin-DNA probe	SA-biotin DNA probe	AuNPs-DNA probe	Wu *et al*., 215
IgE	0.7 pM	Sandwich assay	Anti-IgE antibody	Anti-M13 antibody	Aptamer-phage	Adhikari *et al*., 2015
Ochratoxin A	4.7 nM	Competitive	SA-biotin-cDNA	SA-biotin-poly T	QD-aptamer	Wang *et al*., 2011
Ramos cells	4000 Ramos cells visual, 800 Ramos cells in strip	Sandwich assay	SA-biotin-TE02 aptamer	SA-biotin-Control DNA	AuNPs-aptamer	Liu *et al*., 2009
Thrombin	2.5 nM	Sandwich assay	SA-biotin-aptamer	SA-biotin-DNA complementary primary aptamer	AuNPs-primary aptamer	Xu *et al*., 2009
Thrombin	0.25 nM	Sandwich assay	Anti-thrombin antibody	SA-biotin-poly A	AuNPs-DNA1/DNA 2-AuNPs-aptamer	Shen *et al*., 2013
Vaspin	0.137 nM	Sandwich assay	SA-biotin-aptamer	SA-biotin-DNA complementary aptamer	AuNPs-aptamer	Raston *et al*., 2017
β-conglutin	55 pM	Competitive assay	β-conglutin	SA-biotin-DNA complementary aptamer	AuNPs-aptamer	Jauset-Rubio *et al*., 2016

1.5 The aim of the study

The of the study was to develop an aptamer-based LF strip detection of a diabetes biomarker at PoC device that is versatile, cost effective, rapid, portable and easy for use at the PoC will be developed. This research will focus on developing a LF test strip based on diabetes-biomarker- specific aptamers.

The specific objectives of this research are as follows:

a) Characterize aptamers specific for T2DM biomarkers.
b) Identify dual aptamers that bind to T2DM biomarker.
c) Synthesize and characterize AuNPs for detection of T2DM biomarkers.
d) Conjugate and characterize aptamer-AuNPs conjugate.
e) Develop and characterize LF test strips.

CHAPTER 2: MATERIALS AND METHODS

2.1 Materials

Table 2.1: Reagents and their suppliers.

Reagents/materials	Suppliers	Company location
Absorbent pad	Ahlstrom	Helsinki, Finland
40% Acrylamide Bis Solution (37: 5: 1)	BioRad	California. (United States of America) USA
Ammonium Persulfate	Merck (Pty) Ltd	New Jersey, USA
Boric acid	Merck (Pty) Ltd	New Jersey, USA
Calcium chloride ($CaCl_2$)	Promega	Wisconsin, USA
Carboxymethylated dextran surface (CM5) sensor chip	GE Healthcare	Illinois, USA
Certified low range ultra-agarose	BioRad	California, USA
DNA loading dye	Thermo Fischer scientific	Massachusetts, USA
Disposable folded capillary cell	Malvern	Worcestershire, UK
Disposal polystyrene cuvette (10 mm)	Malvern	Worcestershire, UK
EDTA	Merck (Pty) Ltd	New Jersey, USA
Empigen detergent	Sigma-Aldrich Co.	Missouri, USA
Ethanolamine hydrochloride	Sigma-Aldrich Co.	Missouri, USA
1-Ethyl-3-(3-dimethylaminopropyl) - carbodiimide (EDC)	Sigma-Aldrich Co.	Missouri, USA
GelRed	Biotium Inc.	Barcelona, Spain
Gold (III) chloride trihydrate ($HAuCl_4$)	Sigma-Aldrich	Missouri, USA
Gold sensor chips	GE Healthcare	Illinois, USA
Greiner 96 well plates	Lasec	Cape Town, SA

HF180 nitrocellulose	Millipore	Germany
Immunoglobulin G (IgG)	Sino Biologicals	Beijing, China
Magnesium Chloride ($MgCl_2$)	Promega	Wisconsin, USA
Maleimide activated plate	Thermo Fischer scientific	Massachusetts, USA
N-hydroxysuccinimide (NHS)	Sigma-Aldrich Co.	Missouri, USA
O'GeneRuler® 100bp Plus DNA ladder	Thermo Fischer scientific	Massachusetts, USA
Phosphate buffered saline (PBS)	Sigma-Aldrich Co.	Missouri, USA
Polystyrene 96-well microtiter plate	Th. Geyer GmbH & Co. KG	Renningen Germany
Potassium Chloride (KCl)	Merck (Pty) Ltd	New Jersey, USA
Potassium dihydrogen phosphate (KH_2PO_4)	Sigma-Aldrich Co.	Missouri, USA
Qubit high-sensitivity assay	Invitrogen	California, USA
Recombinant Human RBP4 (His-tag)	Sino Biologicals	Waltham, Massachusetts, USA
Recombinant Human RBP4	AdipoGen Life Sciences	San Diego, USA
Retinol binding aptamer (RBA) 1-2	Integrated DNA Technologies	Iowa, USA
RBA-2/15' mer poly-T spacer	Biomers.net GmbH	Ulm, Germany
Sodium Hydroxide (NaOH)	Sigma-Aldrich Co.	Missouri, USA
Sodium Chloride (NaCl)	Merck (Pty) Ltd	New Jersey, USA
SA poly-horseradish peroxidase (SA-poly HRP)	Thermo Fischer Scientific	Massachusetts, USA
N,N,N',N'-tetramethylethane-1,2-diamine (TEMED)	Sigma-Aldrich Co.	Missouri, USA
3,3',5,5'-tetramethylbenzidine (TMB)	Sigma-Aldrich Co.	Missouri, USA
Tris-base	Sigma-Aldrich Co.	Missouri, USA
Tris(2-carboxyethyl)phosphine (TCEP)	Sigma-Aldrich Co.	Missouri, USA

Tris(hydroxymethyl)aminomethane	Merck (Pty) Ltd	New Jersey, USA
Tween-20	Sigma-Aldrich Co.	Missouri, USA

Table 2.2: Equipment's and their suppliers.

Equipment	Suppliers	Company location
Biacore 3000 Surface Plasmon Resonance (SPR)	GE Health	Illinois, USA
Cary 100 Bio UV-visible spectrophotometer	Agilent technologies	California, USA
Centrifuge 5417 R	Eppendorf	Hamburg, Germany
Eppendorf Thermomixer comfort	Eppendorf	Hamburg, Germany
Field Emission TEM (Tecnai F20)	FEI Company	Oregon, USA
POLARstar Omega Plate reader	BMG Labtech	Ortenberg, Germany
Qubit® 2.0 Fluorometer	Invitrogen	California, USA
SpectraMax 340PC384	BioNova Scientific S.L	California, USA
UVP Trans-illuminator	Analytik Jena AG	Jena, Germany
Malvern Zetasizer Nano-ZS90	Malvern	Worcestershire, UK

2.2 Methodology

2.2.1 *In silico* identification and selection of aptamers

Aptamers against RPB4 protein were selected by Su Jin Lee in Man Bock Gu's lab, using the Flu-Mag SELEX protocol (Lee *el al.*, 2008). Out of 7 aptamer sequences which were reported, 4 aptamer sequences (RBA-1 – RBA-4) were chosen for further characterization in the current study. The aptamer sequences are highlighted in **Table 2.3**. These sequences were then sent to IDT for synthesis and two types of modifications (thiol on RBA-1 and biotin on RBA-1, RBA-2 and RBA-3) were introduced at the 5' end. RBA-2/15 mer' poly-T sequence was sent to Biomers.net GmbH for synthesis and two modifications (biotin and thiol) were introduced at 5' end, yielding two vials.

Table 2.3: ssDNA aptamer sequences.

Aptamer ID	Aptamer sequence	Modification
RBA-1	ATACCAGCTTATTCAATTACGGTGCGGAGGGGGAGGGTGGCGGGTTG TGTCGGTGTGGAGATAGTAAGTGCAATCT	5' biotin
RBA-2	ATACCAGCTTATTCAATTACAGTAGTGAGGGGTCCGTCGTGGGGTAGT TGGGTCGTGGAGATAGTAAGTGCAATCT	5'Thiol Modifier C6 S-S
RBA-2/15' mer poly-T	TTTTTTTTTTTTTTTATACCAGCTTATTCAATTACAGTAGTGAGGGGTC CGTCGTGGGGTAGTTGGGTCGTGGAGATAGTAAGTGCAATCT	5' biotin
RBA-2/15' mer poly-T	TTTTTTTTTTTTTTTATACCAGCTTATTCAATTACAGTAGTGAGGGGTC CGTCGTGGGGTAGTTGGGTCGTGGAGATAGTAAGTGCAATCT	5'Thiol Modifier C6 S-S
RBA-3	ATACCAGCTTATTCAATTACGGTGTGGGCAGTCCAGTTCCAATGTTGG GGTCGTGGGGAGATAGTAAGTGCAATCT	5' biotin
RBA-4	ATACCAGCTTATTCAATTGGCGACGGACCTGTGATGTGTGTATGGCTC ATAGGGGTGTAGATAGTAAGTGCAATCT	5' biotin

2.2.2 Characterization of RBA's

2.2.2.1 Secondary structure prediction of the selected aptamers

M-fold web server was used to analyse and predict the secondary structure of the full-length enriched RBA aptamers. Free-energy minimization was used to predict the secondary structures of the aptamers. The ionic conditions in the server were set as follows: 138 mM $NaCl_2$, 1.2 mM $MgCl_2$, and a fixed temperature of 25 ^oC. Quadruplex- forming G-Rich Sequence (QGRS) mapper was used to predict the possibility of the sequences to fold into a quadruplex structure. The default parameters were set with a maximum QGRS length of 30 nucleotides (nts), minimum G-group of 2 and loop size between 0-36 nt.

2.2.2.2 Binding assay and determination of the dissociation constant

a) SPR analysis

To investigate the binding interaction of the aptamers to RBP4 protein, four candidate aptamers were resuspended in Nuclease-free H_2O to make final concentrations of 100 µM. The SPR experiments were performed as follows:

SPR experiments were performed by Dr. Marketa Svobodová (Department of Chemical Engineering, Universitat Rovira i Virgili) using the BIAcore 3000 at the Centre for Omic Science (Reus, Spain). After insertion of the CM5 sensor chips, the sensor chips were primed using 1× SELEX buffer (100 mM NaCl, 20 mM Tris-HCl, 2 mM $MgCl_2$, 5 mM KCl, 1 mM $CaCl_2$, 0.02% Tween-20, pH 7.6). This was followed by activating channel one on the sensor chip, using EDC/NHS buffer (35 µL of a 4:1 mixture of EDC (400 mM) and NHS (100 mM), at a flow rate of 5 µL/min. The human RBP4 recombinant protein was prepared in NaAc (10 mM), at a final concentration of 200 µg/mL, and 50 µL was injected into channel two, at a flow rate of 5 µL/min. IgG (control) was prepared and injected in a similar manner, into channel three. Following immobilization of the proteins, any unreacted NHS esters were deactivated by injecting 35 µL of ethanolamine hydrochloride (1 M, pH 8). To remove the unbound proteins, the sensor chip surface was then regenerated three times, by injecting 35 µL of NaCl/NaOH buffer (2 M/50 mM) at a flow rate of 5 µL/min. The sensor chip was then regenerated, three times, as previously described; and the baseline was allowed to stabilise by allowing the selection buffer to flow over the sensor chip for approximately 1-2 hrs. The RBA aptamer candidates were prepared as follows: RBA-1 (10 µM - 41 nM), RBA-2, RBA-3

and RBA-4 (1 µM - 15 µM), in a final volume of 100 µL of 1× SELEX buffer. Immediately thereafter, the RBA aptamers were injected, sequentially, at their respective concentrations into all the channels of the sensor chip, at a flow rate of 5 µL/min. The sensor chip was then regenerated, three times. The baseline was allowed to stabilise by allowing the selection buffer to flow over the sensor chip for approximately 1-2 hrs. SPR data analysis was performed using BIAevaluation software.

b) Electrophoresis mobility shift assay analysis

Binding of the RBA aptamers (RBA-1 and RBA-2) to RBP4 was further analysed through a native gel electrophoresis mobility shift assay (EMSA). The two aptamers were prepared in 1× SELEX buffer and conditioned for binding by heating at 95 °C followed by 10 min incubation at 25 °C and the samples were left to cool for 15 min at 4 °C. Each folded RBA aptamer (1 µM) was incubated with 100 µg/mL of RBP4 protein in a total volume of 30 µL, at 25 °C for 30 min. After incubation, 10 µL of the samples were loaded onto a 10% non-denaturing polyacrylamide gel (composition of the gel is shown in **Table 2.4**). The gel was electrophesed in 1× Tris-Borate-EDTA (TBE) buffer (89 mM Tris, 89 mM Boric acid and 2 mM EDTA) at 105 V for 1 h. The gels were stained with 3 µL of GelRed stain in 15 mL of 1× TBE buffer and incubated for 15 min. The gel images were visualized and captured using the UVP Trans-illuminator. The experiment was repeated following the above protocol with slight modification: 500 nM of the RBA aptamers were incubated with increasing concentrations of RBP4 (12.5 - 500 µg/mL) in a total volume 20 µL, at 25 °C for 30 min.

Table 2.4: Composition of 10% non-denaturing polyacrylamide gel.

Reagents	Volume (mL)
40% Acrylamide Bis Solution (37: 5: 1)	2.25
5× TBE buffer	1.8
Milli Q H_2O	4.851
10% Ammonium Persulfate	0.09
TEMED	0.009

c) Enzyme Linked Aptamer Assay (ELAA) analysis

To validate the results obtained from SPR and EMSA analysis, direct-ELAA was conducted by first immobilizing 50 µL/well of 20 µg/mL RBP4 protein in 50 mM carbonate-bicarbonate buffer (pH 9.0) in a polystyrene 96-well microtiter plate. The plate was then incubated for 30 min at 25 ^{o}C. The buffer containing the unbound RBP4 protein was decanted and the plate was washed three times with 200 µL of washing buffer (1× PBS containing 0.05% Tween 20 pH 7.4). The wells were blocked with 200 µL of 5% skim milk powder in PBS-tween 20 pH 7.4 for 30 min at 25 °C, followed by three more washes with 200 µL of washing buffer. A total of 50 µL of 100 nM biotinylated RBA-1 in 1× SELEX buffer was added to each well and the plate was incubated at 25 ^{o}C for 30 min. The buffer containing the unbound aptamer was decanted and the wells were washed three times with 200 µL of washing buffer. To each well 50 µL of 0.5:10000 dilutions of SA-poly HRP (1 mg/mL stock) was added, followed by an incubation at 25 °C for 30 min. The wells were then washed five times with 200 µL of washing buffer. Thereafter, 50 µL of TMB substrate solution was added to each well and incubated for 15 min at 25 °C, in the dark. The reaction was stopped by the addition of 50 µL/well of 0.5 M H_2SO_4 and the optical density was measured at 450 nm using the SpectraMax 340PC384. The above experiment was followed for the biotinylated RBA-2/15 mer' poly-T.

2.2.2.3 Identification of dual aptamers for RBP4

a) Characterization of dual aptamers for RBP4 by SPR

The duality of these aptamers were evaluated using a sandwich based SPR. The same equipment as described in **Section 2.2.1.3** was used. After insertion of the Au sensor chips, the sensor chips were primed using KH_2PO_4 (1 M, pH 3.8). This was followed by activating channel one on the sensor chip, using EDC/NHS buffer (35 µL of a 4:1 mixture of EDC (400 mM) and NHS (100 mM), at a flow rate of 5 µL/min. The thiolated RBA-2 aptamer, at a final concentration of 10 µM, was prepared in KH_2PO_4 (1 M, pH 3.8) and 50 µL was injected into channel two, at a flow rate of 5 µL/min. Following immobilization of the thiolated RBA-2, any excessive groups were deactivated by injecting 20 µL 10 mM of 6-mercapto-1-hexanol. To remove the unbound proteins, the sensor chip surface was then regenerated three times, by injecting 35 µL of NaCl/NaOH buffer (2 M/50 mM) at a flow rate of 5 µL/min. RBP4 protein was diluted in 1× SELEX buffer to a final concentration of 100 nM and injected for 6 min at

a flow rate of 10 µL/min. The baseline was allowed to stabilise by allowing the selection buffer to flow over the sensor chip for approximately 1-2 hrs. Subsequently, 50 µL of each aptamer (RBA-2, RBA-3 and RBA-3) at increasing concentrations (31.25 - 1000 nM), prepared in 1× SELEX buffer, were injected for 6 min at a flow rate of 5 µL/min. Thereafter, 200 µg/mL of streptavidin was injected for 6 min at a flow rate of 5 µL/min. The sensor chip was then regenerated, three times, as previously described; and the baseline was allowed to stabilise by allowing the selection buffer to flow over the sensor chip for approximately 1-2 hrs. SPR data analysis was performed using BIAevaluation software.

b) Characterization of dual aptamers for RBP4 by ELAA

To validate the results obtained from the sandwich-SPR analysis, an ELAA was conducted by washing the melaimide activated plate with 200 µL/well of washing buffer (1× PBS containing 0.05% Tween 20 pH 7.4). The wells were coated with 50 µL of 20 nM of thiolated aptamer in 1× PBS buffer and incubated at 25 ^{o}C, overnight. The buffer containing the unbound RBP4 was decanted and the plate was washed three times with 200 µL of washing buffer (1× PBS containing 0.05% Tween 20 pH 7.4). The wells were blocked with 200 µL of 5% skim milk powder in PBS-tween 20 (pH 7.4) for 30 min at 25 °C, followed by three more washes with 200 µL of washing buffer. A total of 50 µL of 100 µg/mL RBP4, made in 1× SELEX buffer, was added to each well and incubated at 25 °C for 30 min, followed by washing the wells three times with 200 µL of washing buffer. Then, 50 µL of different concentration (1 - 100 nM) of the 5'-biotinylated RBA (RBA-1, RBA-2 and RBA-3) in 1× SELEX buffer were added to the wells, and followed by incubation at 25 °C for 30 min. The buffer containing the unbound aptamer was decanted and the wells were washed three times with 200 µL of washing buffer. To each well, 50 µL of 0.5:10000 dilutions of SA-poly HRP (1 mg/mL stock) was added, followed by an incubation at 25 °C for 30 min. The wells were then washed five times with 200 µL of washing buffer. Thereafter, 50 µL of TMB substrate solution was added to each well and incubated for 15 min at 25 °C in the dark. The reaction was stopped by the addition of 50 µL/well of 0.5 M H_2SO_4 and the optical density was measured at 450 nm using the SpectraMax 340PC384.

2.2.3 Synthesis and characterization of AuNPs

AuNPs were prepared by citrate reduction of $HAuCl_4$ according to the previously reported protocol (Sibuyi *et al*., 2017). After the synthesis, characterizations were done with respect to the optical properties using the following techniques:

2.2.3.1 UV-vis spectrophotometric analysis

To measure the absorbance spectra, 100 µL of the AuNP sample was added in a flat bottom Greiner 96 well plate and the absorbance's were measured using a POLARstar Omega microplate reader set to a wavelength (λ) range of 400 to 700 nm. The data was analyzed using Microsoft Excel.

2.2.3.2 Hydrodynamic size, Polydispersity Index and Zeta Potential measurements

The hydrodynamic size, polydispersity index (PDI) and zeta potential (ζ-potential) of the AuNPs were analyzed using a Malvern Zetasizer Nano-ZS90. To determine the hydrodynamic size and PDI, 1 mL of the AuNPs was placed into 10 mm o.d. square polystyrene cuvette and the content was analyzed at 25 °C using dynamic light scattering (DLS). For ζ-potential measurements, 0.7 mL of the AuNPs was transferred into a disposable folded capillary cell and then analyzed at a voltage of 4 mV at 25 °C.

2.2.3.3 Transmission Electron Microscopy and Energy dispersive x-ray analysis

The AuNPs were centrifuged at 14000 rpm at 25 °C for 30 min, resuspended into 1 mL of deionized H_2O (dH_2O) and sent for Transmission Electron Microscopy (TEM) analysis (Department of Physics, University of the Western Cape). The sample solution was prepared by drop-coating one drop of the sample solution onto a carbon coated copper/nickel grid. The sample solution was then dried under a xenon lamp for 10 min and analyzed by the High-Resolution TEM. Transmission electron micrographs were collected using an FEI Tecnai G2 20 field-emission gun (FEG) TEM, operated in bright field mode at an accelerating voltage of 200 kV. Energy dispersive x-ray spectrum (EDX) was collected using an EDAX liquid nitrogen-cooled lithium doped silicon detector. The core diameter of the AuNPs was calculated by measuring the circumference of individual particles in the TEM micrographs using Image J software.

2.2.4 Functionalization of ssDNA aptamer probe to AuNPs

2.2.4.1 Conjugation and characterization of the apt-AuNPs

For conjugation, 5 µL of thiolated RBA-2 aptamer at different concentrations (25, 50, 75 and 85 µM) was stabilized with 1 µL of 10 mM TCEP, and incubated for 1 hr at 25 ^{o}C, shaking at 650 rpm. Following incubation, 0.5 mL of prepared AuNPs was added to the thiolated RBA-2, in each tube and the mixture was left to incubate for 16 hrs at 25 ^{o}C, shaking at 650 rpm. Subsequently, the mixture was aged (by adding 10 µL for every 20 min) with 50 µL of 1 M NaCl and 5 µL of 500 mM Tris-acetate buffer (pH 8.2). The mixture was further incubated for 24 hrs under the same conditions. Thereafter, the apt-AuNPs conjugates were characterized by measuring the absorbance spectra, size, PDI and ζ-potential as previously described in **Section 2.2.3.1** and **2.2.3.2**. The apt-AuNPs colour change was detected by visual observation. The unconjugated aptamers were removed by centrifuging the sample mixture at 10 000 rpm for 20 min at 4 ^{o}C and resuspending the pellet in 250 µL of dH_2O (three times). The apt-AuNPs conjugates were concentrated by centrifuging using the above conditions and resuspended in 30 µL of dH_2O. The apt-AuNPs conjugates were then characterized by the UV-vis spectrophotometer (as previously described in **Section 2.2.3.1**) and the concentration of the unconjugated aptamers for each sample was quantified using Qubit assay according to the manufacturer's protocol (Invitrogen, 2010).

2.2.4.2 Conjugation and characterization of the apt-AuNPs (Large scale)

For conjugation, 10 µL of 5'-thiolated RBA-2 aptamer (50 µM) was stabilized with 2 µL of 10 mM TCEP, and incubated for 1 hr at 25 ^{o}C, shaking at 650 rpm. Following incubation, 1 mL of prepared AuNPs was added to the thiolated RBA-2 and the mixture was left to incubate for 16 hrs at 25 ^{o}C, shaking at 650 rpm. Subsequently, the mixture was aged (by adding 10 µL for every 20 min) with 100 µL of 1 M NaCl and 10 µL of 500 mM Tris-acetate buffer (pH 8.2). The mixture was further incubated for 24 hrs under the same conditions. The unconjugated aptamers were removed by centrifuging the sample mixture at 10 000 rpm for 20 min at 4 ^{o}C and resuspending the pellet in 250 µL of dH_2O (three times). The apt-AuNPs conjugates were concentrated by centrifuging using the above conditions and resuspended in 30 µL of dH_2O. The experiment was done eight times and the 30 µL of the apt-AuNPs from each tube were combined to make a final volume of 240 µL. Thereafter, the apt-AuNPs conjugate was evaluated and characterised by the Cary 100 Bio UV-vis spectrophotometer

(scan from 200 nm to 800 nm) and by gel electrophoresis. The gel was performed using ultra low pure agarose gel (1%) in 1× TBE buffer and ran for 20 min at 120 V. The gel was stained with 3 µL of GelRed and the UVP Trans-illuminator and a camera phone were used to take images for analysis. The experiment was repeated using biotinylated RBA-2/15 mer' poly-T.

2.2.5 Preparation and evaluation of the LF test strips

To prepare the lateral flow test strips, HF180 nitrocellulose membrane, and the absorbent pad (composed of cotton litter fibers grade 320) were used. The test line was prepared by drawing a line with a yellow micropipette tip containing 12 µL of a pre-incubated (15 min at 25 ºC) mixture of 1.7 mg/mL of streptavidin and 100 µM of the biotinylated RBA-1 in 1× PBS buffer. The control line was prepared by drawing a line with a yellow micropipette tip containing 12 µL of RBP4 (0.5 mg/mL) in 1× PBS buffer. Subsequently, the membrane was allowed to dry at 25 ºC for 1 hr, followed by blocking with 1% w/v skimmed milk powder and 0.1% v/v empigen detergent in PBS-Tween20 (pH 7.4) for 15 min. The membrane was left to dry overnight, at 25 ºC. The test strips were then cut into strips of 4 mm wide. Then, 5 µL of the RBA-2-AuNPs prepared in **Section 2.2.4.2**, was mixed with 10 µL of 1× SELEX buffer. The mixture was incubated for 10 min at 25 ºC before being wicked onto the test strip. A Smartphone camera was used to take an image of the test strip. The experiment was repeated following the above protocol with slight modification: A) 2 mg/mL of the RBP4 protein was immobilized on the control line; B) the biotinylated poly-A aptamer was immobilized on the control line and 2 mg/ml of the RBP4 was immobilized on the test line. The thiolated RBA-2/15' mer poly-T was used for this experiment.

2.2.6 Development of a colorimetric aptasensor

2.2.6.1 Optimization of the aptamer and NaCl concentration

For aptamer and NaCl concentration optimization, a total of 200 µL of different concentrations of the biotinylated RBA-2/15' mer poly-T was added to 360 µL of AuNPs in different 1.5 mL tubes (final aptamer concentration: 0, 25, 50, 75 and 100 nM). The tubes were vortexed, followed by incubation at 25 ºC for 30 min. A total of 75 µL of the apt-AuNPs was added to a 96-well microtiter plate, followed by the addition of different concentrations (0, 20, 40, 60, 80 and 100 mM) of NaCl. The samples were incubated at 25 ºC for 5 min. The UV-vis spectra were measured using the SpectraMax 340PC384 and the absorption ratio A620/520 was calculated to determine the aggregation kinetics.

2.2.6.2 RBP4 detection based on colorimetric technique

For this experiment, 450 µL of AuNPs and 225 µL of 100 nM biotinylated RBA-2 /15' mer poly-T solution were added into a 1.5 mL tube, mixed and incubated at 25 ºC for 30 min. Subsequently, 75 µL of the apt-AuNPs was added into 1.5 mL tubes. Then, 25 µL of different concentrations of RBP4 protein (0, 7, 15, 31, 62, 125, 250 nM) were added into the apt-AuNPs conjugate, mixed thoroughly, and incubated for another 15 min under the same conditions. The apt-AuNPs-RBP4 was transferred into their respective wells on a 96 well microtiter plate and 5 µL of 1 M NaCl solution was added to the wells. The absorbance of the above solutions at 520 nm and 600 nm were recorded using a SpectraMax 340PC384. The experiment was performed in duplicate and the average absorbance was calculated and used for the standard curve.

CHAPTER 3: RESULTS AND DISCUSSION

3.1 Secondary structure predictions of the selected aptamers

The aptamer secondary structure prediction plays a vital role in binding to the target because different folds allow the aptamer to exploit various binding mechanisms. Aptamers assume their structures upon binding to their target through a "lock and key" mechanism whereby they organise themselves to fit to the target. This allows aptamers to bind to their target with a greater specificity and affinity (Gold *et al*., 1995, Eaton *et al*., 1995). For this reason, it is absolutely necessary to evaluate the secondary structures of the aptamers in order to have a better understanding of their versatility. This analysis was carried out using M-Fold mapper.

The M-fold program predicted multiple secondary structured for RBA-1 (**Appendix A**); whereas, RBA-2, RBA-3 and RBA-4 had only one structure (**Figure 3.1** and **3.2**). However, only one predicted structure of RBA-1 will be reported in this study as it is assumed to be the most stable structure due to having the lowest minimum free energy. The predicted structures of all aptamers contained random region sequences and both the forward and reverse primers. The primer sequences are highlighted in colours whereby the green colour represent the forward and the blue colour represent the reverse primer. Looking closely at the predicted structures, it was apparent that both primers were involved in the formation of part of the stem-loop structures on RBA-1, RBA-3 and RBA-4, whereas, only the reverse primer was involved in the formation of part of a stem loop on RBA-2. Interestingly, RBA-1 showed to have a bulge composed of -CAG- at base 5-7 which is not observed on other aptamer structures (**Figure 3.1**). Furthermore, a stem-loop composed of -TAGTAAGTGCAA- was present at base 62-73 for all four predicted structures, which is a component of the reverse primer (highlighted by the red boxes). Although the primer regions are involved in the formation of the secondary structure, they are not expected to have recognition sites. However, these stem-loops may play an ancillary role in the binding of these aptamers to the target protein.

The results in the present study indicated that RBA-1 and RBA-3 shared a conserved motif of -GTTG- at base 44-47; whereas, RBA-1 and RBA-2 shared a motif of -AGGGG- at base 26-32. This provided a possibility of these aptamers binding to RBP4 with a higher affinity. Qin *et al*. (2013) previously reported that conserved motifs which are often located in stem-loop structures are most likely to be responsible for aptamer binding to the target.

The results further revealed that RBA-3 had the lowest minimum free energy (ΔG = -5.48 kJ mol^{-1}). Therefore, this aptamer may be highly stable and may have a high binding affinity as compared to other aptamers. RBA-1 and RBA-4 had relatively similar structures; however, RBA-4 (ΔG = -4.35 kJ mol^{-1}) had the second lowest minimum free energy while RBA-1 (ΔG = -2.37 kJ mol^{-1}) had the highest minimum free energy. The minimum free energy of RBA-1 was comparable with that of RBA-2 (ΔG = -2.84 kJ mol-1). despite having slightly different structures. Li *et al*. (2015) have isolated four ssDNA aptamers (Q2, Q3, Q4 and Q5) of which the M-fold results revealed that all aptamers contained stem-loop structures, with Q4 exhibiting the lowest minimum energy value of -25.14 kJ mol^{-1}.

Even though we have assumed that RBA-3 will bind to the RBP4 with a higher affinity, it was also possible that the non-binding domain may interfere with the interaction between the aptamer and target protein by formation of complex secondary structures, which in turn may inhibit the binding domain to fold into the desired confirmation for binding the target. In order, to validate the binding affinity and specificity of these aptamers, kinetic studies were used.

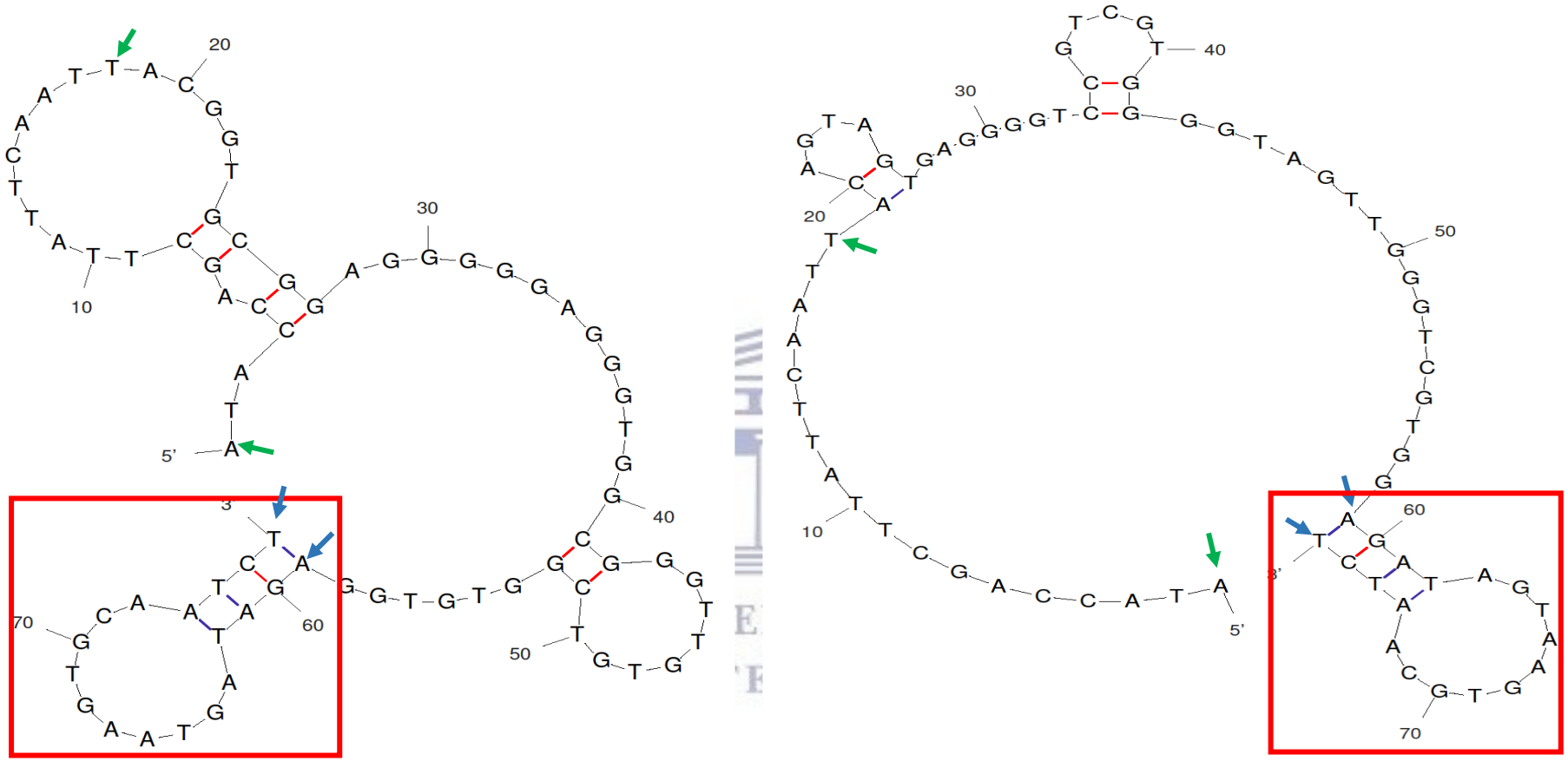

Figure 3.1: Secondary structure prediction of RBA-1 (ΔG= -2.37 kJ mol^{-1}) and RBA-2 (ΔG= -2.84 kJ mol^{-1}) as predicted by the M-fold program. The ΔG represents the minimum free energy of each aptamer. The forward primer sequence (base 1-18) is shown by the green colour and the reverse primer (base 59-76) are shown by the blue colour. Common stem loops within each aptamer are depicted using red boxes.

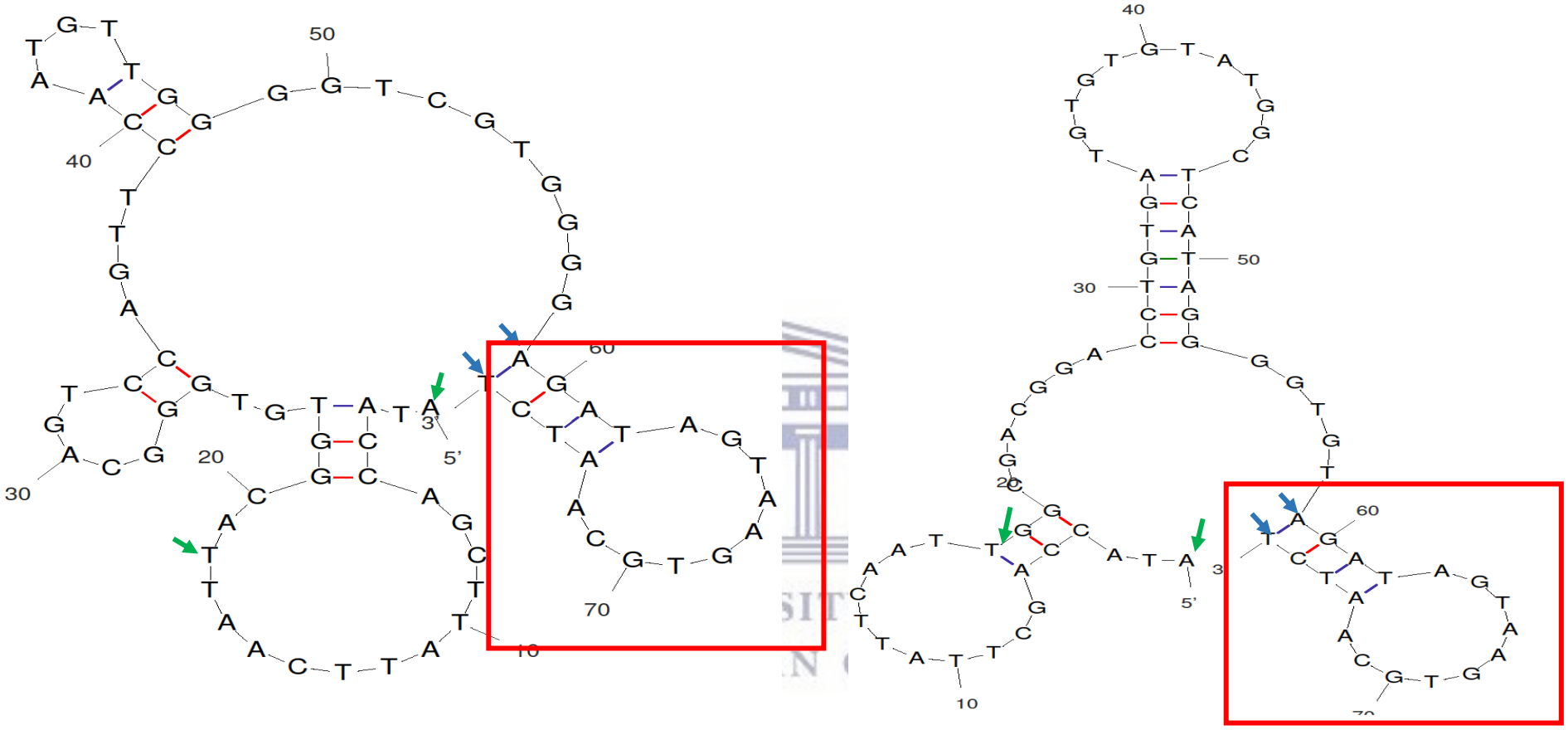

RBA-3 **RBA-4**

Figure 3.2: Secondary structure prediction of RBA-3 (ΔG= -5.48 kJ mol^{-1}) and RBA-4 (ΔG= -4.35 kJ mol^{-1}) as predicted by the M-fold. The ΔG represents the minimum free energy of each aptamer. The forward primer sequence (base 1-18) is shown by the green colour and the reverse primer (base 59-76) are shown by the blue colour. Common stem loops within each aptamer are depicted using red boxes.

An alternative way of predicting secondary structure is by analyzing the G-quadruplex of the aptamers. G-quadruplexes are usually formed in the presence of a guanine-rich nucleotide sequence in a square planar array. Each G-quadruplex is then assigned a G-score which can be defined as the probability of the aptamer and the number of guanines present to form Quadruplex forming G-Rich Sequences (QGRS) (Viglasky and Hianik, 2013). For the present study, the predictions of the G-quadruplex secondary structures were made computationally using a QGRS Mapper.

The results obtained in this analysis demonstrated that RBA-1, RBA-2 and RBA-3 were able to form G-quadruplexes with G-scores of 21, 18 and 3, respectively (**Table 3.1**). On the other hand, RBA-4 was not able to form the G-quadruplex structures; however, this was acceptable because not all aptamers are able to form/contain such structures. The number of bases responsible for forming G-quadruplex structure for RBA-1 was 14 nucleotide's (nts), starting at position 31 on the sequence of 76 nts full length aptamer sequence. RBA-2 had 28 nts also starting at position 31; whereas, RBA-3 had 30 nts starting at position 21 of the full length aptamer sequence. Furthermore, RBA-1 and RBA-2 had the highest G-Scores of 21 and 18, respectively. This indicates that both aptamers had a higher number of guanines which are responsible for forming QGRS secondary structures. In addition, these aptamers were also stable. This is because the importance of G-quadruplexes lies in the stability of their 3D aptamer structure and in the improvement of electrostatic interactions to the positively charged binding sites on the ligands. This is mostly attributed to the fact that the negative charge density of G-quadruplexes is twice as high as that of linear DNA (Gatto *et al*., 2009). Using the same software, an independent study by Espiritu *et al*. (2018) identified three aptamers (AP65A1, AP65A3 and AP65A6) that had a G-score of more than 20, indicating a high probability of forming G-quadruplexes.

Table 3.1: G-quadruplex structure of the aptamer.

Aptamer ID	Position	Length	QGRS	G-Score
RBA-1	31	14	GGGAGGGTGGCGGG	21
RBA-2	31	28	GGTCCGTCGTGGGGTAGTTGGGTCGTGG	18
RBA-3	21	30	GGTGTGGGCAGTCCAGTTCCAATGTTGGGG	3
RBA-4	0	0	N/A	0

3.2 Evaluation of the binding affinity of the selected aptamers

Evaluating the kinetics of these aptamers allow the understanding of how rapidly the aptamers and RBP4 associate and also how soon the aptamer-RBP4 complex dissociates. It is well documented that the tighter the bond of the aptamer ligand, the lower the dissociation constant (K_D) will be. Therefore, an ideal aptamer would have a fast association rate but a slow dissociation rate, resulting in an aptamer-ligand complex maintained for longer, subsequently leading to a lower equilibrium K_D. In regards to the above statement, it is assumed that a low K_D shows higher binding affinity (Stoltenburg *et al*., 2007). And since PoC tests are desired to be fast and accurate, low nM and pM values are preferred ranges which allows binding in seconds to minutes only (Svobodová *et al*., 2012).

3.2.1 Binding of aptamers to RBP4 by SPR

For this study, aptamer interactions were evaluated in real time using the Biacore 3000 SPR instrument. SPR is a phenomenon that happens on the surface of a metal film when the incident light is polarized parallel to the plane of incidence. The electron-plasmon oscillation generates the evanescent electromagnetic field that penetrates the metal film into the sample solution near the film. By fixing the light source and the metal film, the change in the angle of the reflected light is related only to the refractive index of the sample solution near the film (Homola, 2008). The resonance signal is related linearly to the analyte immobilized at a broad concentration range (Zhu *et al*., 2015, Drescher *et al*., 2009).

The target protein (RBP4), was immobilized on the CM5 sensor chip, to allow for subsequent aptamer binding (**Figure 3.3**). Four channels were used in this study, the first channel was activated with EDC/NHS, the second channel was allotted for immobilization of the RBP4 and the third channel was used as control (IgG) and the fourth channel was blocked with EDC/NHS. When the protein was immobilized on the chip, there was interaction between the His-tagged RBP4 via the amino group on the surface of the chip. The association followed a single exponential curvature until it reached equilibrium. When the surface of the chip became saturated, an association constant was observed. IgG was used as the counter protein; thus, it was immobilized in the same manner as above. After immobilization of the two proteins on the surface, the four aptamers were injected in their respective channels on the sensor chip to investigate their binding affinities. The aptamers were injected at different

concentrations, at a constant flow rate. The binding affinities of the aptamers to RBP4 were measured by the changes in the resonance unit.

Figure 3.4 shows that the response units increased with the sampling time and reached the steady value at 700 s. According to the results, RBP4 bound to the aptamer with a fast association rate constant and the relative response return to the baseline at 450 s after sample injection. RBA-1 at 10 µM gave a response unit (RU) of 327, while RBA-2, RBA-3 and RBA-4 at 1 µM had a RU of 153, 147 and 91, respectively. The sensorgrams also indicated that the dissociation curve did not show any decrease; thus, indicating that there was a tighter binding of the aptamers to RBP4.

The K_D of the aptamers was estimated using the Langmuir 1:1 model, with a range of concentrations (10 - 40 nM). This model is the simplest and most widely used in literature (Chang *et al*., 2014; Kaur and Yung; 2012). The obtained sensorgrams showed specific shift at the beginning of association phase in majority of curves which complicated the fitting. This specific shift in the sensorgram may be attributed to the presence of 0.02% Tween which was part of the constituents in the binding buffer. Hence, for the calculation of K_D, different selections for fitting (part of association and dissociation curve) were used and resulted in different K_D values.

Based on the selections used, a good fit to the Langmuir 1:1 model was obtained for RBA-1, RBA-3 and RBA-4, as demonstrated by the Chi^2 (χ^2) values (**Table 3.2)**. The χ^2 is a statistical measure of closeness of fit of experimental data to the theoretical model used to determine the K_D. It describes how well the results agree with the curve-fitting of the model used. The χ^2 values lower than the noise RU (in this case, ~ 20 RU), indicate a good fit. Therefore, for kinetic evaluations, the results were found to be within acceptable ranges of the relevant statistical measures (Gopinath, 2010). However, RBA-2 displayed a kinetic parameter that does not fit the Langmuir 1:1 model used for analysis. This is sometimes experienced as SPR-based kinetic evaluations can be affected by several factors such as the purity of reagents, the immobilization procedure and level, ligand activity, flow rate and analyte concentration range (Gopinath, 2010). However, the encountered problem could not be attributed to the above factors as the aptamers were injected over the same ligand surface using the same immobilization procedure. Therefore, it can be hypothesized that the

conditions in which the binding reactions took place were much suitable for the other three aptamers and may be unfavorable for RBA-2.

The results further demonstrated that all four aptamers had a higher binding affinity for RBP4. RBA-1, RBA-2 and RBA-4 had K_D values within a nM range and RBA-3 showed a K_D value within a pM range; which are the preferred ranges for aptamer-protein interactions (**Table 3.2**). O'Sullivan and her team were able to select an aptamer that bind with a high affinity to *Trichomonas vaginals* Adhesion protein. This aptamer (AP65_A1) had a K_D value of 56 nM and a χ^2 value of 3.21 which indicated a good fit to the Langmuir 1:1 model (Espiritu *et al.*, 2018).

Interestingly, the present study has shown that RBA-2 exhibit a dissociation constant of 3.74 nM which is much lower than that of the reported K_D value of RBA-2 ($K_D = 0.2 \pm 0.03$ µM) by Lee *et al.* (2008). In the present study, RBA-2 showed higher affinity to RBP4 which may be attributed to the modification introduced at the 5' end. It is common to see such differences in the binding affinities of aptamers free in solution and immobilized, as the immobilization process may obstruct the folding of the aptamer into its optimum 3D structure for target binding. This is often resolved by using spacers to extend the aptamer from the surface and facilitate its 3D formation optimum target binding (Espiritu *et al.*, 2018). An independent study investigated how the immobilization orientation of the aptamers affects their functionality in SPR measurements. The study demonstrated that the immobilization of aptamer (PA#2/8) at its 5' end resulted in low binding affinity to the target protein (Protein A). However, a high binding affinity of the aptamer to Protein A was observed with a 3' end immobilized aptamer. This indicated that a free 5' end of the aptamer was necessary for its correct folding as basis for formation of the binding complex with the target (Stoltenburg *et al.*, 2015). In contrast to the study by Stolenburg *et al.* (2015), the present study showed that a 5' end immobilized aptamer resulted in high binding affinity of the aptamer to the target.

Furthermore, to corroborate the statements made above regarding the binding affinities of these aptamers, the intrinsic relationship between the affinities and structures were investigated. Aptamers were compared with regards to their binding affinities and secondary structures. The results revealed that the aptamer (RBA-3) with the highest binding affinity had a complex structure with an extra stem-loop (**Figure 3.1**). This indicated that the closeness of the loops did not affect the binding affinity of this aptamer to the target.

Moreover, this aptamer had the lowest minimum free energy, indicating that it was more stable; hence, it was not surprising that it had a higher binding affinity to RBP4. Interestingly, despite a huge difference of minimum free energies between RBA-4 and other two aptamers (RBA-1 and RBA-2) and also their structures, there was no significant difference in their binding affinities.

IgG was used as a control to conclusively confirm aptamer selectivity to the target protein. The results demonstrated that all the aptamers had a high binding affinity to RBP4 whilst having no interaction with IgG. This suggested that the aptamers used in this study were only specific to RBP4. A previous study used adiponectin, visfatin, bovine serum albumin and human serum albumin proteins as counter targets to evaluate the aptamers' specificity. Their study revealed that RBA-1, RBA-3 and RBA-4 were not specific to RBP4; thus, they were not considered for further characterization (Lee *et al.*, 2008). A second study by the same group also showed that RBA-2 was only specific to RBP4 (Lee *et al.*, 2012); thus, making this aptamer a good candidate for downstream applications due to its specificity.

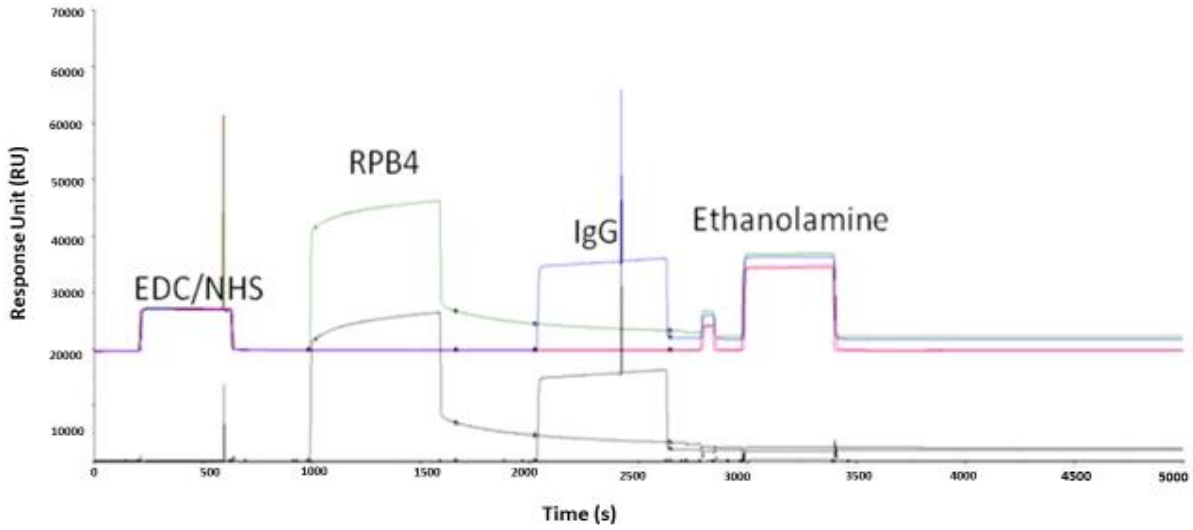

Figure 3.3: Representative sensorgram for the coupling of RBP4 on an SPR sensor chip surface. RBP4 and IgG were immobilized using amine coupling chemistry. Activation of the sensor chip was achieved by injecting the EDC: NHS over the surface of the chip to activate the carboxyl groups of the ligand. Activated carboxyl groups which had no proteins bound were then blocked with ethanolamine. The surface was regenerated and unbound proteins were removed with 2 M NaCl + 50 mM NaOH.

Table 3.2: Affinity dissociation constant of the candidate aptamer by SPR.

Aptamer ID	K_D	Chi^2
RBA-1	3 nM	6.2
RBA-2	3.74 nM	33.9
RBA-3	2.52 pM	1.71
RBA-4	3.65 nM	15.7

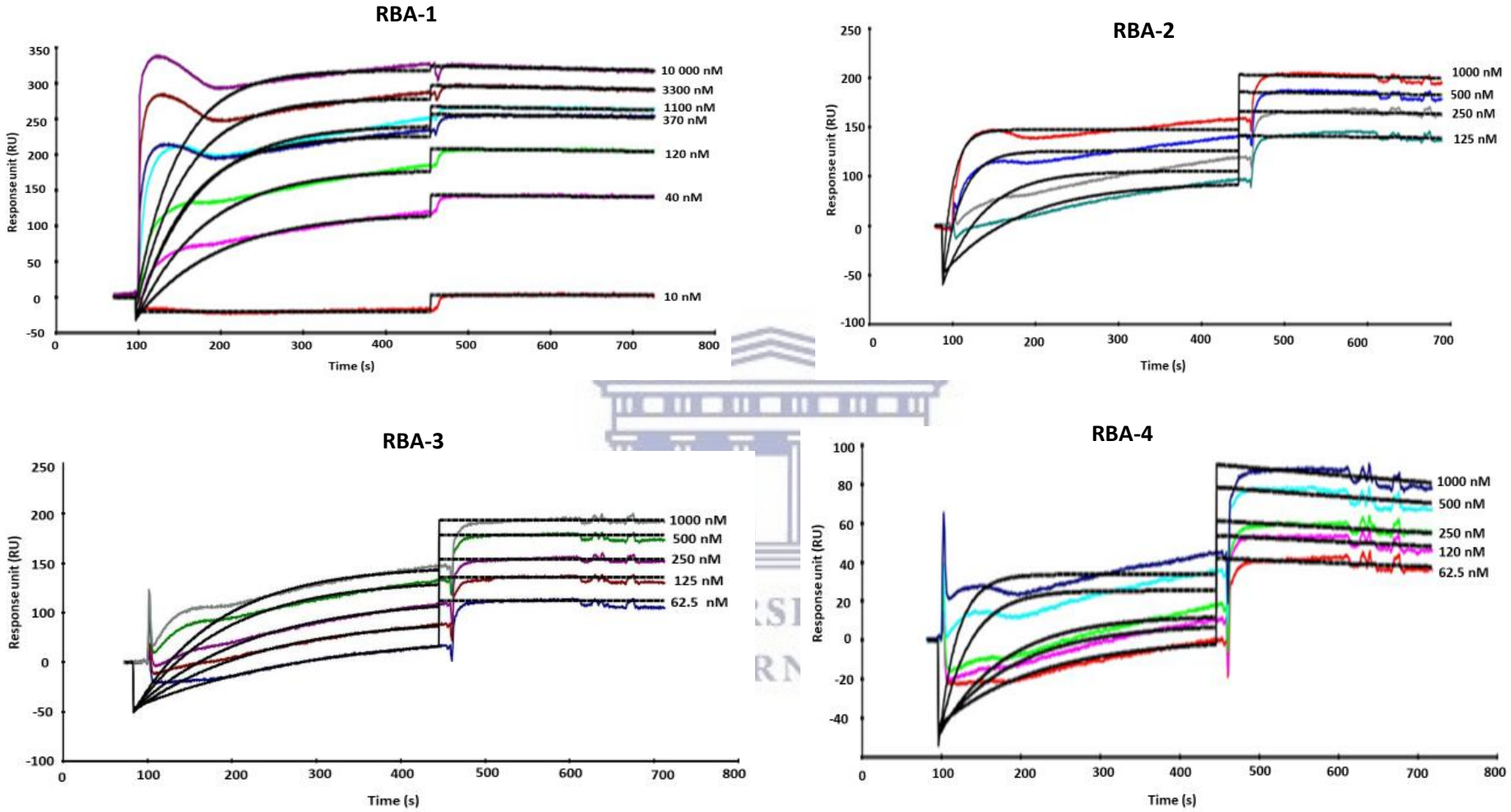

Figure 3.4: Measurement of the interaction of aptamers with RBP4 by SPR. Dissociation constants for the selected aptamers immobilized on a CM5 sensor chip were determined by SPR. Data are presented as real-time graphs of response units against time and were evaluated using BIAevaluation 3.0 software (Biacore).

3.2.2 Binding of aptamers to RBP4 by EMSA

To further confirm the interaction of the protein and the selected aptamers, an electrophoretic mobility shift assay (EMSA) was employed. EMSA is a rapid and a sensitive method for the detection of protein-nucleic acid interactions. It is based on the principle that a nucleic acid bound to the target protein will migrate slower through a gel matrix than the free nucleic acid. This technique is used for qualitative purposes; however, under suitable conditions, it can also be employed to provide quantitative data for the determination of binding stoichiometry, affinities and kinetics (Hellman and Fried, 2007).

For this study, RBA-1 and RBA-2 were selected to validate their interaction with RBP4. The selection of RBA-2 was based on the results published from a previous study which demonstrated RBA-2 was specific to RBP4 (Lee *et al*., 2008); whereas, the selection of was based on the secondary structure prediction analysis. As shown in **Figure 3.5**, there were bands appearing near the 75 bps band, which corresponds to the free aptamer. The migration of the band produced for RBA-1/RBP4 was much slower than the migration of the band produced for the free RBA-1. This suggested that RBA-1 was able to interact/bind with RBP4; thus, validating the results obtained from the SPR analysis. However, the same shift was not observed with RBA-2/RBP4. This could be attributed to rapid dissociation during electrophoresis which prevented detection of complexes or slow dissociation which resulted in underestimation of binding density. It was postulated that the His-tag modification on the target protein might also be preventing the aptamers from binding. In addition, the control (lane 6) had a band at around 200 bps which was also found in the protein/aptamer complex suggesting that the band could have found during the refolding of the aptamer.

Based on the results from the previous experiment, a second experiment was performed with different concentrations of RBP4 incubated with a fixed concentration of the RBA-1. As shown in **Figure 3.6**, there were bands appearing near the 75 bps band which corresponded to the free RBA-1. There were also bands obtained on top of the wells which were associated with the aptamer/protein complex; however, the same effect was observed in lane 1 (RBA-1 only); thus, suggesting that the bands were not due to the slow migration of the protein/aptamer complex. Therefore, the results obtained by EMSA analysis did not provide conclusive evidence of molecular interaction and must be done in combination with other methods.

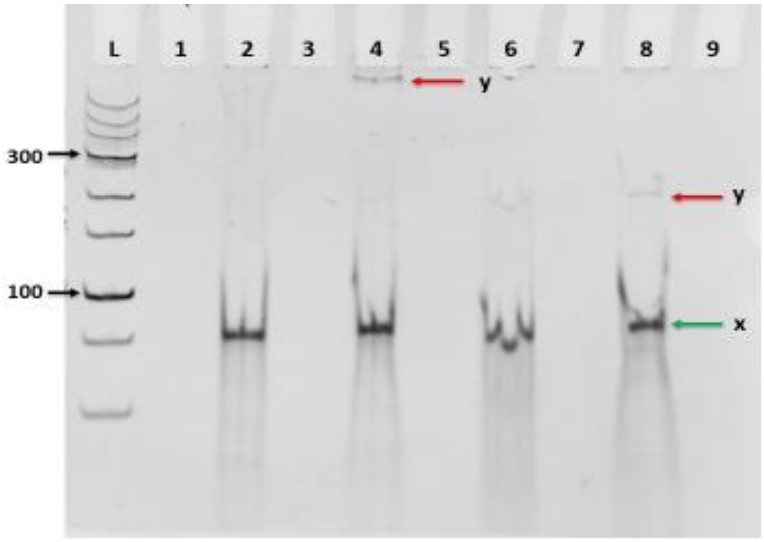

Figure 3.5: Evaluation of RBP4 binding to RBA-1 and RBA-2 aptamers using EMSA. RBP4 was incubated in 100 mg/mL of aptamers for 30 min, the samples were electrophoresed in a native polyacrylamide gel. The red arrow (y) indicate the migration of the aptamer/protein complex, while the green arrow (x) indicate the migration of the free aptamers.

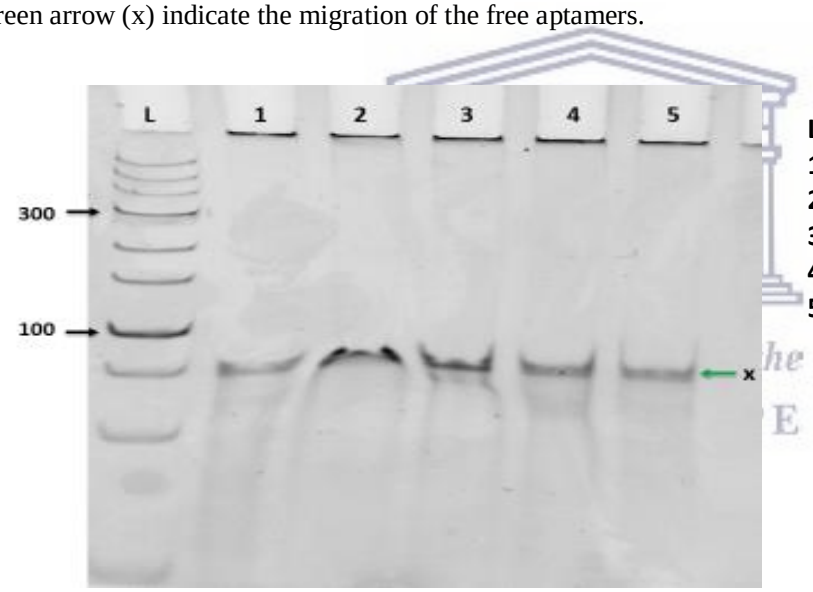

Figure 3.6: Evaluation of RBP4 binding to RBA-1 aptamer using EMSA. RBP4 was incubated in different aptamer concentrations for 30 min, the samples were electrophoresed in a native polyacrylamide gel. The green arrow (x) indicate the migration of the free aptamers.

3.2.3 Binding of aptamers to RBP4 by ELAA

Due to the inconclusive results obtained using EMSA analysis, a direct enzyme linked aptamer assay was established to confirm the interaction between the two aptamers (RBA-1 and RBA-2) with RBP4, respectively. ELAA is a fundamental tool of immunological, medical, and biochemical research. It is based on the principle of target-aptamer interactions in combination with photometric visualisation of the binding results and is typically performed in microtiter plates (Stoltenburg *et al*., 2016). The use of a plate-based ELAA is a generally rapid and a simple way to screen and characterize aptamer binding to protein targets.

Figure 3.7: A shows that when RBA-1 was immobilized, a slight increase in the signal was observed; however, there was also a signal in the control which was attributed to the background signal. The results were inconclusive and indicated that there was no interaction between RBA-1 and RBP4. However, **Figure 3.7: B** shows that when RBA-2/15 mer' poly-T was immobilized, an increased signal was obtained; and a negligible background signal was observed in the control (0 mg/mL). The results demonstrated that the RBA-2/15 mer' poly-T was able to bind to RBP4. The enhanced affinity of this aptamer to the protein may be attributed to the poly-T modification introduced at the 5' end. This is because the use of a spacer decreases steric hindrance resulting in a better folding and target recognition (Zhu *et al*., 2011).

The results obtained by ELAA supported the results obtained by SPR analysis; however, the results demonstrated the use of spacers are required for ELAA. Using the same technique, Stoltenburg *et al.* (2016) evaluated the binding interaction between protein A aptamer and *Staphylococcus aureus*. Their study demonstrated that ELAA allowed a high affinity detection of Protein A by the aptamer as compared to other methods which were previously used for analysis and that the truncated 3′-biotinylated aptamer PA#2/8 showed the best binding features $K_D = 11.3 \pm 1.4$ Nm.

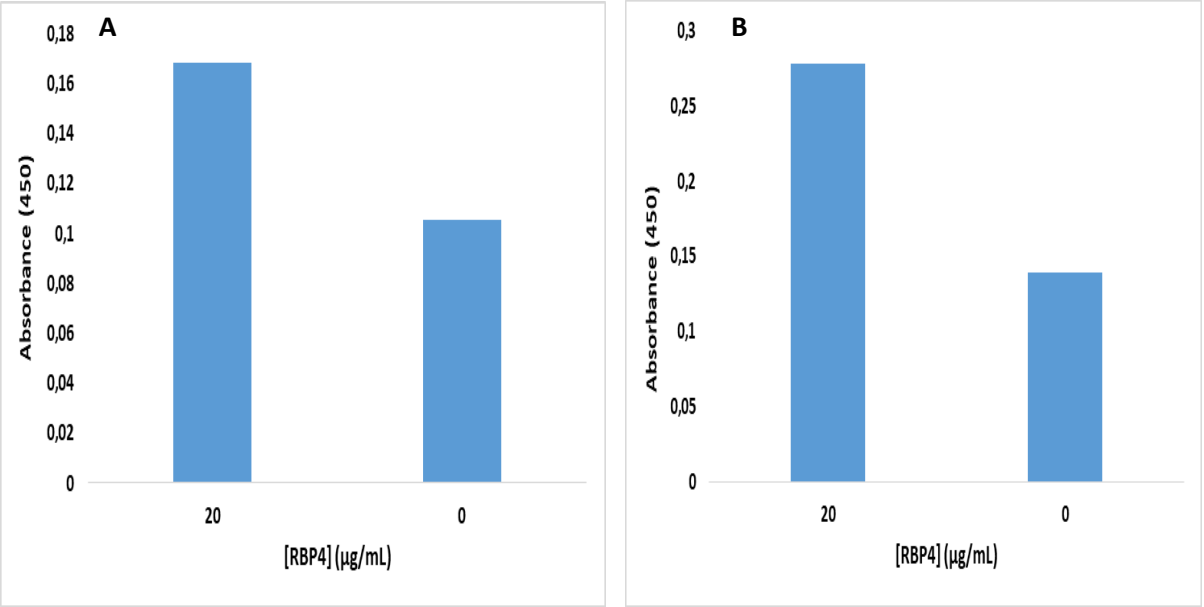

Figure 3.7: Evaluation of target binding of aptamer (RBA-1 and RBA-2) using ELAA. Protein solution of 20 µg/mL was used for coating the microtiter plates. 100 nM of 5′-biotinylated RBA-1 and of 5′-biotinylated RBA-2/15 mer' poly-T were added for binding (A and B), respectively. The blank reaction (0 µg/mL) represents the control without any protein coating.

3.3 Identification of dual aptamers

We further investigated the possibility of having dual aptamers that bind to two different sites of RBP4. The first mention of dual aptamers that bound to distinct sites of human thrombin was reported in 1997 by Tasset and colleagues (Tasset *et al.*, 1997). These thrombin dual aptamers have been used in several analytical techniques and diagnostic applications (Xu *et al.*, 2009). The biggest advantage of having dual aptamers is an easy and broad modification of the capture and reporter aptamers in order to enhance the detection of target in sensing platforms (Raston and Gu, 2015). Herein, two assays (SPR and ELAA) were used to evaluate the possibility of having two aptamers that bind to RBP4 at two different sites.

Due to the high specificity of RBA-2 as previously reported in **Section 3.2**, this aptamer was chosen as the capture aptamer. The SPR analysis showed that RBA-1 bound to RBA2-captured/immobilized RBP4 as indicated by an increase in the sensorgram. In contrast, there were no significant changes observed when RBA-3 and RBA-4 were injected into RBA2-captured/immobilized RBP4 (**Figure 3.8)**. The results indicated that there was an interaction of RBA-2 and RBA-1 with RBP4; thus, suggesting that these dual aptamers bind distinctively to different sites on RBP4 protein. However, the results also indicated that the aptamers-RBP4 complex dissociate rapidly. In contrast, the lack of observed changes with RBA-3 and

RBA-4 suggested that they bind at the same site on RBP4 as RBA-2. However, it is possible that by reversing the immobilization and using RBA-3 and RBA-4, we could have found different interactions. Similarly, Ahmad Raston and Gu (2015), have successfully developed cognate dual aptamers for another diabetes biomarker (vaspin). Jauset Rubio *et al*. (2016) also reported on β-conglutin dual aptamers binding distinct sites. The SPR analysis in their study showed that two aptamers were able to bind to β-conglutin as indicated by an increase in the sensorgram when the full-length (β-CA I and β-CA II) were used.

In order to validate the obtained results, evaluation of the dual aptamer was performed using an ELAA. Once again, RBA-2 was used as a capture probe and was immobilized on the plate. RBP4 was incubated with the aptamers and the unbound was removed by washing. **Figure 3.9** shows that at 100 µg/ml RBP4 concentration, RBA-1 showed a concentration dependent increase in signal. This suggests that with an increasing concentration of RBP4; RBA-1 and RBA-2 bound to RBP4, again validating the results obtained using SPR. In contrast, incubation with RBA-3 and RBA-4 did not increase the signal, further proof that they bind to same site as RBA-2. Using a similar method, dual aptamers that bind to platelet-derived growth factor B-chain homodimer (PDGF-BB) were conjugated to the surface of a green fluorescent ferritin nanoparticle (which functioned as a reporter aptamer) and the bottom of wells respectively for a sandwich ELISA. This aptamer-based ELISA was capable of detecting PDGF-BB at a concentration as low as 100 fM, with higher sensitivity than antibody-based ELISA due to the multivalency effect of aptamer-conjugated nanoparticles (Kim *et al*., 2011). Li *et al*. (2018) also identified dual aptamers that bind distinctively to rongalite using ELAA. The aptamers were further used in the development of a sandwich LF test strips.

The results obtained in the current study supported that RBA-1 and RBA-2 indeed had different secondary structures (as shown by M-Fold) and that they bind at different sites of RBP4. Therefore, RBA-2 was selected as capture aptamer and RBA-1 as reporter aptamer for RBP4 detection in the development of the LF test strips.

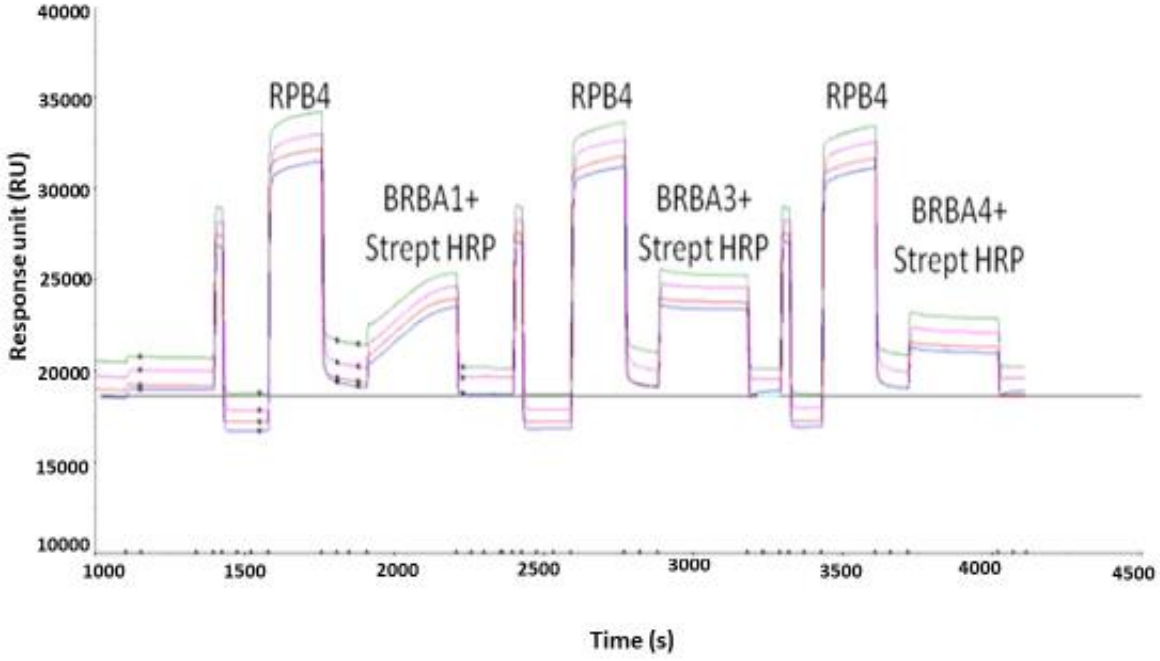

Figure 3.8: Dual aptamer based sandwich assay by SPR: the binding assays were performed using 10 µM thiol-RBA-2 as capture aptamer immobilized on gold sensor chip.

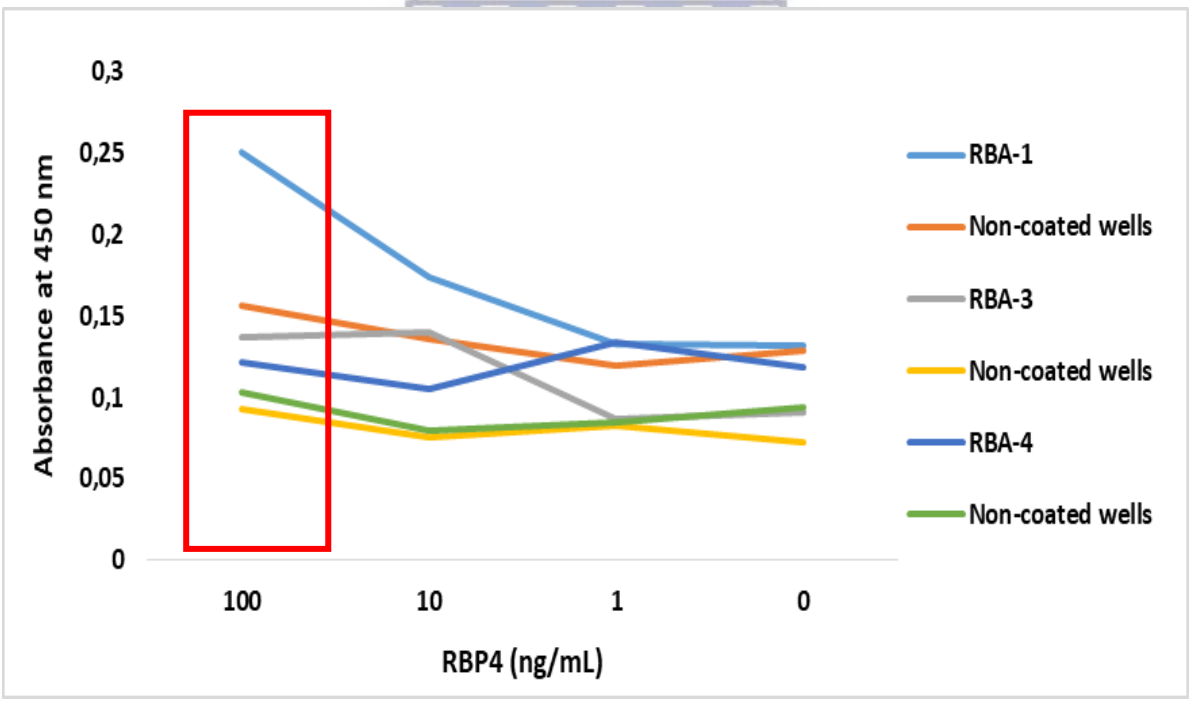

Figure 3.9: Dual aptamer based sandwich assay by ELAA: using 500 µM of thiol-RBA-2 immobilized on the plate, RBP4 (0 - 100 µg/mL) and 10 µM reporter aptamer (RBA-1, RBA-3 and RBA-4).

3.4 Synthesis and characterization of AuNPs

Recent advances in nanotechnology have provided a depth of insight and new opportunities for the application of nanomaterials in biological analysis and disease diagnosis (Matsui *et al*., 2004; Saji *et al*., 2010; Zhu *et al*., 2004). These nanomaterials are usually integrated in various parts of existing sensing platforms in order to offer innovative detection systems (Quesada-Gonza´lez and Merkoçi, 2017). Among these sensing nanomaterials, AuNPs have been mostly used in the development of colorimetric biosensors due to their unique optical properties, strong SPR and high extinction coefficient in the visible wavelength spectrum/range (He *et al*., 2008; Kim *et al*., 2016; Lin *et al*., 2005; Liu and Lu, 2004). In addition, they are highly stable and available in large quantities with controlled size and shape (Zhang *et al*., 2012). Hence, their application has remarkably increased the speed and success of PoC testing. For this experiment, AuNPs were synthesized by using citrate reduction method (Sibuyi *et al*., 2017) and characterized using UV-vis spectrophotometer, DLS, ζ-potential and TEM.

3.4.1 UV-vis spectrometry of AuNPs

UV-vis spectrometry is an important aspects of characterizing AuNPs. With increase in NPs size, the absorption spectra shift to longer wavelengths and the width of the adsorption spectra is related to the size distribution range. Generally, AuNPs display a single absorption spectrum between ranges of 510 - 550 nm with a bright ruby-red colour, which may vary depending on their size (Verma *et al*., 2014). In this study, the absorption maximum (λ_{max}) was observed at 517 nm, which indicated that the AuNPs were approximately 14 nm in size (**Figure 3.10**). The AuNPs had an absorbance value of 1,084 OD, and a concentration of 6.94 nM which is within the preferred concentration range for conjugation. The concentration of the AuNPs was calculated based on the formula:

$C=A450/\varepsilon 450$

Where: C = concentration, A450 = absorbance at 450 nm, ε450 = molar extinction coefficient at 450 nm.

Furthermore, the absorption spectra of the AuNPs was sharp, thus indicating that the AuNPs were uniform and stable. Similar findings were reported on AuNPs of variable sizes between

13-20 nm with λ_{max} around 520 nm (Agnihotril and Bhide, 2012; Liu *et al*., 2010; Qadami *et al*., 2018).

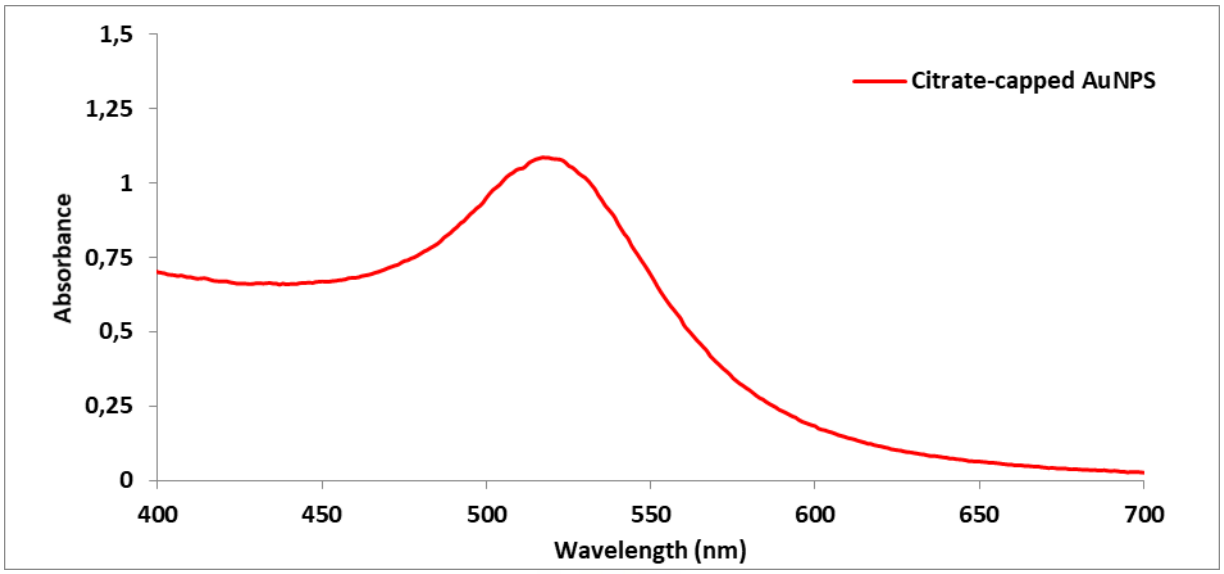

Figure 3.10: UV-vis spectrum of the citrate-capped AuNPs.

3.4.2 DLS and PDI analysis of the AuNPs

Hydrodynamic size of AuNPs was measured by DLS, which is one of the most preferred analytical methods for the characterization of AuNPs size. In the measurement, particles are exposed to a laser beam and the particles size is specified from the scattered light generated as a result, using the dependence of particles size on the spatial intensity and distribution pattern (Bhattacharjee, 2016)

As shown in **Figure 3.11**, the AuNPs had an average hydrodynamic diameter of 16.82 nm, which could be due to the hydrodynamic capacity of H_2O surrounding the AuNPs. About 97.8% of the AuNPs were within 17,93 nm and only 2.2% were about 5077 nm in size. This indicated that most of the AuNPs were of a smaller size. The PDI of the AuNPs was found to be 0.228, which indicated that the AuNPs were mostly monodispersed.

			Size (d.nm):	% Intensity:	St Dev (d.nm):
Z-Average (d.nm):	16,82	Peak 1:	17,93	97,8	6,034
PdI:	0,228	Peak 2:	5077	2,2	584,1
Intercept:	0,927	Peak 3:	0,000	0,0	0,000
Result quality :	Refer to quality report				

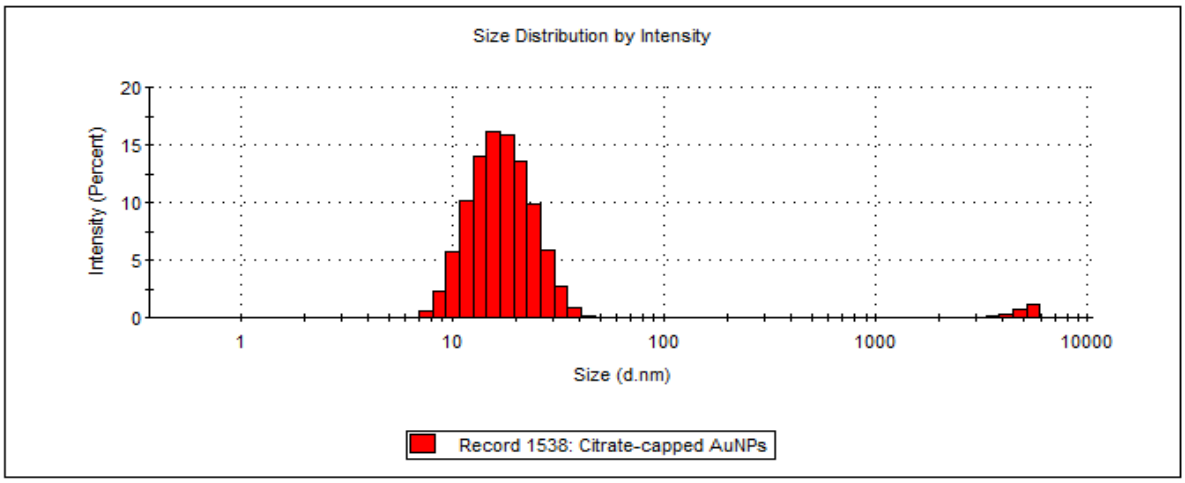

Figure 3.11: Size distribution of the citrate-capped AuNPs determined by the Malvern Zetasizer.

3.4.3 ζ-potential of the AuNPs

In this experiment, ζ- potential of the AuNPs was measured. The term ζ- potential describes the electrostatic potential around the particle surface. NPs bearing a ζ- potential between -10 mV and +10 mV are considered to be neutral, whereas NPs with a ζ- potential less than -30 mV or greater +30 mV are considered as charged and more likely remain stable in the solution. This is because they will not aggregate and will repel each other due to their electrostatic forces around the charges. On the other hand, the NPs with a ζ- potential greater than -30 mV or less than +30 mV are considered unstable and will eventually aggregate due to Van Der Walls inter-particle attraction (Nanocomposix, 2012).

The AuNPs showed a ζ- potential of -30.1 mV (**Figure 3.12**) which indicated that the AuNPs were highly stable and convenient for conjugation. The negative charge also indicated that the particle size was smaller than 100 nm, which was confirmed with the data obtained from UV-vis spectrophotometry and DLS. Other studies have reported synthesis of AuNPs with a ζ- potential of -43.2 mV (Lata *et al.*, 2015) and -44 mV (Nara *et al.*, 2010).

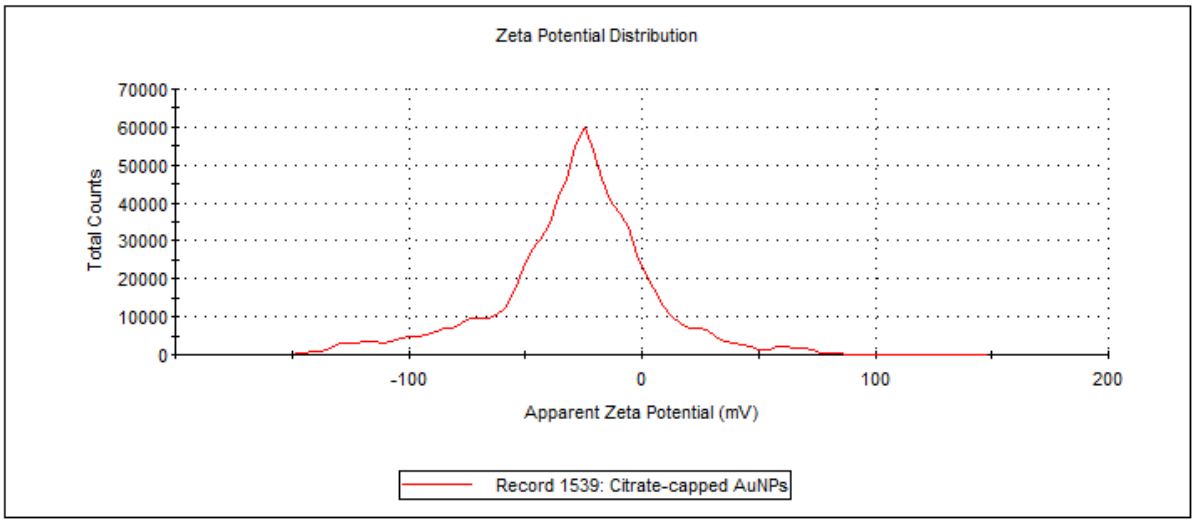

Figure 3.12: Zeta potential analysis of the citrate-capped AuNPs determined by the Malvern Zetasizer.

3.4.4 TEM analysis of the AuNPs

In order to confirm the results obtained, the AuNPs were further characterized by TEM. This technique is the most commonly used technique to determine the size, morphology, topography, composition and crystallography of the sample (Wang, 2001).

TEM images showed that the AuNPs were mostly spherical in shape (**Figure 3.13: A**). The images further revealed that the AuNPs were relatively monodispersed, this is due to the negatively charged layer of citrate ions which makes them to repel each other (Verman *et al*., 2014). The AuNPs dispersion showed no sign of aggregation. The core diameters of AuNPs were found to be 13.59 ± 3.04 nm which corroborate the results obtained from the UV-vis spectrophotometry (**Figure 3.13 B**). This data corroborates other published results of citrate-capped AuNPs (cAuNPs) (Bai *et al*., 2015; Verma *et al*., 2014).

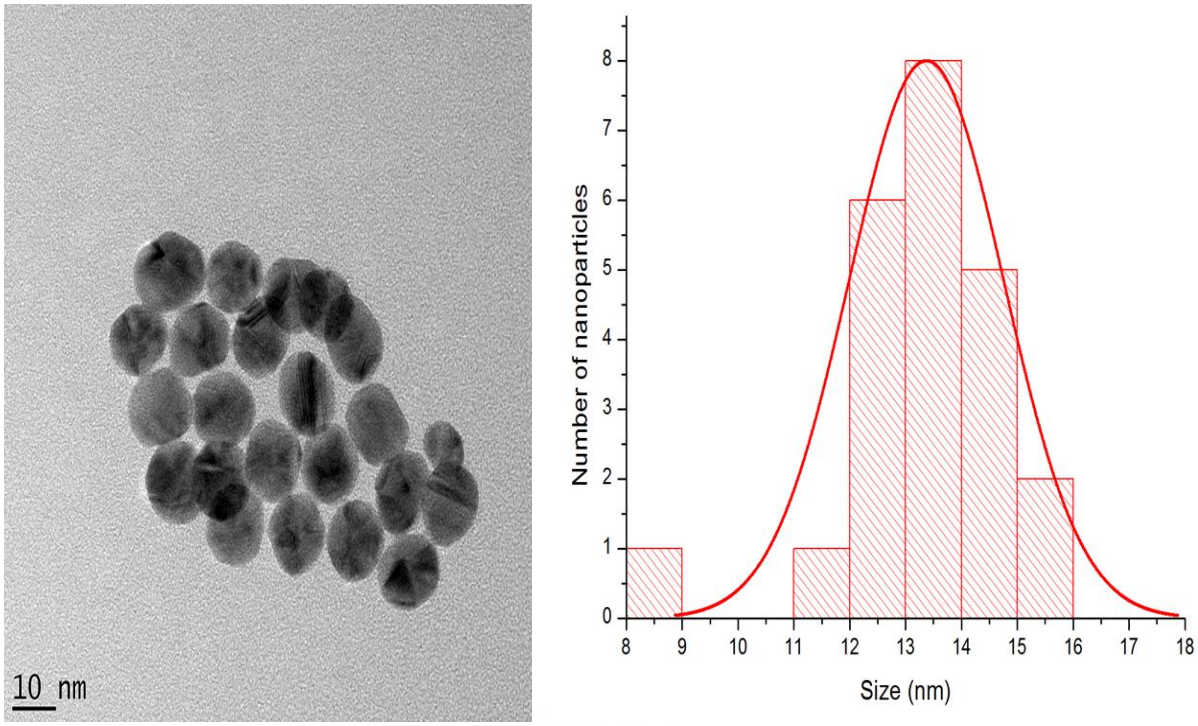

Figure 3.13: (A) TEM images of the citrate-capped AuNPs and (B) their size distribution. The magnification was at 10 nm. The core diameter of the AuNPs was calculated by measuring the circumference of 23 individual particles of the TEM images of AuNPs using the Image J software.

3.4.5 EDX analysis of the AuNPs

In order to validate the presence of Au in the NPs solutions, the energy dispersive x-ray spectra (EDX) of the AuNPs was carried. EDX is a techniques used to obtain the elemental and chemical composition of NPs. It relies on the unique atomic structure of each element. Therefore, the x-ray spectrum emitted by different atomic structures is clearly distinct between different elements (Rao and Biswas, 2009).

The EDX spectrum of the AuNPs, in **Figure 3.14** shows the presence of gold (Au), which was expected. However, there are other traces of other elements such copper (Cu), carbon (C) and oxygen (O). The presence of Cu and C was due to the holey carbon coated Ni/Cu grid that the AuNPs were placed on during the analysis whereas O may have been adsorbed onto the samples surfaces. The results are corroborated by Tejaswi *et al*. (2016) in which Au, Cu and O were also observed.

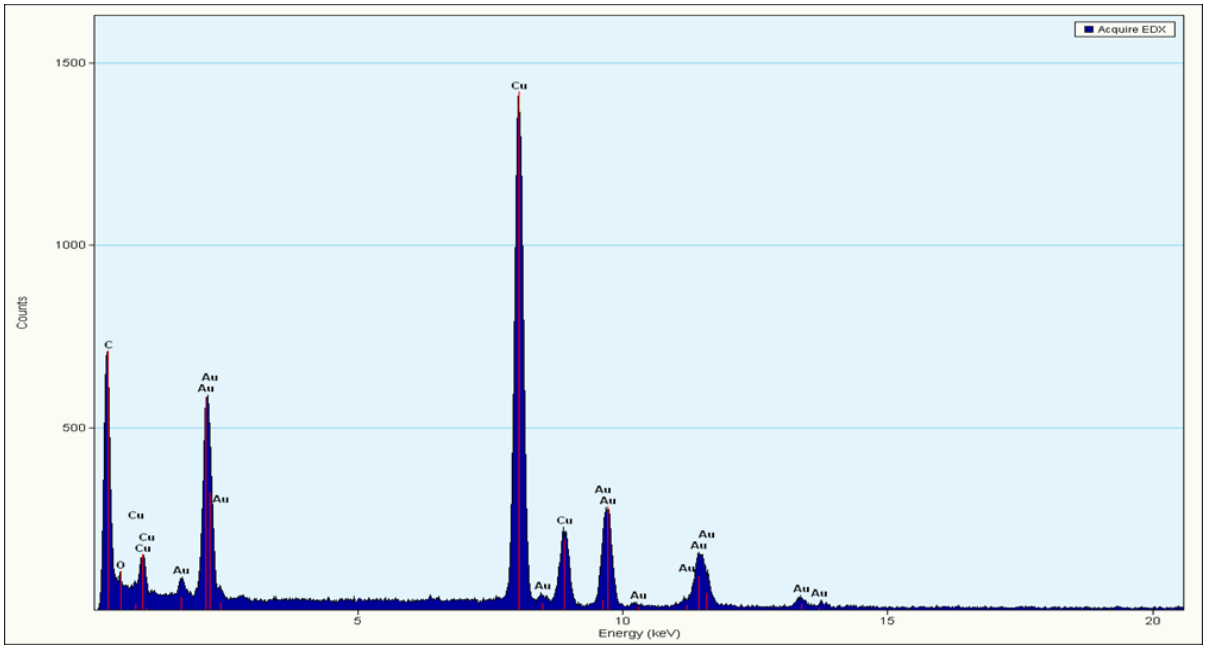

Figure 3.14: The chemical composition/EDX spectrum of the AuNPs.

3.5 Functionalization of ssDNA aptamer probe to AuNPs

3.5.1 Conjugation and characterization of apt-AuNP

The multifunctional properties of AuNPs offer unique opportunities for their use in the development of various diagnostic methods and devices. AuNPs prepared via citrate reduction method show uniformity, stability and wider applications in immunoassays (Thobhani *et al*., 2010). Moreover, thiolated compounds (aptamers, antibodies, peptides) can adsorb onto the AuNPs due to the high affinity of gold for thiol; thus, enhancing their stability and functionality (Zhang *et al*., 2012). Therefore, in this study, RBA-2 which was modified with thiol at its 5' end was used for conjugation to the AuNPs. To confirm that the thiolated aptamer probe conjugated to the AuNPs, samples were characterized using the UV-vis spectrophotometry, Zetasizer and Qubit assay. Stability tests were also done to detect any colour changes after conjugation.

3.5.1.1 UV-vis spectrometry of the apt-AuNPs

The UV-vis spectrophotometry has been widely used to determine the absorption spectrum of AuNPs in order to indicate immobilization of aptamers or other biomolecules on the surface of the AuNPs. AuNPs exhibit a strong λ_{max} in the visible region that can be used to determine whether modification of the NP surface has been successful (Philip, 2008). The colloidal SPR depends on several factors such as the size, solvent and surface modification, and is useful in

distinguishing AuNPs conjugates as well as to monitor adsorption of the ssDNA aptamers on the surface of the AuNPs.

Figure 3.15 shows the UV-vis spectra of the AuNPs, and apt-AuNPs with and without NaCl. The red shift in optical properties of the apt-AuNPs conjugates indicated the adsorption of the aptamers on the surface of the AuNPs was successful. The λ_{max} of AuNPs was obtained at 517 nm and shifted to 522 nm for 25 µM, 519 nm for 50 µM, 518 nm for 75 µM, and to 525 nm for 85µM upon conjugation. The red shift could be attributed to successful conjugation of the aptamers to the AuNPs; whereas, a small decrease in the peak intensity of the AuNPs can be attributed to the decrease in the interparticles distance as a result of conjugation (Liu and Lu, 2006, Qadami *et al.*, 2018).

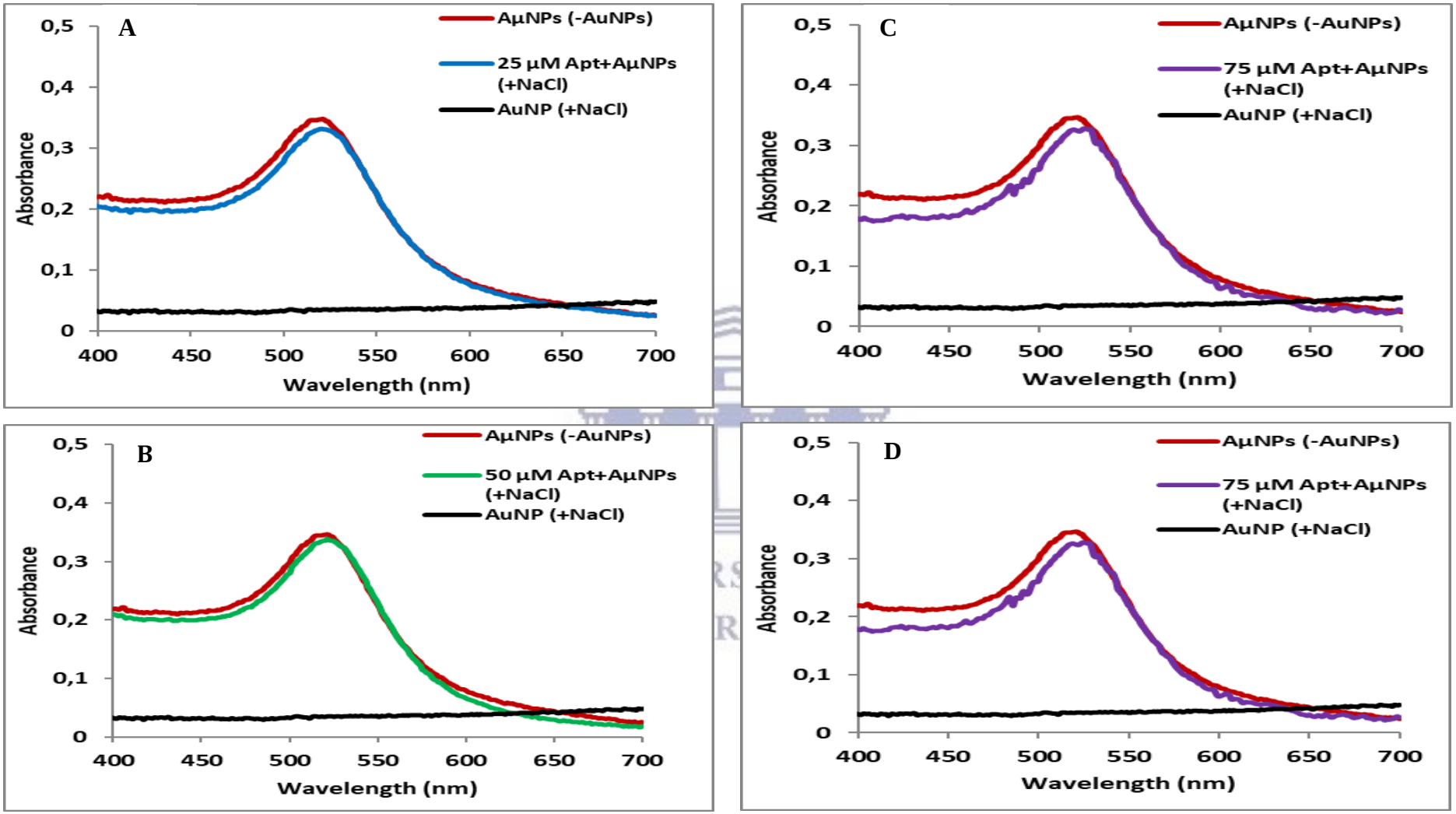

Figure 3.15: Comparison of the UV-Vis spectra of the AuNPs, apt-AuNPs conjugate with and without NaCl as indicated by +NaCl and -NaCl, respectively.

A: 25 μM aptamer concentration; B: 50 μM aptamer concentration; C: 75 μM aptamer concentration; D: 85 μM aptamer concentration.

3.5.1.2 Analysis of the stability of the apt-AuNPs conjugate

Visual detection, in which the changes in the colour of the AuNPs can be directly observed by the eyes, has gained a wide attention and serves as a preliminary characterization which does not require using any expensive and complicated instruments. It helps researchers to explore the stability of the AuNPs under various concentrations of proteins or aptamers. It is mostly applied in colorimetric assays in the presence of a target molecule (Guan *et al.*, 2014; Zhang *et al.*, 2012). Hence, this technique was used in this study to analyze the stability of the apt-AuNPs conjugates.

Figure 3.16, shows the obvious ruby-red to purple/blue colour change observed upon addition of NaCl in tube 1 (AuNPs). Addition of NaCl led to a slight colour change when 25 µM aptamer was used. This indicated that the surface of AuNPs was not fully covered by aptamers, hence the addition of NaCl caused aggregation (Ou *et al*., 2010). In contrast, the colour of apt-AuNPs at 50 - 85 µM remained ruby-red which is the same colour as the AuNPs (tube 0). This indicated that the surface of the AuNPs was fully covered with aptamers via the thiol group. The absence of a color change at higher concentrations indicated that the apt-AuNPs were stable. Thus, the minimal aptamer concentration required to stabilize the AuNPs was 50 µM. The results are corroborated by the results obtained by Zhang *et al*. (2016) and Chen *et al.* (2015).

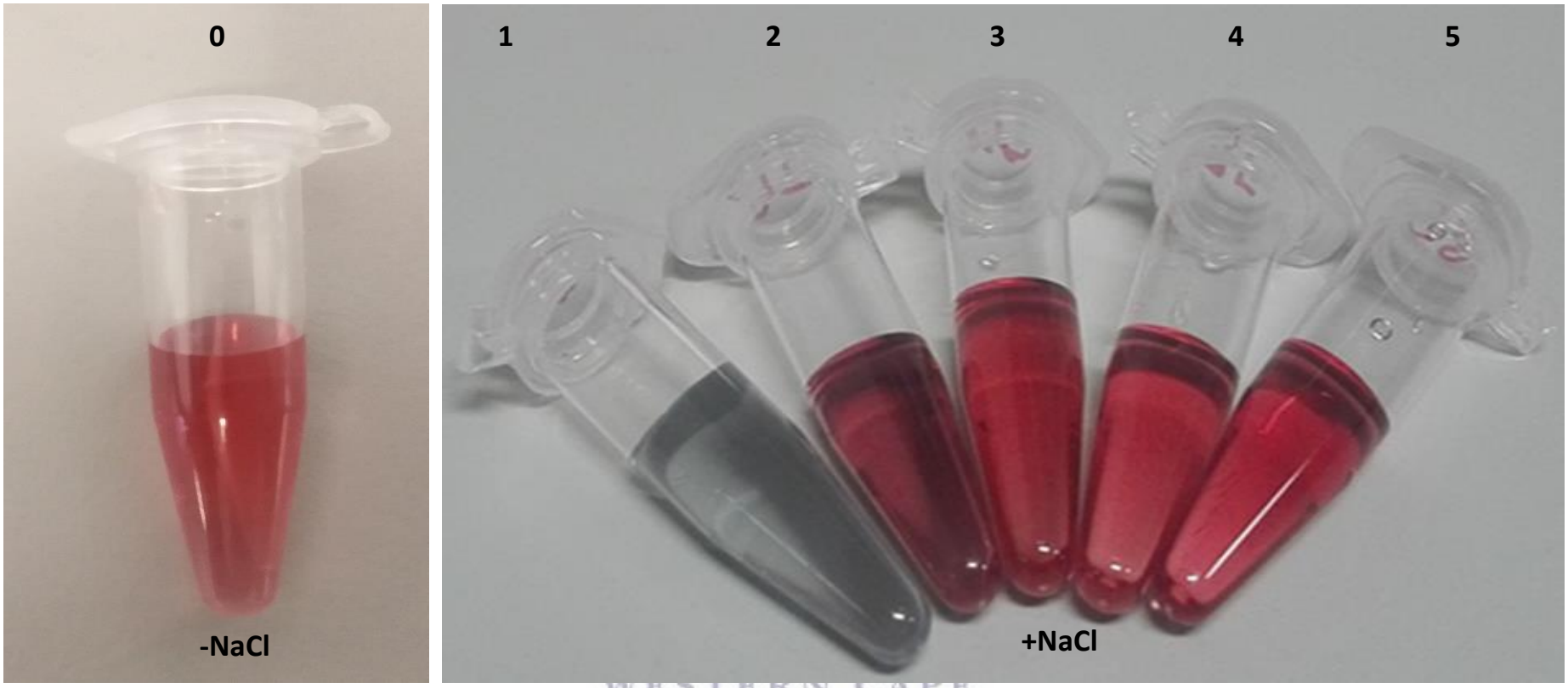

Figure 3.16: Colour change detection by naked eyes. Tube 0: AuNPs (-NaCl); Tube 1: 0 µM; Tube 2: 25 µM; Tube 3: 50 µM; Tube 4: 75 µM; Tube 5: 85 µM aptamer concentration and AuNPs (+NaCl).

3.5.1.3 DLS, PDI and ζ-potential analyses of the apt-AuNPs

DLS is able to monitor not only the core of NPs but also the surface modifications. Because adsorption of ssDNA probes onto AuNPs would cause an increase in the size of particles, DLS was used to evaluate adsorption by measuring sizes of the modified particles It is well established that, at a low surface coverage, the ssDNA probe lays flat on the surface, due to non-specific binding. However, as the surface coverage increases, the aptamers starts to adopt a more perpendicular conformation due to electrostatic repulsion between the aptamers and the AuNPs, which may lead to an increase in the hydrodynamic diameter (Liu and Liu, 2017).

In this experiment, the hydrodynamic diameter of the AuNPs was 16.82 and conjugation of aptamers to AuNPs had no significant effect on the hydrodynamic diameter, ~ 18 nm (17.85 - 18.42 nm) in the absence of NaCl. At 25 µM aptamer concentration, the hydrodynamic diameter of the AuNPs increased to 54.66 nm; for 50 - 85 µM, the hydrodynamic diameter increased upon the addition of salts to 31 nm (30.94 - 31.71 nm). The results further indicated that the optimal loading capacity of apt-AuNPs was at a concentration of 50 µM.

The PDI results (**Table 3.3**) indicated that in the absence of NaCl, the AuNPs at all aptamer concentrations remained monodispersed. However, in the presence of NaCl, the PDI of the AuNPs at 0 and 25 µM increased to 0.378 and 0.44, respectively. This indicated that the AuNPs were polydispersed; whereas, the results for higher concentrations (50 - 85 µM) indicated that the AuNPs were still monodispersed with a PDI of 0.257 - 0.266. There were no major changes observed on the PDI (0.134 - 0.244) in the absence of NaCl.

Addition of aptamers had no effect on the ζ-potential of conjugated AuNPs compared to control (**Table 3.3**). The ζ-potential increased from -30.31 to -20.93 after exposing the apt-AuNPs to NaCl. These changes can be attributed to molecules attached to the AuNPs surfaces and could be used to predict how these AuNPs are going to behave when used in the LFA and also the shelf life of the LF.

Table 3.3: DLS, PDI and ζ-potential of the apt-AuNPs conjugate determined using the Zetasizer.

[Aptamer] (µM)	-NaCl			+NaCl		
	Z ave (nm)	PDI	Zeta pot.	Z ave (nm)	PDI	Zeta pot.
0	16.82	0.228	-30.31	658.2	0.378	-25.8
25	17.89	0.244	-35.2	54.66	0.44	-22.8
50	17.85	0.223	-28.9	30.94	0.266	-20.93
75	18.04	0.221	-34.8	31.71	0.265	-22.2
85	18.42	0.134	-29.6	31.70	0.257	-25.4

3.5.1.4 UV-vis spectrometry of the apt-AuNPs

The UV-vis spectrophotometry was used to check the absorption spectra after removing the unbound aptamers from the apt-AuNPs. The UV-vis spectra show (**Figure 3.17**) that the apt-AuNPs at 50 - 85 µM in the presence of NaCl were stable while apt-AuNPs in the absence of NaCl were not stable. There SPR shifted to longer wavelength which resulted in a formation of a new peak between 600 - 700 nm, which indicated that there was aggregation (Zimbone *et al*., 2014). This results were further corroborated by the visible colour change from ruby-red to dark purple/blue (shown by photograph insert).

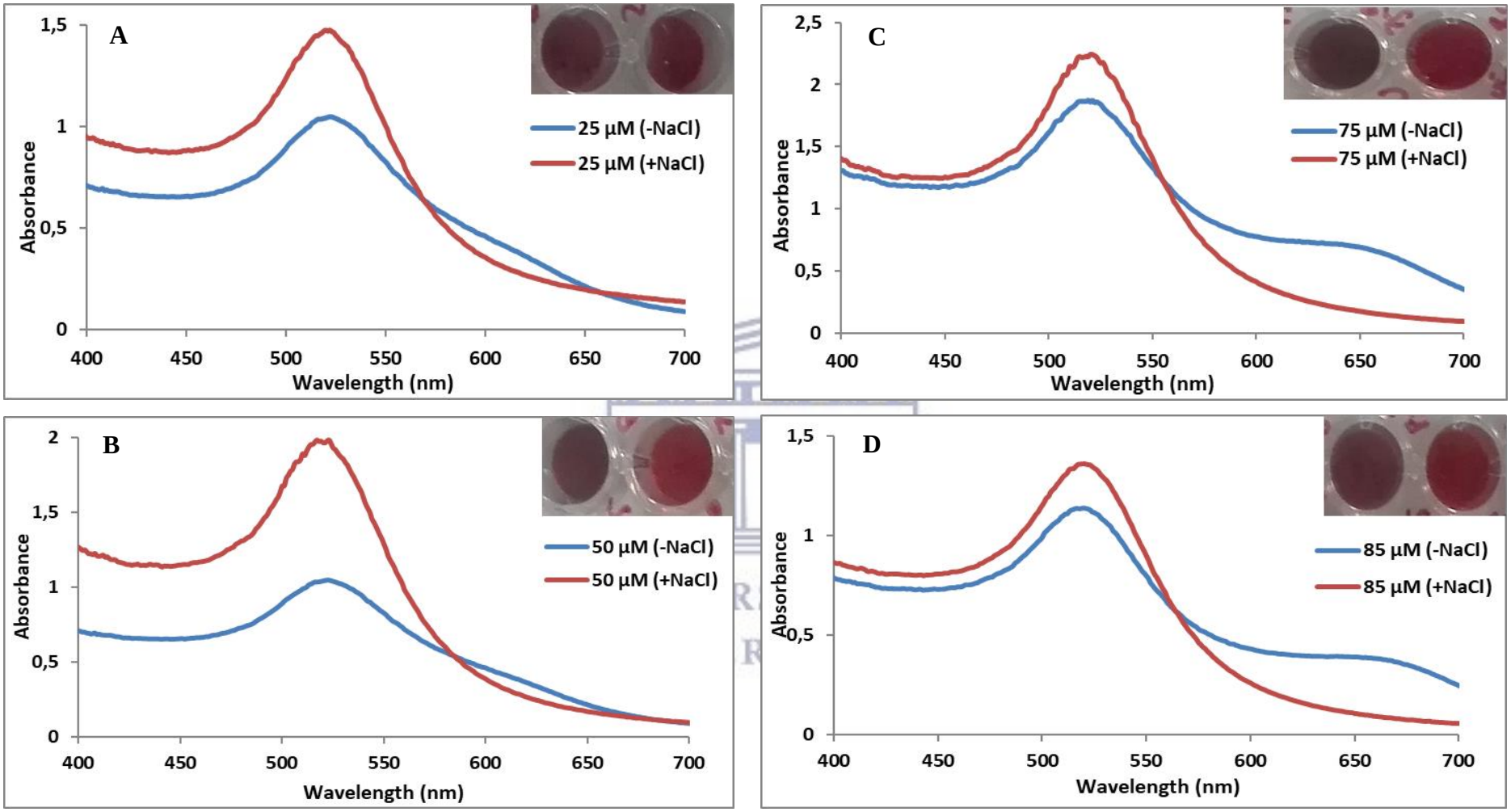

Figure 3.17: UV-vis spectra of the apt-AuNPs after removing the unbound aptamers. The maroon colour represent the apt-AuNPs in the presence of 1 M NaC1 (+NaCl) and blue colour represent the apt-AuNPs in the absence of NaCl (-NaCl). A: 25 µM aptamer concentration; B: 50 µM aptamer concentration; C: 75 µM aptamer concentration; D: 85 µM aptamer concentration.

3.5.1.5 Quantification of ssDNA aptamer bound to AuNPs

To determine the concentration of the aptamers bound to the AuNPs, a reliable quantification of the ssDNA aptamer is important. The amount of the ssDNA aptamer after conjugation may be very low due to insufficient breaking of the disulphide bonds by TCEP, therefore, a sensitive assay for quantification is needed. The Qubit high-sensitivity assay which is able to accurately detect as little as 50 pg/µL of the sample was used for quantification. Besides its specificity, this assay is more advantageous than the Nanodrop as common contaminants such as salts, free nucleotides, solvents, detergent or protein that may be present in the sample are tolerated in the assay.

The results shown in **Table 3.4** indicated that a reliable quantification of 25 µM was not possible. This could be attributed to the concentration not being sufficient to cover the whole surface of the AuNPs; thus, indicating that an increase in concentration is still needed. On the other hand, a reliable quantification of 14.6, 17.8 and 11.6 ng/mL were detected for 50, 75 and 85 µM, respectively. Although the aptamer concentration in the conjugates was not directly quantified due to the quenching effect of AuNPs on the dye, the method used in this study support the results given by preliminary characterization and suggest that the aptamers at certain concentration were able to fully cover the surface of the AuNPs.

Table 3.4: Quantification of ssDNA by Qubit assay.

[Apt] (µM)	[Apt in H_2O] (ng/mL)	[Unbound apt] (ng/mL)	[Bound apt] (ng/mL)
25	10.4	Samples too low	Not calculated
50	20.7	14.6	6.1
75	33.3	17.8	15.5
85	36.4	11.6	24.8

3.5.2 Conjugation and characterizations of RBA-2 to AuNPs (Large scale)

3.5.2.1 UV-vis spectrophotometry of the apt-AuNPs

Conjugation of the RBA-2 aptamer to AuNPs was done in a large scale for use in the development of the LF test strips. **Figure 3.18** shows the UV-vis spectra of the AuNPs, and apt-AuNPs conjugate. The λ_{max} of AuNPs is obtained at 522 nm with a high symmetry and narrow width, which indicated that the prepared AuNPs were monodisperse and had narrow size distribution. The λ_{max} of the AuNPs shifted to 525 nm upon conjugation with aptamers. The intensity of the apt-AuNPs conjugate peak was reduced compared with the unconjugated AuNPs peak. The red shift and the decrease in the peak intensity of the AuNPs may be attributed to the decrease in the interparticles distance as a result of apt-AuNPs conjugation (Aaryasomayajula *el al*., 2014). However, the results were inconclusive because the presence of aptamers was not further confirmed by a peak at 260 nm because the AuNPs also showed a peak at 260 nm. Similar data was observed when the biotinylated RBA-2/15 mer' poly-T was used.

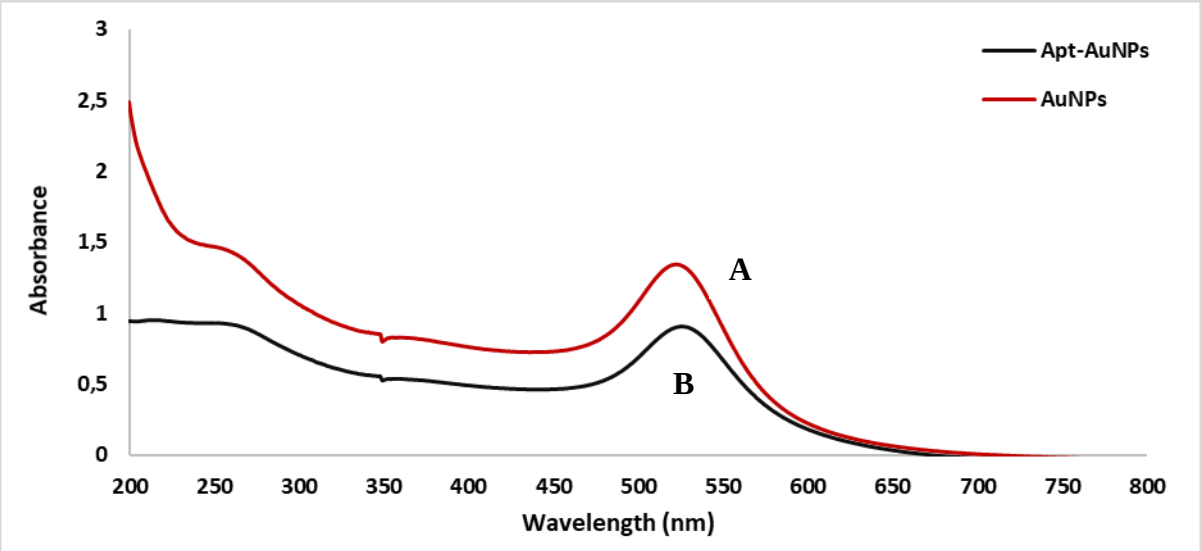

Figure 3. 18: UV-vis analysis of AuNPs and apt-AuNPs conjugates. (A) citrated-capped AuNPs; (B) 50 µM of the biotinylated-RBA-2 was conjugated to the AuNPs.

3.5.2.2 Gel electrophoresis analysis of the apt-AuNPs

Gel electrophoresis was also used to confirm successful conjugation of the aptamer to the AuNPs based on the mobility shift effect. As indicated in **Figure 3.19**, in lane 2, the unconjugated AuNPs did not migrate into the gel and formed a black precipitate immediately after mixing with the loading dye. In lane 3, a distinct band, which corresponded with the apt-

AuNPs conjugates was observed. Lane 4 showed the aptamer band (arrow; at about 75 bp). The band was faint, which could be attributed to the low aptamer concentration used. There is a clear retardation in the apt-AuNPs migration along the gel (lane 3) compared to AuNPs alone. This can be attributed to both the increased size of the apt-AuNPs complex, as well as to each AuNPs bearing multiple copies of the aptamer. Furthermore, the colour of the AuNPs remained ruby-red, indicating that the AuNPs were still stable. Similar data was observed when the biotinylated RBA-2/15 mer' poly-T was used.

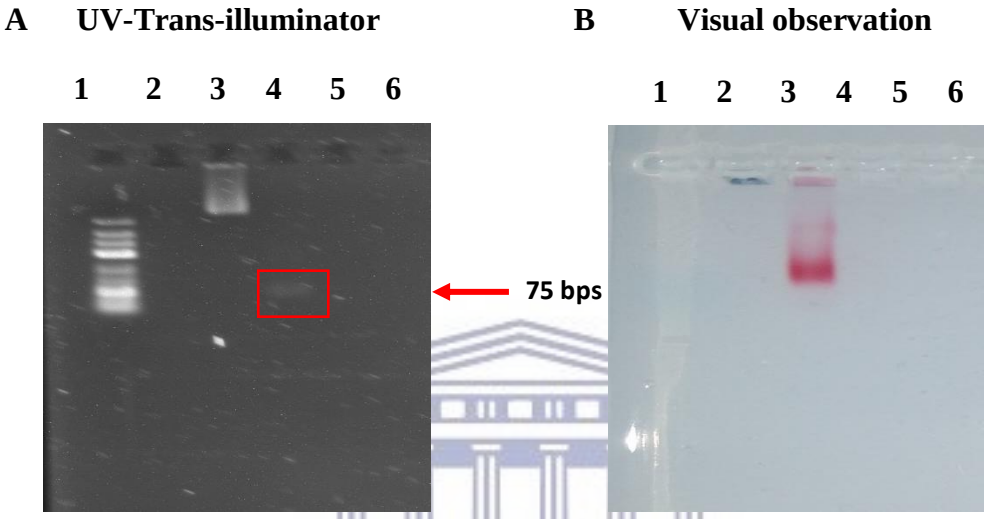

Figure 3.19: Analysis of apt-AuNPs conjugation by 1% agarose gel electrophoresis. Images were analyzed by (A) UVP Trans-illuminator and (B) visual observation. 1: 100 bp O'gene ruler; 2: AuNPs; 3: apt-AuNPs conjugate; 4: free aptamer (arrow).

3.6 Development of the lateral flow test strips

Previous studies have demonstrated the feasibility of developing strip biosensors based on aptamer-functionalized AuNPs for the detection of thrombin (Xu *et al.*, 2009), ochratoxin A (Zhou *et al.*, 2016) and vaspin (Raston *et al.*, 2017). For the extended application of RBP4 aptamers selected by Lee *et al.* (2008), we combined the high affinity, specificity, and stability of aptamers to develop an aptamer-based lateral flow test strips for rapid and sensitive detection of RBP4.

For the preparation of the test line on the lateral flow test strips, streptavidin was set as a bridge, which can be immobilized on the nitrocellulose membrane by electrostatic adsorption and linked biotin-modified aptamer through the specific reaction of streptavidin and biotin. This was done to prevent nucleic acid from being washed away easily by the sample flow when sprayed onto the nitrocellulose membrane directly because they have no specific

binding force to the nitrocellulose membrane. Then, RBP4 (0.5 mg/mL) prepared in PBS buffer was directly immobilized on the control line. When the apt-AuNPs conjugate mixture was wicked on the edge of the nitrocellulose membrane, it migrated through capillary action to interact with RBP4 on the control line.

Based on the results on **Figure 3.20**, there was an appearance of a line on the control line which was observed within five min. The presence of a line was regarded as positive results; however, the intensity of the line was weak and decreased gradually until it disappeared after washing with the 1× SELEX buffer which indicated that there is no interaction between the aptamer and the protein. It was postulated that the negative results obtained may be due to low concentration of the RBP4; thus, the concentration was increased to 2 mg/mL and the test strips were prepared in the similar manner as before. Nevertheless, the results were still negative. This could be attributed to the protein being subjected to desorption upon direct immobilization on the LF test strips. The presence of His-tag modification on the protein might also be a key factor that resulted to negative results.

Hence, a new experiment was performed with a new RBP4 protein (1.3 mg/mL) and thiolated RBA-2/15-mer poly-T. The use of spacers allows more space for the aptamers to fold into their active structure and therefore result in a higher ratio of functional aptamers. A biotin-modified poly-A aptamer was immobilized on the control. The choice of using the biotin-modified complementary poly-A aptamer was because the new set of aptamer incorporated a 15 mer' poly-T spacer.

The results obtained in **Figure 3.21** indicated that before wash, there was a band obtained at the test line and the unbound labelled reporter aptamer conjugate migrated along the nitrocellulose membrane and was captured at the control line by the biotinylated poly-A aptamer; whereas, other excessive solutions went to the absorption pad. The intensity of the colour at the control line corresponds to the amount of the unbound aptamer captured by the complementary aptamer. The band, which was initially obtained at the test line, had a weak intensity and gradually disappeared after washing with 1× SELEX buffer.

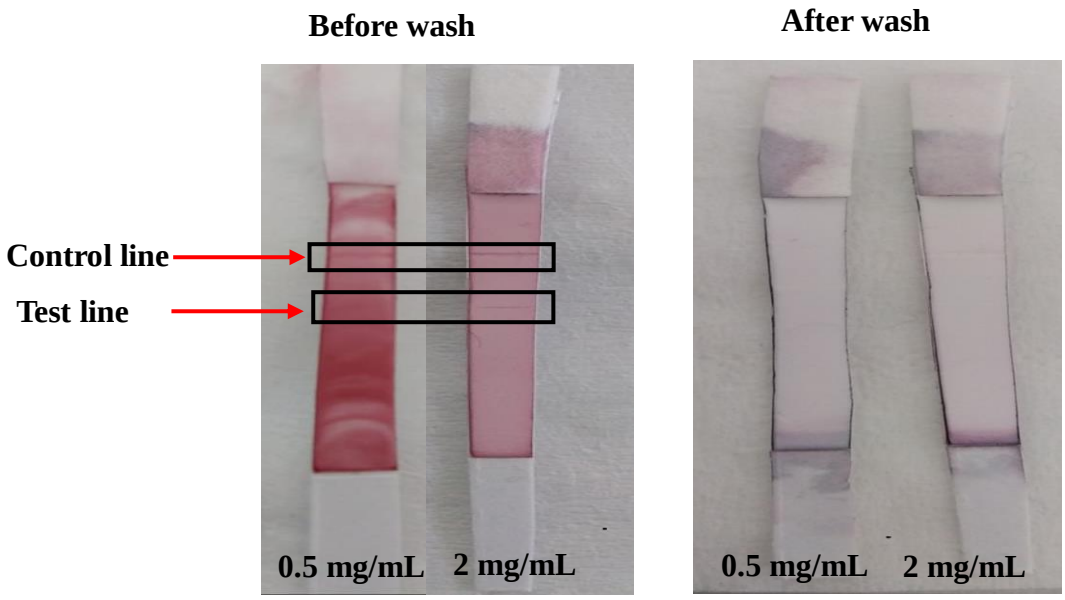

Figure 3.20: Detection of RBP4 (0.3 - 2 mg/mL) by the conventional LFA. RBP4 was immobilized on the control line and RBA-1 was immobilized on the test line.

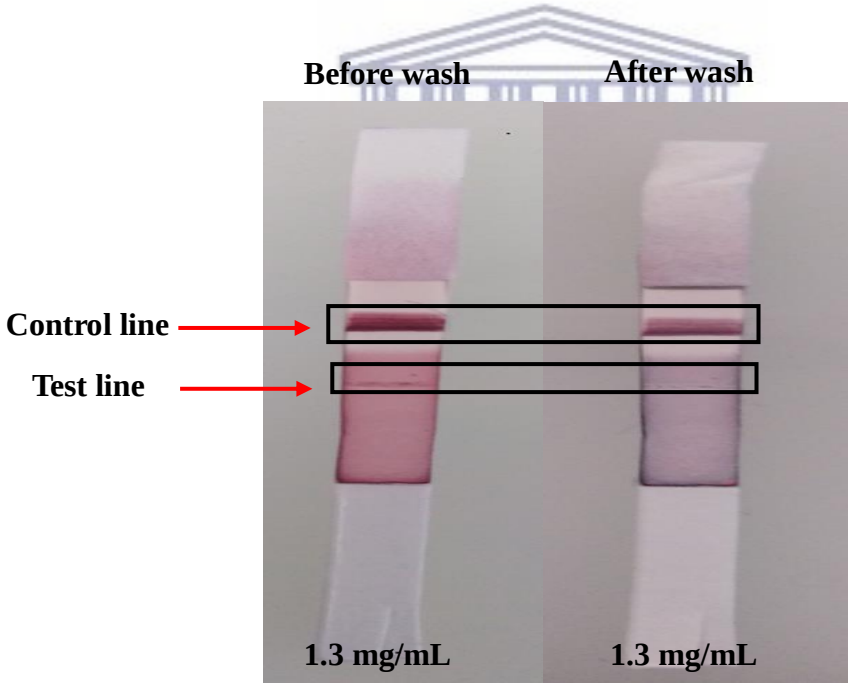

Figure 3.21: Detection of RBP4 (1.3 mg/mL) by the conventional LFA. RBP4 was immobilized on the test line and biotinylated poly-A aptamer was immobilized on the control line.

3.7 Development of a colorimetric aptasensor

The present study further investigated the possibility of developing a colorimetric aptasensor for the detection of RBP4. This assay is based on colour change from ruby-red to blue/purple due to conformational change of aptamer in the presence of the target molecule, and the phenomenon of salt-induced AuNPs aggregation which could be monitored by eyes or UV-vis spectrophotometer.

3.7.1 Determination of the optimum concentration of NaCl and aptamer

It is well known that AuNPs are highly reactive and aggregate easily in the presence of salts, so it is important to monitor the salt-induced AuNPs aggregation kinetics for the development of a colorimetric aptasensor. To optimize the performance of the developed assay, various conditions such as, RBA-2/15 mer' poly-T and NaCl concentrations were investigated, as described in **Section 2.2.6.1**.

Figure 3.22 indicate the photograph insert of the reaction conditions **(A)** and the absorbance ratio (A660/520) **(B)**. It was apparent that the AuNPs with and without aptamers barely aggregated under 20 mM NaCl solution. The control AuNPs (without the aptamer) changed colour from ruby-red to purple/blue with an increased NaCl concentration (40 - 100 mM) and the percentage aggregation kinetics increased and reached saturation at 80 and 100 nM. Thus, the minimum required NaCl is 60 nM. The observation suggested that the Na^+ and Cl^- ions destroyed the ionic environment and led to the aggregation of AuNPs in the absence of aptamers. Addition of 25 nM aptamer, partially protected the AuNPs; whereas, it can be seen that when the aptamer concentration were 50 - 100 nM, the protection efficiency against salt-aggregation of AuNPs was excellent which was indicated by the ruby-red colour and a lower percentage aggregation kinetics.

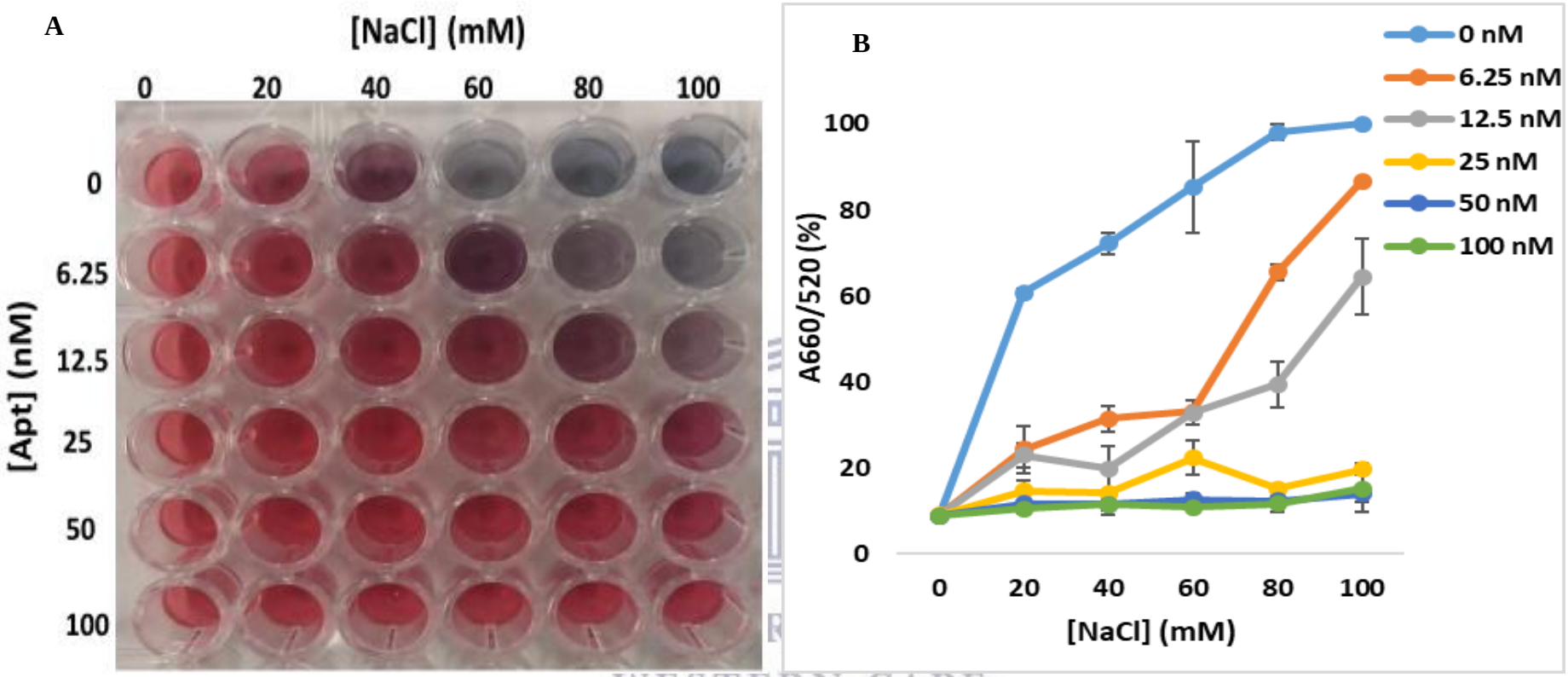

Figure 3.22: Optimization of the biotinylated-aptamer and NaCl concentrations for the development of the aptasensor. (A) Photograph insert; (B) Absorbance ratio. Final aptamer concentrations: 0, 6.25, 12.5, 25, 50 and 100 nM; final NaCl concentrations: 0, 20, 40, 60, 80 and 100 mM.

3.7.2 Sensitivity of the aptasensor for RBP4 detection

The sensitivity of the colorimetric sensor for the detection of RBP4, under the optimized experimental conditions, was measured with different concentrations of RBP4 as described in **Section 2.2.6.2**.

Figure 3.23 shows that the colour of the AuNPs changed from ruby-red to purple/blue (insert) and the absorbance ratio (A600/A520) gradually increased with an increase of RBP4 concentration. The results demonstrate that RBA-2 bound to RBP4; thus, detached from the AuNPs, leaving the AuNPs unprotected. In the presence of 60 mM NaCl, the AuNPs aggregated. The aggregation was confirmed by the red shift from 520 nm to 600 nm as indicated by **Figure 3.23: A.** The assay was reproducibly sensitive with a limit of detection of 45.32 nM (R^2 = 0.9656) (**Figure 3.23: B**). The detection limits of the same protein obtained using ELAA and aptamer-based SPR analysis were 0.45 and 75 nM (**Table 3.5**), respectively (Lee *et al.*, 2012; Lee *et al.*, 2008). This indicated that the colorimetric aptasensor was more sensitive compared to the aptamer-based SPR; but, less sensitive as compared to the ELAA. The results in this study were obtained within 5 min. One of the major advantages of POCT is that it provides much faster access to test results, allowing for more rapid clinical decision making and more appropriate treatments and interventions. Moreover, the method required much smaller sample volume than those needed for testing in the central clinical laboratory.

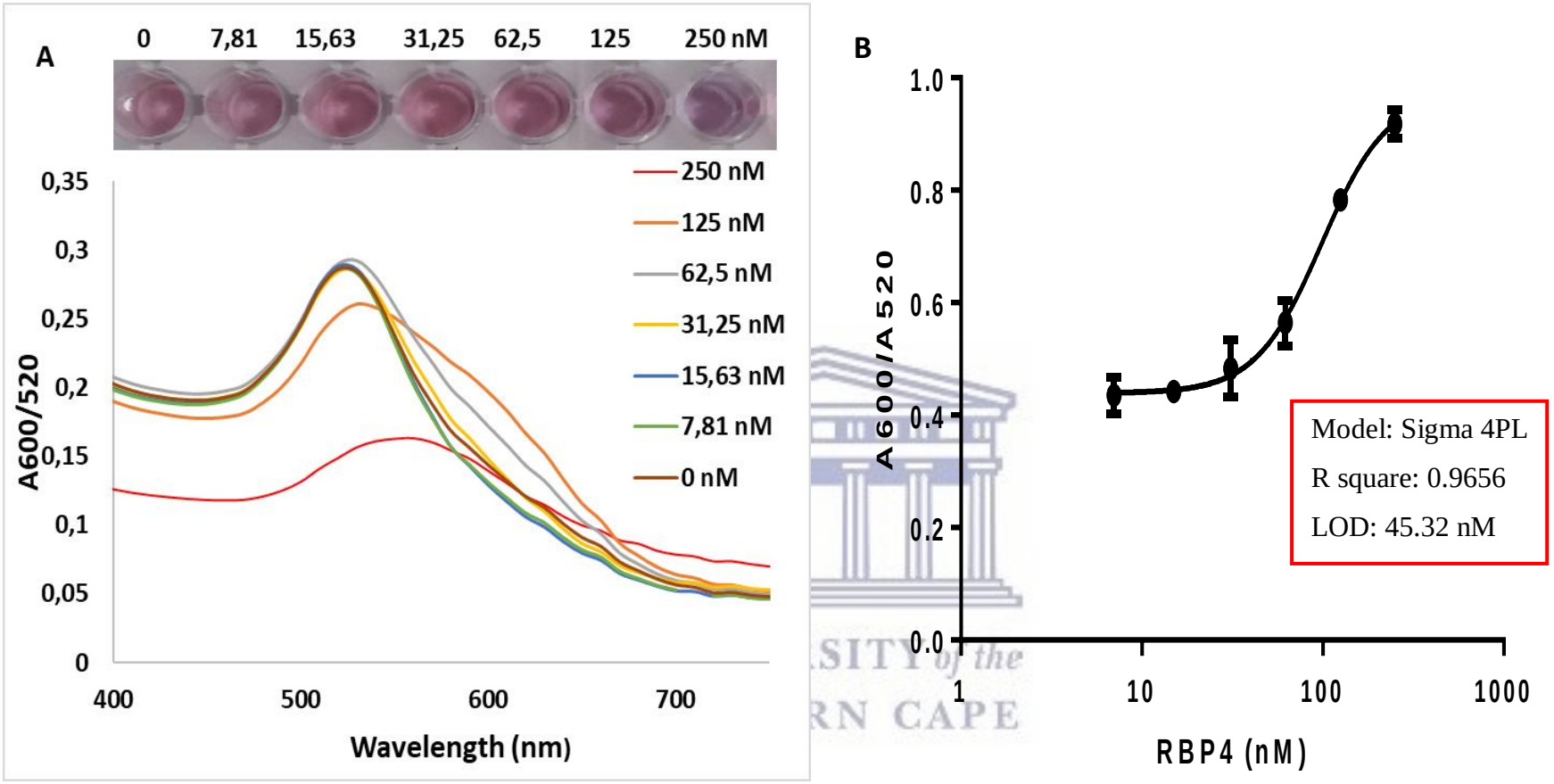

Figure 3.23: Sensitivity analysis of the colorimetric aptasensor. A: Absorption spectra of apt-AuNPs solutions treated with different RBP4 concentrations. Inset: visual colour changes of the sensing solution treated with 0, 7.81, 15.63, 31.25, 62.5, 125, 250 nM RBP4. B: Standard curve for different absorbance intensity (A600/A520) corresponding to different concentrations of RBP4. Each data point represents the averaged results of four separate experiments, each with two replicates.

Table 3. 5: Comparison of the colorimetric aptasensor with other methods for RBP4 detection.

Materials	Method	Limit of detection (nM)	Ref.
AuNPs and aptamer	Colorimetric	45.32	Present study
Aptamer and antibodies	ELAA	0.46	Lee *et al*. (2012)
Aptamer	SPR	75	Lee *et al*. (2008)

CHAPTER 4: CONCLUSION

4.1 Conclusion

The aim of the present study was to characterize RBP4 aptamers for the development of aptamer-based PoC diagnostic kit for diabetes. The aptamer were previously selected by Lee *et al.* (2008) and the sequences were analysed using bioinformatics tools in order to determine their secondary structures. The interactions of these aptamers with RBP4 was evaluated by SPR (**Section 3.2**). The secondary structures correlated with the findings of kinetic studies which revealed high binding affinities of aptamers to RBP4 and enhanced stability as denoted by the stem hairpin loops. Binding of the aptamers to RBP4 was in a low nM range for three aptamers and pM for one aptamers, which is the preferred range that allows binding in seconds to minutes only (Svobodová, *et al.*, 2012). The results were further validated by ELAA and EMSA; however, the EMSA results were inconclusive. Even though ELAA showed binding of the aptamers to RBP4, there should be more optimization steps for improving the results. Sandwich-SPR demonstrated that RBA-1 and RBA-2 bind to different sites on RBP4 and the results were validated by sandwich-ELAA.

AuNPs were successfully synthesized and characterized. The AuNPs had an average size of 14 nm and λ_{max} of 517 nm; a PDI of 0.226 and ζ- potential of -30.31 mV. The latter indicated that the AuNPs were indeed stable. TEM analysis revealed that the AuNPs were monodispersed and spherical. All the characterizations indicate that AuNPs are negatively charged, stable and convenient for the functionalization with aptamers. Conjugation of the aptamers to the AuNPs was achieved and used for the development of lateral flow test strips.

The development of the LF test strips was unsuccessful. Only one test strip showed positive results; however, the intensity was low and the results were not reproducible when different apt-AuNPs dilutions and also high concentrations of the RBP4 were used. Although, the LF test strips gave negative results, the present study has demonstrated the feasibility of developing an aptamer-based LFA for the detection of T2DM biomarker. Thus, further optimizations of different types of membranes, buffers, pH and target concentrations, are needed in order to obtain better resolutions and intensity on the test strips. The present study has successfully developed label-free aptasensor assay for RBP4 detection with a detection limit of 45.32 nM. The principle of such high sensitivity for RBP4 detection was based on the aggregation of AuNPs controlled by the salt induced and the special interactions between

RBA-2 and RBP4. The results indicated that the developed method had a relatively stable precision and satisfactory reproducibility. Therefore, the study has shown successful development of a simple yet effective colorimetric assay for RBP4 detection and the assay is not limited to this target, but also other targets with aptamers available without any special laborious instruments.

4.2 Limitation of the study

The present study has limitations that need to be addressed. The obtained sensorgrams showed specific shift at the beginning of association phase in majority of curves which complicated the fitting. The ELAA results for the identification of dual aptamers were not reproducible. The limitation factor was the newly ordered protein. Furthermore, the results obtained by EMSA analysis does not provide conclusive evidence of interaction, which may be due to the aptamers binding near the His-tag modification and or the incorrect gel percentage used.

The size, PDI and ζ- potential of the apt-AuNPs analysis was not repeated because the AuNPs were no longer stable after 10 months' storage. The development of LF test strips was not successful; perhaps, due to less concentration of the target protein, incorrect buffers and pH used.

4.3. Future studies

Future studies will include aptamer characterizations using different techniques such as a BLI and MST to validate the binding affinities of the aptamers and to identify dual aptamers. Different parameters such as different membranes, buffers, and target concentration will be optimized for the development of LF test strips. The stability of the AuNPs over a certain period will also be monitored in order to provide an insight on the shelf life of the LF test strips to be designed.

REFERENCES

Aaryasomayajula, V.S.R., Severs, T., Ghosh. K., DeLong, R., Zhang, X., Talapatra, S. and Wanekaya, A.K. (2014). Assembly of a Dual Aptamer Gold Nanoparticle Conjugate Ensemble in the Specific Detection of Thrombin when Coupled with Dynamic Light Scattering Spectroscopy *Journal of Nanomedicine and Nanotechnology*, **5**(4): 1–6.

Abel, E.D., Peroni, O., Kim, J.K., Kim, Y.B., Boss, O., Hadro, E., Minnemann, T., Shulman, G.I. and Kahn, B.B. (2001). Adipose-selective targeting of the GLUT4 gene impairs insulin action in muscle and liver. *Nature*, **409:** 729–733.

Adhikar, M., Strych, U., Kim, J., Goux, H., Dhamane, S., Poongavanam, M.V., Hagstrom, A.E.V., Kourentzi, K., Conrad, J.C. and Willson, R.C. (2015). Aptamer-phage reporters for ultrasensitive lateral flow assays. *Analytical Chemistry*, **87:** 11660-11665.

Agnihotril, N.P. and Bhide, M. (2012). Design of Aptamer-Gold Nanoparticles Based Colometric Assay for the Early diagnosis of Breast Tumour. *International Journal of Science and Research*, **3**(11): 2319–7064.

Al-Tarawneh, S.K., Border, M.B., Dibble, C.F., Bencharit, S. (2011). Defining salivary biomarkers using mass spectrometry-based proteomics: a systematic review. *OMICS*, **15:** 353 – 361.

Al-Tarawneh, S.K., Bencharit, S. (2009). Applications of Surface-Enhanced Laser Desorption/Ionization Time-Of-Flight (SELDI-TOF) mass spectrometry in defining salivary proteomic profiles. *Open Dentistry Journal*, **3:** 74–79.

Almasi, F., Mousavi Gargari, S.L., Bitaraf, F. and Rasoulinejad, S. (2016). Development of a single stranded DNAaptamer as a molecular probe for lncap cells using cell-selex. *Avicenna Journal of Medical Biotechnology*, **8:** 104–111.

Alsager, O.M., Alotaibi, K.M., Alswieleh, A.M., and Alyamani, B.J. (2018). Colorimetric Aptasensor of Vitamin D3: A Novel Approach to Eliminate Residual Adhesion between Aptamers and Gold Nanoparticles. *Scientific reports*, **8:** e12947.

American Diabetes Association, (2018). Classification and Diagnosis of Diabetes: Standards of Medical Care in Diabetes. *Diabetes Care*, **41**(1): S13–S27.

American Diabetes Association, (2014). Diagnosis and classification of diabetes mellitus. *Diabetes Care*, **37**(l1): 8S1–S90.

American Diabetes Association. (2011). Standards of medical care in diabetes—2011. *Diabetes Care*, **34**(1): S11–S61.

American Diabetes Association (ADA). (2009). Diagnosis and Classification of Diabetes Mellitus. *Diabetes Care*, **40**(11): S9.

Amendola, V. and Meneghetti, V. (2009). Size evaluation of gold nanoparticles by UV - vis

spectroscopy. *Journal of Physical Chemistry C*, **113**(11): 4277–4285.

American Diabetes, Association (2007). "Diagnosis and classification of diabetes mellitus". Diabetes Care. **30**(1): 42–47.

Aravindaha Babu N., Masthan, N.K.M.K., Tathagat Bhattacharjee, T. and Elumali, M. (2014). Saliva the key regulator of oral changes in diabetes patients. *International Journal of Pharmaceuticals Science and Reseach*, **5**(7): 2579–2583.

Arguedas, J.A, Leiva, V. and Wright, J.M. (2013). Blood pressure targets for hypertension in people with diabetes mellitus. *The Cochrane Database of Systematic Reviews*, **10:** CD008277.

Aring, A.M., Jones, D.V., Falko, J.M. (2005). Evaluation and prevention of Diabetic Neuropathy. *American Family Physician*, **71:** 2123–2128.

Assadollahi, S., Reininger, C., Palkovits, R., Pointl, P. and Schalkhammer, T. (2009). From lateral flow devices to a novel nano-color microfluidic assay. *Sensors (Basel, Switzerland)*, **9**(8): 6084– 6100.

Backus, K.M., Correia, B.E., Lum, K.M., Forli, S., Horning, B.D., González-Páez, G.E., Chatterjee, S., Lanning, B.R., Teijaro, J.R., Olson, A.J., Wolan, D.W, and Cravatt B.F.

(2016). Proteome-wide covalent ligand discovery in native biological systems. *Nature*, **534**(7608): 570–574.

Bai, W., Zhu, C., Liu, J., Yan, M., Yang, S. and Chen, A. (2015). Gold nanoparticle–based colorimetric aptasensor for rapid detection of six organophosphorous pesticides. *Environmental Toxicology and Chemistry*, **34**(10): 2244–2249.

Berg, K., Lange, T., Mittelberger, F., Schumacher, U. and Hahn, U. (2016). Selection and Characterization of an α6β4 Integrin blocking DNA Aptamer. *Molecular Thererapy-Nucleic Acids*, **5:** e294.

Berlanga-Acosta, J., López-Saura, P., Guillen-Pérez, I., Guillen-Nieto, G., Acevedo-Castro B, and Herrera- Martínez, L. (2013). Type 2 Diabetes Mellitus (T2DM): Biological Overview from Pathways to Organelles and its Translation toward a Torpid Wound Healing Process. *Journal of diabetes and metabolism*, **4:** e285.

Bertram, M.Y., Jaswal, A.V., Van Wyk, V.P., Levitt, N.S. and Hofman, K.J. (2013). The non-fatal disease burden caused by type 2 diabetes in South Africa, 2009. *Global Health Action*, **6:** e19244.

Bhalla, N., Jolly, P., Formisano, N. and Estrela, P. (2016). Introduction to biosensors. *Essays in Biochemistry*, **60**(1): 1–8.

Bian, C., Zhang, F., Wang, F., Ling, Z., Luo, M., Wu, H., Sun, Y., Li, J., Li, B., Zhu, J., Tang, L., Zhou, Y., Shi, Q., Ji, Y., Tian, L., Lin, G., Fan, Y., Wang, N. and Sun, B. (2010). Development of retinol-binding protein 4 immunocolloidal gold fast test strip using high-sensitivity monoclonal antibodies generated by DNA immunization. *Acta Biochim Biophys Sin*, **42:** 847–853.

Blind, M. and Blank, M. (2015). Aptamer selection technology and recent advances. *Molecular Therapy-Nucleic Acids*, **4**(1): e223.

Borth, W. (1992). Alpha 2-macroglobulin, a multifunctional binding protein with targeting characteristics. *The FASEB Journal*, **6**(15): 3345–3353.

Brereton, M.F., Rohm, M., Shimomura, K., Holland, C., Tornovsky-Babeay, S., Dadon, D., Iberl, M., Chibalina, M.V., Lee, S., Glaser, B., Dor, Y., Rorsman, P., Clark, A. and Ashcroft, F.M. (2016). Hyperglycaemia induces metabolic dysfunction and glycogen accumulation in pancreatic β-cells. *Nature Communications*, **(7):** e13496.

Cabrera Escobar MA, Veerman JL, Tollman SM, Bertram MY, Hofman KJ (2013) Evidence that a tax on sugar sweetened beverages reduces the obesity rate: a meta-analysis. *BMC Public Health*, **13:** e1072.

Campfield, L.A, Smith, F.J., and Burn, P. (1996). The OB protein (leptin) pathway—a link between adipose tissue mass and central neural networks. *Hormone and Metabolic Research*, **28**(12): 619–632.

Carvalhal, R.F., Kfouri, M.S., Piezzate, M.H., Gobbi, A.L. and Kubota, L.T. (2010). Electrochemical detection in a paper-based separation device. *Analytical Cheistry*, **82**(3): 1162–1165.

Cella, L.N., Sanchez, P., Zhong, W., Myung, N. V., Chen, W., and Mulchandani, A. (2010). Nano Aptasensor for Protective Antigen Toxin of Anthrax. *Analytical Chemistry*, **82**(5): 2042–2047.

Chang, A.L., McKeague, M., Liang J.C. and Smolke C.D. (2014). Kinetic and Equilibrium Binding Characterization of Aptamers to Small Molecules using a Label-Free, Sensitive, and Scalable Platform. *Analytical Chemistry*, **86:** 3273−3278.

Chen, D., Zhang, C., Lin, J., Song, X. and Wang, H. (2018.) Screening differential circular RNA expression profiles reveal that hsa_circ_0128298 is a biomarker in the diagnosis and prognosis of hepatocellular carcinoma. *Cancer Management and Research*, **10:** 1275–1283.

Chen, A. and Yang, S. (2015). Replacing antibodies with aptamers in lateral flow immunoassay. *Biosensors and Bioelectronics*, **71:** 230–242.

Chen, C., Luo, M., Ye, T., Li, N., Ji, X. and He, Z. (2015). Sensitive colorimetric detection of protein by gold nanoparticles and rolling circle amplification. Analyst, **140:** 4515–4520

Chen, F., Zhou, J., Luo, F.L., Mohammed, A.B. and Zhang, X.L. (2007). Aptamer from whole-bacterium SELEX as new therapeutic reagent against virulent Mycobacterium tuberculosis. *Biochemical and Biophysical Research Communications*, **357:** 743–748.

Chovelon, B., Durand, G., Dausse, E., Toulmé, J., Faure, P., Peyrin, E. and Ravelet, C. (2016). ELAKCA: Enzyme-Linked Aptamer Kissing Complex Assay as a Small Molecule Sensing Platform. *Analytical Chemistry*, **88**(5): 2570–2575.

Chung, T., Hsu, K., Chen, J., Liu, J., Chang, H., Li, P., Huang, C., Shieh, Y. and Lee, C. (2016). Association of salivary alpha 2-macroglobulin levels and clinical characteristics in type 2 diabetes. *Journal of Diabetes Investigation*, **7**(2): 190–196.

Comucci, E.B., Vasques, A.C., Geloneze, B., Calixto A.R., Pareja J.C. and Tambascia, M.A. (2014). Serum levels of retinol binding protein 4 in women with different levels of adiposity and glucose tolerance. *Brazilian Society of Endocrinology and Metabolism*, **58**(7):709–714.

Coppari R (2017). Diabetes present and future. *The International Journal of Biochemistry and and Cell Biology*, **88:** e197.

Cordera, R. and Adami, G.F. (2016). From bariatric to metabolic surgery: Looking for a "disease modifier" surgery for type 2 diabetes. *World Journal of Diabetes*, **7**(2): 27–33.

Covantev, S., Chiriac, A., Perciuleac, L. and Zozina, V. (2016). Maturity onset diabetes of the young: Diagnosis and treatment options. *Russian Open Medical Journal*, **5**(4): e402

Daniels, D.A., Chen, H., Hicke, B.J., Swiderek, K.M. and Gold, L. (2003). A tenascin-c aptamer identified by tumor cell selex: Systematic evolution of ligands by exponential enrichment. *Proceedings of the National. Academy of Science USA*, **100:** 15416–15421.

Darmostuk, M., Rimpelova, S., Gbelcova, H. and Ruml, T. (2015). Current approaches in SELEX: An update to aptamer selection technology. *Biotechnology Advances*, **33:** 1141–1161.

Deshpande, A.J., Harris-Hayes, M. and Schootman, M. (2008). Epidemiology of diabetes and diabetes related complications. *Physical Therapy*, **88** (11): 1254–1264.

Dhiman, A., Kalraa, P, Bansal, V., Bruno J.G. and Sharma T.K. (2017) Review: Aptamer-based point-of-care diagnostic platforms. *Sensors and Actuators B: Chemical*, **246**: 535–553.

DiMatteo, M.R., Giordani, P.J., Lepper, H.S. and Croghan, T.W. (2002). Patient adherence and medical treatment outcomes: A meta-analysis. *Medical Care*, **40**(9):794–811.

Dinneen, S.F. (2006). What is diabetes? *MPMED Medicine,* **34**(2): 45-46.

Dizgah, I.M. (2013). Stimulated saliva glucose as a diagnostic specimen for detection of diabetes mellitus. *Journal of Archives in Military Medicine*, **1**(1): 24–27.

Drescher, D.G., Ramakrishnan, N.A. and Drescher M.J. (2009). Surface Plasmon Resonance (SPR) Analysis of Binding Interactions of Proteins in Inner-Ear Sensory Epithelia. *Methods in Molecular Biology*, **493:** 323–343.

Duan, N., Gong, W., Wu, S. and Wang, Z. (2017). An ssDNA library immobilized SELEX technique for the selection of an aptamer against Ractopamine. *Analytica Chimica Acta*, **961:** 100–105.

Duan, N., Ding, X.Y., Wu, S.J., Xia, Y., Ma, X.Y., Wang, Z.P. and Chen, J. (2013). In vitro selection of a DNA aptamer targeted against *Shigella dysenteriae*. *Journal of Microbiological. Methods*, **94:** 170–174.

Dunmore, S.J. and Brown, J.E. (2013). The role of adipokines in beta cell failure of type 2 diabetes. *Journal of Endocrinology*, **216**(1): 37–45.

Eaton BE, Gold L and Zichi DA (1995). Let's get specific: the relationship between specificity and affinity. *Chemistry and Biology*, **2:** 633–638.

Ellington, A.D. and Szostak, J.W. (1990). In vitro selection of RNA molecules that bind speci fic ligands. *Nature*, **346** (30): 818–822.

Entzian, C. and Schubert, T. (2016). Studying small molecule-aptamer interactions using MicroScale Thermophoresis (MST). *Methods*, **97:** 27–34.

Espiritu, C.A, Justo, C.A.C., Jauset Rubio, M., Svobodova, M., Bashammakh, A.S., Alyoubi, A.O., Rivera, W.L., Rollon, A.P. and O'Sullivan C.K. (2018). Aptamer selection against Trichomonas vaginalis adhesion protein for diagnostic application. *ACS Infectious Diseases*, **4:** 1306–1315.

Estruch, R., Ros, E., Salas-Salvadó, J., Covas, M., Corella, D., Arós, F., Gómez-Gracia, E., Ruiz-Gutiérrez, V., Fiol, M., Lapetra, J., Lamuela-Raventos, R.M., Serra-Majem, L., Pintó, X., Basora, J., Muñoz, M.A., Sorlí, J.V., Martínez, J.A. and Martínez-González, M.A. (2013). Primary prevention of cardiovascular disease with a Mediterranean diet. *The New England journal of medicine,* **368**(14): 1279–1290.

Fang, X., Sen, A., Vicens, M. and Tan. W. (2003). Synthetic DNA Aptamers to detect Proteins Molecular Variants in a High-Throughput Fluorescence Quenching Assay. *ChemBioChem*, **4**(9): 829–834.

Festa, A., D'Agostino, R Jr., Tracy, R.P. and Haffner, S.M. (2002). Insulin Resistance Atherosclerosis Study Elevated levels of acute-phase proteins and plasminogen activator inhibitor-1 predict the development of type 2 diabetes: the insulin resistance atherosclerosis study. *Diabetes*, **51**(4): 1131–1137.

Florinel-Gabriel, B. (2012). Chemical Sensors and Biosensors: Fundamentals and Applications. Chichester, UK: John Wiley & Sons. 576. ISBN 9781118354230

Gatto, B., Palumbo, M. and Sissi, C. (2009). Nucleic acid aptamers based on the G-quadruplex structure: therapeutic and diagnostic potential. *Current Medicinal Chemistry*, **16:** 1248–1265

Gold, L. and Tuerk, C. (1993). Methods for identifying nucleic acid ligands. US5270163

Gold, L.B.P., Uhlenbeck, O. and Yarus, M. (1995). Diversity of oligonucleotide functions. *Annual Review of Biochemistry*, **64:** 763–797.

Gopinath, S.C., Lakshmipriya, T., Chen, Y., Phang, W.M. and Hashim, U. (2016). Aptamer-based 'point-of-care testing, *Biotechnology Advances*, **34:** 198–208.

Graham, T.E., Yang, Q., Bluher, M., Hammarstedt, A., Ciaraldi, T.P., Henry, R.R., Wason, C.J., Oberbach, A., Jansson, P.A., Smith, U. and Kahn, B.B. (2006). Retinol-binding protein 4 and insulin resistance in lean,obese, and diabetic subjects. *New England Journal of Medicine*, **354:** 2552–2563.

Groop, L. and Pociot, F. (2013). Genetics of diabetes - Are we missing the genes or the disease? *Molecular and Cell Endocrinology*, **25**(1): 726–739.

Guo, L.H. and Kim, D.H. (2012). LSPR biomolecular assay with high sensitivity induced by aptamer-antigen-antibody sandwich complex. *Biosensors and Bioelectronics*, **31:** 567–750.

Han, H.S., Kang, G., Kim J.S, Chooi, B. and Koo S.H. (2016). Regulation of glucose metabolism from a liver-centric perspective. *Experimental and Molecular Medicine*, **48:** e218; doi:10.1038/emm.2015.122

Hermann, T. and Patel, D.J. (2000). Adaptive Recognition by Nucleic Acid Aptamers. *Science*, **287:** 820–825.

Henry, N.L. and Hayes D.F. (2012). Cancer biomarkers. *Molecular Oncology*, **6**(2):140–146.

Hirtz, C., Chevalier, F., Sommerer, N., Raingeard, I., Bringer, J., Rossignol, M. de Périere D.D. (2006). Salivary protein profiling in type I diabetes using two-dimensional electrophoresis and mass spectrometry. *Clinical Proteomics*, **2:** 117–127.

Hoinka, J., Zotenko, E., Friedman A., Sauna, Z.E. and Przytycka1 T.M. (2012). Identification of sequence–structure RNA binding motifs for SELEX-derived aptamers. *Bioinformatics*, **28**(12): i215-23.

Hyle, E.P., Jani, I.V., Lehe, J., Su, A.E., Wood, R., Quevedo, J., Losina, E., Bassett, I.V., Pei, P.P., Paltie,l D.A., Resch, S., Freedberg, K.A., Peter, T. and Walensky, R.P. (2014). The Clinical and Economic Impact of Point-of-Care CD4 Testing in Mozambique and Other Resource-Limited Settings: A Cost-Effectiveness Analysis. *PLoS Medicine*, **11**(9): 1–15.

Hu, J., Wang, S., Wang, L., Li, F., Pingguan-Murphy, B., Lu, T.J. and Xu, F. (2014). Advances in paper-based point-of-care diagnostics. *Biosensors and Bioelectronics*, **54:** 585–597.

Hung, P.H., Lu, Y.C., Chen, Y.W., Chou, H.C., Lyu, P.C., Lee, Y.R. and Chan, H.L. (2011). Proteomic identification of plasma signatures in type 2 diabetic nephropathy. *Journal of Integrated Omics*, **1**(1): 151–156.

Hurst, S.J., Lytton-Jean, A.K. and Mirkin, C.A. (2006). Maximizing DNA loading on a range of gold nanoparticle sizes. *Analytical Chemistry*, **78:** 8313–8318.

Insel, R.A., Dunne, J.L., Atkinson, M.A., Chiang, J.L., Dabelea, D., Gottlieb, P.A., Greenbaum C.J., Herold, K.C., Krischer, J.P., Lernmark, A., Ratner, R.E., Rewers, M.J., Schatz, D.A., Skyler, J.S., Sosenko, J.M. and Ziegler, A.G. (2015). Staging Presymptomatic Type 1 Diabetes: A Scientific Statement of JDRF, the Endocrine Society and the American Diabetes Association. *Diabetes Care*, **38:** 1964–1974.

International Diabetes Ferderation (IDF). (2018) Diabetes atlas - Home. Available: http://www.diabetesatlas.org/. (Retrieved April 2018)

International Diabetes Ferderation (IDF). (2017) Diabetes Atlas. 8th edition, 2017. Available: http://www. diabetesatlas. org/resources/. (Retrieved 03 May 2018).

Invitrogen (2010) Molecular Probes Handbook: A Guide to Fluorescent Probes and Labeling Technologies. Invitrogen, Waltham, MA, USA.

James, W. (2000). Aptamers. In: Meyers, R.A. (Ed.), Encyclopedia of Analytical Chemistry. John Wiley & Sons Ltd., Chichester, 4848–4871.

Järvelä, I.Y., Juutinen, J., Koskela, P., Hartikainen, A.L., Kulmala, P., Knip, M. and Tapanainen, J.S. (2006). Gestational diabetes identifies women at risk for permanent type 1 and type 2 diabetes in fertile age: Predictive role of autoantibodies. *Diabetes Care*, **29** (3): 607–612.

Jauset-Rubio, M., El-Shahawi M.S., Bashammakh A.S., Alyoubi A.O. and O′Sullivana C.K. (2017). Advances in aptamers-based lateral flow assays. *Trends in Analytical Chemistry*, **97:** 385–398.

Jauset-Rubio, M., Svobodova, M., Mairal, T., McNeil, C., Keegan, N., El-Shahawi, M.S., Bashammakh, A.S., Alyoubi, A.O. and O'Sullivan C.K. (2016). Aptamer lateral flow assays

for ultrasensitive detection of beta-conglutin combining recombinase polymerase amplification and tailed primers, *Analytical Chemistry*, **88**(21): 10701–10709.

Jauset-Rubio, M., Svobodová, M., Mairal, T., Schubert, T., Künne, S., Mayer. G. and O'Sullivan, C.K. (2016). β-Conglutin dual aptamers binding distinct apatopes. *Analytical and Bioanalytical Chemistry*, **408**(3): 875–884.

Jenison, R.D., Gill, S.C., Pardi, A. and Polisky, B. (1994). High-resolution molecular discrimination by RNA. *Science*, **263:** 1425–1429.

Joubert, J., Norman, R, Bradshaw, D., Goedecke, J.H., Steyn, N.P. and Puoane, T. (2007). Estimating the burden of disease attributable to excess body weight in South Africa in 2000. *S*outh *African Medical Journal*, **97:** 683–90.

Kaku, K. (2010). Pathophysiology of Type 2 Diabetes and its treatment policy. *Japan Medical Association Journal*, **53**(1): 41–46.

Kamnev, A. A. (2013). Infrared Spectroscopy in Studying Biofunctionalised Gold Nanoparticles. *Nanomaterials Imaging Techniques, Surface Studies, and Applications*, **146:** 35–50.

Kapustin, J.F (2008). Postpartum management for gestational diabetes mellitus: Policy and practice implications. *Journal of the American Academy of Nurse Practitioners*, **20:** 547–554

Keefe, A.D., Pai, S. and Ellington, A. (2010). Aptamers as therapeutics. *Nature Reviews Drug Discovery*, **9:** 537–550.

Kengne, A.P., Echouffo-Tcheugui, J.B., Sobngwi, E., and Mbanya J.C. (2013). New insights on diabetes mellitus and obesity in Africa-part 1: prevalence, pathogenesis and comorbidities. *Heart*, **99**(14): 979–983.

Kim, S.E., Ahn, K.Y., Park, J.S., Kim, K.R., Lee, K.E., Han, S.S. and Lee, J. (2011). Fluorescent Ferritin Nanoparticles and Application to the Aptamer Sensor. *Analytical Chemistry*, **83**(15):5834–5843.

Koczula, K.M. and Gallotta, A. (2016). Lateral flow assays. *Essays in Biochemistry*, **60:** 111–120.

Kolberg J. A., Jorgensen T., Gerwien R. W., Hamren, S., McKenna, M.P., Moler, E., Rowe, M.W., Urdea, M.S., Xu, X.M., Hansen, T., Pedersen, O. and Borch-Johnsen, K. (2009). Development of a type 2 diabetes risk model from a panel of serum biomarkers from the Inter99 cohort. *Diabetes Care*, **32**(7): 1207–1212.

Kumar, B., Smita, K., Cumba L., Debut, A. and Pathak, R.N. (2014). Sonochemical Synthesis of Silver Nanoparticles Using Starch: A Comparison. *Bioinorganic Chemistry and Applications*, 2014:784268.

Kumar, P.J. and Clark, M. (2002). Textbook of Clinical Medicine. Pub: Saunders,London, UK. 1099–1121.

Kaur, H. and Yung L-Y.L. (2012). Probing High Affinity Sequences of DNA Aptamer against VEGF165. *PLoS One*, **7**(2): e31196.

Lauridsen, L.H., Shamaileh, H.A., Edwards, S.L., Taran, E. and Veedu, R.N. (2012). Rapid One-Step Selection Method for Generating Nucleic Acid Aptamers: Development of a DNA Aptamer against a-Bungarotoxin. *PLoS One*, **7**(7): e41702.

Lee, Y.J., Han, S.R., Maeng, J.S., Cho, Y.J. and Lee, S.W. (2012). In vitro selection of Escherichia coli O157:H7-specific RNA aptamer. *Biochemical and Biophysical Research Communications*, **417:** 414–420.

Lee, S.J., Youn, B., Park, J.W., Niazi, J.H., Kim, S.K. and Gu, M.B. (2008). SsDNA APTAMER-BASED Surface Plasmon Resonance biosensor for the detection of Retinol Binding Protein 4 for the early detection if Type 2 Diabetes. *Analytical Chemistry*, **80:** 2867–2873.

Lenčová, E., Broukal, Z. and Spížek, J. (2010). Point-of-care salivary microbial tests for detection of cariogenic species-clinical relevance thereof-review, *Folia Microbiologica*, **55**(6): 559–568.

Li, L., Yang, G., Li, Q., Tang, Y., Yang, M., Yang, H. and Li, K. (2006). Changes and relations of circulating visfatin, apelin, and resistin levels in normal, impaired glucose tolerance, and type 2 diabetic subjects. *Experimental and Clinical Endocrinology and Diabetes*, **114**(10): 544–548.

Li, J., Jing, L., Song, Y., Zhang J., Chen, Q., Wang, B., Xia, X. and Han, Q. (2018). Rapid detection of Rongalite via a sandwich lateral flow strip assay using a pair of aptamers. *Nanoscale Research Letters*. **13**(1): 296.

Lin, H.I., Wu, C.C., Yang, C.H., Chang, K.W., Lee, G.B and Shiesh, S.C. (2015) Selection of aptamers specific for glycated haemoglobin and total haemoglobin using on-chip SELEX. *Lab Chip*, **15**(2): 486–494.

Liu, J., Cao, Z. and Lu, Y. (2009). Functional nucleic acid sensors. *Chemical Review*, **109**(5): 1948–1998.

Liu, G.D., Mao, X., Phillips, J.A., Xu, H., Tan, W.H. and Zeng, L.W. (2009). Aptamer-Nanoparticle Strip Biosensor for Sensitive Detection of Cancer Cells. *Analytical Chemistry*, **81:** 10013–10018.

Liu, J. and Lu, Y. (2006). Preparation of aptamer-linked gold nanoparticle purple aggregates for colorimetric sensing of analytes. *Nature Protocols*, **1:** 246–252.

Lowe, J., Taveira-da-Silva, R. and Hilario-Souz, E. (2017). Dissecting Copper Homeostasis in Diabetes Mellitus. *International Union of Biochemistry and Molecular Biology Life*, **69**(4): 255–262.

Lowe W.L. and Karban J. (2015). Genetics, genomics and metabolomics: new insights into maternal metabolism during pregnancy. *Diabetic Medicine*, **31**(3): 254–262.

Lowe, W.L (2005). Principles of Molecular Medicine, Humana Press, New Jersey, NJ, USA, 16th edition.

Luong, J.H., Male, K.B. and Glennon, J.D. (2008). Biosensor technology: technology push versus market pull. *Biotechnology Advances*, **26**(5): 492–500.

Malamud, D. (2011). Saliva as a Diagnostic Fluid. *Dental Clinics of North America*, **55**(1) 159–178.

Malathi, N., Mythili, S. and Vasanthi, H.R. (2014). Salivary diagnostics: a brief review. *ISRN dentistry*, 158786.

Mallikaratchy, P., Tang, Z., Kwame, S., Meng, L., Shangguan, D. and Tan, W. (2007) Aptamer directly evolved from live cells recognizes membrane bound immunoglobin heavy mu chain in Burkitt's lymphoma cells. *Molecular and Cell Proteomics*, **6**(12): 2230–2238.

Mao, X., Phillips, J.A., Xua, H., Tanb, W., Zengc, L. and Liua, G. (2009). Aptamer-Nanoparticle Strip Biosensor for Rapid and Sensitive Detection of Cancer Cell. *Analytical Chemistry*, ***81*(**24): 1001–1008.

Mason, J.M., Hancock, H.C., Close, H., Murphy, J.J., Fuat, A., de Belder, M., Singh, R., Teggert, A., Wood, E., Brennan, G., Hussain, N., Kumar, N., Manshani, N., Hodges, D., Wilson, D. and Hungin, A.P.S. (2013). Utility of Biomarkers in the Differential Diagnosis of Heart Failure in Older People: Findings from the Heart Failure in Care Homes (HFinCH) Diagnostic Accuracy Study. *PLoS ONE*, **8**(1), e53560.

McDermott, J.E., Wang, J., Mitchell, H., Webb-Robertson, B., Hafen, R., Ramey, J., and Rodland, K.D. (2013). Challenges in Biomarker Discovery: Combining Expert Insights with Statistical Analysis of Complex Omics Data. *Expert Opinion on Medical Diagnostics*, Expert **7**(1): 37–51.

Mendonsa, S.D and Bowser, M.T. (2004). In vitro selection of high-affinity DNA ligands for human IgE using capillary electrophoresis. *Analytical Chemistry*, **76**(18): 5387–5392.

Melmed, S., Kenneth, P., Larsen, P.R. and Henry, K. (eds.). Williams textbook of endocrinology (12th ed.). *Philadelphia: Elsevier/Saunders*, 1371–1435. ISBN 978-1-4377-0324-5.

Miller, K., Kim, A., Kilimnik, G., Jo, J., Moka, U., Periwal, V. and Hara, M. (2009). Islet formation during the neonatal development in mice. *PLoS One*, **4**(11): e7739.

Millipore (2009) Rapid Lateral Flow Test Strips: Consideration for Product Development. http:www.millipore.com/techpublications/tech1/tb500en500.

Molesworth, A.M., Ndhlovu, R., Banda, E., Saul, J., Ngwira, B., Glynn, J.R., Crampin, A.C. and French, N. (2010). High accuracy of home-based community rapid HIV testing in rural Malawi. *Journal of Acquired Immune Deficiency Syndromes*, **55**(5): 625–30.

Mondal, B., Ramlal, S., Lavu, P.S., Bhavanashri, N. and Kingston, J. (2018). Highly Sensitive Colorimetric Biosensor for Staphylococcal Enterotoxin B by a Label-Free Aptamer and Gold Nanoparticles. *Frontiers in Microbiology*, **9:** 179. doi: 10.3389/fmicb.2018.00179

Morales-Narvaez, E., Naghdi, T., Zor, E. and Merkoci, A. (2015). Photoluminescent lateral-flow immunoassay revealed by graphene oxide: highly sensitive paper-based pathogen detection. *Analytical Chemistry*, **87:** 8573–8577.

Mosing, R.K., Mendonsa, S.D. and Bowser, M.T. (2005). Capillary electrophoresis-SELEX selection of aptamers with affinity for HIV-1 reverse transcriptase. *Analytical Chemistry*, **77:** 6107–6112.

Nadal, P., Pinto, A., Svobodova, M., Canela, N. and O'Sullivan, C.K. (2012). DNA aptamer against Lup an 1 food allegen. *PLoS ONE*, **7**(4): e35253.

Nakanishi, T., Koyama, R., Ikeda, T. and Shimizu A. (2002). Catalogue of soluble proteins in the human vitreous humor: comparison between diabetic retinopathy and macular hole. *Journal of Chromatography B: Analytical Technologies in the Biomedical and Life Sciences*, **776**(1): 89–100.

Nanocomposix. (2012). Zeta Potential Analysis of Nanoparticles. NanoComposix, **11**: 1-6.

Nara, S., Tripathib, V., Singh, H. and Shrivastav, T.G. (2010). Colloidal gold probe based rapid immunochromatographic strip assay for cortisol. *Analytica Chimica Acta*, **682:** 66–71.

Nathan, D.M., Cleary, P.A., Backlund, J.Y., Genuth, S.M., Lachin, J.M., Orchard, T.J., Raskin, P., Zinman, B. and Diabetes Control and Complications Trial/Epidemiology of Diabetes Interventions and Complications (DCCT/EDIC) Study Research Group (2005). Intensive diabetes treatment and cardiovascular disease in patients with type 1 diabetes. *The New England Journal of Medicine*, **353(**25): 2643–53.

Newcomer, M.E. and Ong, D.E. (2000). Plasma retinol binding protein: structure and function of the prototypic lipocalin. *Biochimica et Biophysica Acta*, **1482:** 57–64.

Newmand, J.D. and Setford, S.J. (2006). Enzymatic biosensors. *Molecular Biotechnology*, **32:** 249–268.

Ng, M., Fleming, T., Robinson, M., Thomson, B., Graetz, N., and Margono, C. (2014). Global, regional, and national prevalence of overweight and obesity in children and adults during 1980-2013: a systematic analysis for the Global Burden of Disease Study 2013. *Lancet*, **384** (9945):766–781.

Ngo V.K.T., Nguyen H.P.U., Huynh T.P., Tran N.N.P., Lam Q.V. and Huynh T.D. (2015). Preparation of gold nanoparticles by microwave heating and application of spectroscopy to study conjugate of gold nanoparticles with antibody E. coli O157:H7. *Advances in Natural Sciences: Nanoscience and Nanotechnology*, **6** (3): e35016.

Ngom, B., Guo, Y., Wang, X. and Bi, D. (2010). Development and application of lateral flow test strip technology for detection of infectious agents and chemical contaminants: a review. *Analytical and Bioanalytical Chemistry*, **397:** 1113–1135.

Nitsche, A., Kurth, A., Dunkhorst, A., Pänk, O., Sielaff, H., Junge, W., Muth, D., Scheller, F., Stöcklein, W., Dahmen, C., Pauli, G. and Kage A. (2007). One-step selection of Vaccinia virus-binding DNA aptamers by MonoLEX. *BMC Biotechnology*, **7**(48): 18–23.

Nomiyama, T. and Yanase, T. (2015). Secondary diabetes. *Nihon Rinsho*, **73**(12):2008–2012.

Onat, A., Hergenç, G., Bulur, S., Ugur, M., Kuç¨ukdurmaz Z and Can G (2010). The paradox of high apo- lipoprotein A-I levels independently predicting incident type-2 diabetes among Turks. *International Journal of Cardiology*, **142:** 72–79.

Ooi, C.P. and Loke, S.C. (2012). Colesevelam for type 2 diabetes mellitus. *The Cochrane Database of Systematic Reviews*, **12:** CD009361. Ottermann, B. (2012). Prevalence of diabetes in South Africa. Available: http://www.health24.com/Medical/Diabetes/About-diabetes/Diabetes-tsunamihits-South-Africa20130210. (Retrived May 2018).

Ou, L.J., Jin, P.Y., Chu, X., Jiang, J.H., Yu, R.Q. (2010). Sensitive and Visual Detection of Sequence-Specific DNA-Binding Protein via a Gold Nanoparticle-Based Colorimetric Biosensor. *Analytical Chemistry*, **82:** 6015−6024.

Panchbhai, A.S. (212). Correlation of salivary glucose level with blood glucose level in diabetes mellitus. *Journal of Oral Maxillofacial Research*, **3**(3):1−6.

Panda, A., Venkatapathy, R. and Oza, N. (2012). Glucose estimation in the salivary secretion of diabetes mellitus patients: diabetes, metabolic syndrome and obesity. *Targets and Therapy*, **5:** 149–54.

Peer, N., Kengne, A.P., Motala, A.A., Mbanya, J.C. (2014). Diabetes in the Africa region: an update. *Diabetes Research and Clinical Practice*, **103:** 197–205.

Pendergrast, P.S., Marsh, H.N., Grate, D., Healy, J.M., Stanton, M. (2005). Nucleic acid aptamers for target validation and therapeutic applications. *Journal of biomolecular techniques*, **16**(3): 224–234.

Philip, D. (2008). Synthesis and spectroscopic characterization of gold nanoparticles. Spectrochimica Acta. Part A, *Molecular and Biomolecular Spectroscopy*, **71**(1): 80–85.

Piganeau, N. and Schroeder, R. (2003). Aptamer structures: a preview into regulatory pathways? *Chemical Biology*, **10**(2): 103–104.

Pociot, F. and Lernmark, A. (2016). Genetic risk factors for type 1 diabetes. *The Lancet*, **387**(10035): 2331–2339.

Porta, M., Toppila, I., Sandholm, N., Hosseini, S,M., Forsblom, C., Hietala, K., Borio, L., Harjutsalo, V., Klein, B.E., Klein, R., Paterson A.D. and Per-Henrik Groop P-H. (2016). Variation in SLC19A3 and Protection from Microvascular Damage in Type 1 Diabetes. *Diabetes*, **65**(4): 1022–1030.

Peer, D., Karp, J.M., Hong, S., FarokHzad, O.C., Margalit, R. and Langer, R. (2007). Nanocarriers as an emerging platform for cancer therapy. *Nature Nanotechnology*, **2:** 751 – 760.

Pultar, J., Sauer, U., Domnanich, P. and Preininger, C. (2009). Aptamer-antibody on-chip sandwich immunoassay for detection of CRP in spiked serum. *Biosensors and Bioelectronics*, **24:** 1457–1461.

Qadami, F., Molaeirad, A., Alijanianzadeh, M., Azizi, A. and Kamali, N. (2018). Localized Surface Plasmon Resonance (LSPR)-Based Nanobiosensor for Methamphetamin Measurements. *Plasmonics*, **13:** 2091–2098.

Quesada-González, D. and Merkoçi, A.M. (2018). Nanomaterial-based devices for point-of-care diagnostic applications. *Chemical Society Reviews*, **47**(13): 4697–4709.

Rao, P.V., Reddy, A.P., Lu, X., Dasari, S., Krishnaprasad, A., Biggs, E., Roberts, C.T. and Nagalla, S.R. (2009). Proteomic identification of salivary biomarkers of type 2 diabetes. *Journal of Proteome Research*, **8**(1): 239–245.

Rao, C.N.R. and Biswas, K. (2009). Characterization of nanomaterials by physical methods. *Annual Review of Analytical Chemistry*, **2:** 435–462.

Raston, N.H.A., Nguyen, V.T. and Gu, M.B. (2017). A new lateral flow strip assay (LFSA) using apair of aptamers for the detection of Vaspin. *Biosensors and Bioelectronics*, **93:** 21–25.

Raston, N.H.A. and Gu, M.B. (2015). Highly amplified detection of visceral adipose tissue derived serpin (vaspin) using a cognate aptamer duo. *Biosensors and Bioelectronics*, **70:** 261–267.

Rey, E., O'Dell, D, Mehta, S. and Erickson D. (2017). Mitigating the hook effect in lateral flow sandwich immunoassays using real-time reaction kinetics. *Analytical Chemistry*, **89**(9): 5097–5100.

Riaz, S. (2009). Diabetes mellitus. *Scientific Research and Essays*, **4**(5): 367–373.

Rodriguez, Z.J. and O'Kennedy, R. (2017). New approaches for the develoment of diagnostic systems. *Medical Sciences*, **38:** 18–23.

Sajid, M., Kawde A. and Daud, M. (2015). Designs, formats and applications of lateral flow assay: A literature review. *Journal of Saudi Chemical Society*, **19**(6): 689–705.

Sajid, V.S., Choe, H.C. and Young, K.W.K. (2010). Nanotechnology in biomedical applications - a review. *International Journal of Nano Biomaterials*, **3:** 119–139.

Sasongko, M.B., Wong, T.Y., Nguyen, T.T., Kawasaki, R., Jenkins, A., Shaw, J. and Wang, J.J. (2011) Serum apolipoprotein AI and B are stronger biomarkers of diabetic retinopathy than traditional lipids. *Diabetes Care*, **34**(2): 474–479.

Schütze T., Wilhelm, B., Greiner, N., Braun, H., Peter, F., Mörl, M., Erdmann, V.A., Lehrach, H., Konthur, Z., Menger, M., Arndt, P.F. and Glökler, J. (2011). Probing the SELEX Process with Next-Generation Sequencing. *PLoS One*, **6**(12): e29604.

Setlem, K., Mondal, B., Ramlal, S. and Kingston, J. (2016). Immuno affinity selex for simple, rapid, and cost-effective aptamer enrichment and identification against aflatoxin B1. *Frontiers in Microbiology*, **7:** e1909.

Sharma, T.K., Bruno, J.G. and Dhiman, A. (2017). ABCs of DNA aptamer and related assay development. *Biotechnology Advances*, **35** (2): 275–301.

Sharma, T. K., Bruno, J. G., and Cho, W. C. (2016). The point behind translation of aptamers for Point of Care Diagnostics. *Aptamers and Synthetic Antibodies*, **3**(1): 36–42.

Sharma S, Julia Zapatero-Rodrgíuez, Estrela P and O'Kennedy R (2015). Point-of-Care Diagnostics in Low Resource Settings: Present Status and Future Role of Microfluidics. *Biosensors-Basel*, **5**(3): 577–601.

Sharma, T.K. and Shukla, R. (2014). Nucleic acid aptamers as an emerging diagnostic tool for animal pathogens. *Advances in Animal and Veterinary Sciences*, **2:** 50–55.

Shen, G., Zhang, S. and Hu, X. (2013). Signal enhancement in a lateral flow immunoassay based on dual gold nanoparticle conjugates, *Clinical Biochemistry*. **46**(16-17): 1734–1738.

Shim, W.B., Kim, M.J., Mun, H. and Kim, M.G. (2014). An aptamer-based dipstick assay for the rapid and simple detection of aflatoxin B1. *Biosensors and Bioelectronics*, **62:** 288–294.

Shukla, S., Leem, H., Lee, J.S. and Kim, M. (2014). Immunochromatographic strip assay for the rapid and sensitive detection of Salmonella Typhimurium in artificially contaminated tomato samples. *Canadian Journal Microbiology*, **60:** 399–406.

Shoback, D. (2011). Chapter 17. Greenspan's basic and clinical endocrinology (9th ed.). New York: McGraw-Hill Medica.

Schüling, T., Eilers, A., Scheper, T. and Walter, J. (2018). Aptamer-based lateral flow assays. *AIMS Bioengineering*, **5**(2): 78–102.

Sibuyi, N.R.S., Thovhogi, N., Gabuza, K.B., Meyer, M.D., Drah, M., Onani, M.O., Skepu, A., Madiehe, A.M. and Meyer M. (2017). Peptide-functionalized nanoparticles for the selective induction of apoptosis in target cells. *Nanomedicine*, **12:** 1631–1645.

Song, Y., Huang, Y.Y., Liu, X., Zhang, X., Ferrari, M. and Qin, L. (2014). Point-of-care technologies for molecular diagnostics using a drop of blood. *Trends in Biotechnology*, **32:** 132–139.

Song, K.M., Lee, S., Ban, C. (2012). Aptamers and their biological applications. *Sensors*, **12:** 612–631.

Stenström, G., Gottsäter, A., Bakhtadze, E., Berger, B., Sundkvist, G. (2005). Latent autoimmune diabetes in adults: definition, prevalence, beta-cell function, and treatment. *Diabetes*, **54**(2): 68–72.

Stofkova, A. (2010). Resistin and visfatin: regulators of insulin sensitivity, inflammation and immunity. *Endocrine Regulations*, **44**(1): 25–36.

Stoltenburg, R., Schubert, T. and Strhlitz, B. (2015). In vitro selection and interaction studies of a DNA aptamer targeting Protein A. *PLoS One*, **10**(7): e1034403.

Stoltenburg, R., Reinemann, C. and Strehlitz, B. (2005). FluMag-SELEX as an advantageous method for DNA aptamer selection. *Analytical and Bioanalytical Chemistry*, **383**(1): 83–91

Strimbu, K. and Tavel J.A. (2010). What are biomarkers? *Current opinion in HIV and AIDS*, **5**(6): 463–466.

Sun, H. and Zu, Y. (2015). A Highlight of Recent Advances in Aptamer Technology and Its Application. *Molecules*, **20:** 11959-11980.

Sun, J.K., Keenan, H.A., Cavallerano J.D., Asztalos, B.F., Schaefer, E.J., Sell, D.R., Strauch, C.M., Monnier, V.M., Doria, A., Paul Aiello, L. and King G.L. (2011). Protection from Retinopathy and Other Complications in Patients with Type 1 Diabetes of Extreme Duration. *Diabetes Care*, **34**(4): 968–974.

Sun, L., Qi, Q., Zong, G., Ye, X., Li, H., Liu, X., Zheng, H., Hu, F.B, Liu, Y. and Lin, X. (2014). Elevated plasma retinol-binding protein 4 is associated with increased risk of type 2

diabetes in middle-aged and elderly Chinese adults. *The Journal of Nutrition*, **144**(5): 722–728.

Sundsten, T. and Ortsäter, H. (2009). Proteomics in diabetes research. *Molecular and Cellular Endocrinology*, **297:** 93–103.

Srinivasan, B. and Tung, S. (2015). Development and Applications of Portable Biosensors. *Journal of Laboratory Automation*, **20**(4): 365–389.

Svobodová, M., Pianto. A., Nadal, P. and O'Sullivan, C.K. (2012). Comparison of different methods for generation of single-stranded DNA for SELEX processes. *Analytical and Bioanalytical Chemistry*, **404**(3): 835–842

Sypabekova, M., Bekmurzayeva, A., Wang, R., Li, Y., Nogues, C. and Kanayeva, D. (2017). Selection, characterization, and application of DNA aptamers for detection of Mycobacterium tuberculosis secreted protein MPT64. *Tuberculosis*, **104:** 70–78.

Tang, Z.W., Shangguan, D., Wang, K.M., Shi, H., Sefah, K., Mallikratchy, P., Chen, H.W., Li, Y. and Tan, W.H. (2007). Selection of aptamers for molecular recognition and characterization of cancer cells. *Analytical Chemistry*, **79:** 4900–4907.

Takebayashi K., Suetsugu M., Wakabayashi S., Aso, Y. and Inukai, T. (2007). Retinol binding protein-4 levels and clinical features of type 2 diabetes patients. *The Journal of Clinical Endocrinology and Metabolism*, **92**(7): 2712–2719.

Tejaswi, M., Rao, M.C., Datta Prasad, P.V., Giridhar, G., Pisipti, V.G.K.M. and Manepalli, R.K.N.R. (2006). Synthesis and characterization of citrate capped gold nanoparticles and their effect on liquid crystals: optical studies. *Rasayan journal of chemistry*, **9**(4): 697–705.

Thebani, A., Afonso, C., Marret, S. and Bekri, S. (2016). Omics-Based Strategies in Precision Medicine: Toward a Paradigm Shift in Inborn Errors of Metabolism Investigations. *International Journal of Molecular Sciences*, **17**(9): e1555.

Thobhani, S., Attree, S., Boyd, R., Kumarswami, N., Noble, J., Szymanski, M. and Porter, R.A. (2010). Bioconjugation and characterisation of gold colloid-labelled proteins. *Journal of Immunological Methods*, **356:** 60–69.

Tolle, F., Wilke, J., Wengel, J. and Mayer, G. (2014). By-Product Formation in Repetitive PCR Amplification of DNA Libraries during SELEX. *PLoS One*, **9**(12): e114693.

Uludag, Y., Narter, F., Sa ˘glam, E., Köktürk, G., Gök, M.Y., Akgün, M., Barut, S. and Budak S. (2016). An integrated lab-on-a-chip-based electrochemical biosensor for rapid and sensitive detection of cancer biomarkers. *Analytical and Bioanalytical Chemistry*, **408:** 7775–7783.

Umeno, A., Yoshino, K., Hashimoto, Y., Schichiri, M., Kataota, M. and Yoshida, Y. (2015). Multi-Biomarkers for Early Detection of Type 2 Diabetes, Including 10- and 12-(Z,E) Hydroxyoctadecadienoic Acids, Insulin, Leptin,and Adiponectin. *PLoS One*, **10**(7): e0130971.

Unnikrishnan, R., Pradeepa, R., Joshi, S.R. and Mohan, V. (2017). Type 2 Diabetes: Demystifying the Global Epidemic. *Diabetes*, **66:** 1432–1442

Vaishya, S., Sarwade, R.D. and Seshadri, V. (2018). MicroRNA, proteins and metabolites as novel biomarkers for prediabetes, diabetes and related complications. *Frontiers in Endocrinology*, **9:** e80.

Verma, H.N., Sighn, P. and Chavan, R.M. (2014). Gold nanoparticles: synthesis and characterization. *Veterinary World*, **7(**2): 72–77.

Viglasky, V. and Hianik, T. (2013). Potential use of G-quadruplex-forming aptamers. *Physiology and Biophysics*, **32:** 149–172.

Vorster, H.H., Venter, C.S., Wissing, M.P. And Margetts, B.M. (2005). The nutrition and health transition in the North West Province of South Africa: a review of the THUSA (Transition and Health during Urbanisation of South Africans) study. *Public Health Nutrition*, **8:** 480–90.

Wang, J.P., Gong, Q., Maheshwar, N., Eisenstein, M., Arcila, M.L., Kosik, K.S. and Soh, H.T. (2014). Particle display: a quantitative screening method for generating high-affinity aptamers. *Angewandte Chemie International Edition*, **53**(19): 4796–4801.

Wang, Y., Luo, Y., Bing, T., Chen, Z., Lu, M., Zhang, N., Shangguan, D. and Gao, X. (2014). DNA Aptamer Evolved by Cell-SELEX for Recognition of Prostate Cancer. *PLoS One*, **9**(6): e100243.

Wang, C.F., Zhang, L.F. and Shen, X.M. (2013). Development of a nucleic acid lateral flow strip for detection of hepatitis C virus (HCV) core antigen. *Nucleosides Nucleotides Nucleic Acids*, **32**(2): 59–68.

Wang, L., Chen, W., Ma, W., Liu, L., Ma, W., Zhao, Y., Zhu, Y., Xu, L., Kuang, H. and Xu, C. (2011). Fluorescent strip sensor for rapid determination of toxins. *Chemical Communications*, **47**(5): 1574–1576

Wilcox, G. (2005). Insulin and insulin resistance. *The Clinical biochemist. Reviews / Australian Association of Clinical Biochemists*, **26**(2): 19–39.

Willett, W.C. and Leibel, R.L. (2002). Dietary Fat Is Not a Major Determinant of Body Fat. *American Journal of Medicine*, **113**(9B): 47–59.

World Health Organization (WHO). (2016) Global report on Diabetes. Available: http://www.who.int/mediacentre/factsheets/fs312/en/. (Retrived: May 2018)

Wright, T.A. (2011). Salivary diagnostic testing: a "game changer" for patient evaluation. *Compendium of Continuing Education in Dentistry*, **32**(4): 28–29.

Wu, W., Zhao, S., Mao, Y., Fang, Z., Lu, X. and Zeng, L. (2015). A sensitive lateral flow biosensor for Escherichia coli O157:H7 detection based on aptamer mediated strand displacement amplification, *Analytica Chimica Acta*, **861:** 62–68.

Wu, Y., Ding, Y., Tanaka, Y. and Zhang, W. (2014). Risk Factors Contributing to Type 2 Diabetes and Recent Advances in the Treatment and Prevention. *International Journal of Medical Sciences*, **11**(11): 1185–1200.

Wu, H., Yu, Z., Qi, Q., Li, H., Sun, Q. and Lin, X. (2011). Joint analysis of multiple biomarkers for identifying type 2 diabetes in middle-aged and older Chinese: a cross-sectional study. *BMJ Open*, **1**(1): p. e000191.

Xiao, N., Long, Q., Tang. X. and Tang, S. (2014). A community-based approach to non-communicable chronic disease management within a context of advancing universal health coverage in China: progress and challenges. *BioMed Central*, **14:** 2–6.

Xu, Y., Tan, S., Liang, Q. and Ding M. (2007). One-Step Facile Synthesis of Aptamer-Modified Graphene Oxide for Highly Specific Enrichment of Human A-Thrombin in Plasma. *Sensors*, **17:** e1986.

Xu, H., Mao, X., Zeng, Q.X., Wang, S.F., Kawde, A.N. and Liu, G. D. (2009). Aptamer-functionalized gold nanoparticles as probes in a dry-reagent strip biosensor for protein analysis. *Analytical Chemistry*, **81:** 669−676.

Xu, J.W., Morita, I., Ikeda, K., Miki, T. and Yamori, Y. (2007). C-reactive protein suppresses insulin signalling in endothelial cells: role of spleen tyrosine kinase. *Molecular Endocrinology*, **21:** 564–573.

Xu, H., Mao, X., Zeng, Q., Wang, S., Kawde, A.N. and Liu, G. (2006). Aptamer-functionalized gold nanoparticles as probes in a dry-reagent strip biosensor for protein analysis. *Analytical Chemistry*, **81:** 669–675.

Yang, Q., Graham, T.E., Mody, N., Preitner, F., Peroni, O.D., Zabolotny, J.M., Kotani, K., Quadro, L. and Kahn, B.B. (2005). Serum retinol binding protein 4 contributes to insulin resistance in obesity and type 2 diabetes. *Nature*, **436:** 356–362.

Yu, L., Ng, S.R., Xu, Y., Dong, H., Wang, Y.J. and Li, C.M. (2013). Advances of lab-on-a-chip in isolation, detection and post-processing of circulating tumour cells. *Lab on a Chip*, **13:** 3163–3182.

Yudkin, J.S., Juhan-Vague, I., Hawe, E., Humphries, S.E., di Minno, G., Margaglione, M., Tremoli, E., Kooistra, T., Morange, P.E., Lundman, P., Mohamed-Ali, V. and Hamsten, A. (2004). Low-grade inflammation may play a role in the etiology of the metabolic syndrome in patients with coronary heart disease: the HIFMECH study. *Metabolism*, **53:** 852–857.

Zhang, X., Servo, M.R. and Liu, J. (2012). Surface science of DNA adsorption onto citrate-capped gold nanoparticles. *Langmuir*, **28:** 3896–3902.

Zhang, J., Wang, X.L. and Yang, X.R. (2012). Colorimetric determination of hypochlorite with unmodified gold nanoparticles through the oxidation of a stabilizer thiol compound. *Analyst*, **137:** 2806–2812.

Zhou, J., and Rossi, J. (2017). Aptamers as targeted therapeutics: current potential and challenges. *Nature Reviews Drug Discovery*, **16:** 181–202.

Zhou, W. L., Kong, W.J., Dou, X.W., Zhao, M., Ouyang, Z. and Yang, M.H. (2016). An aptamer based lateral flow strip for on-site rapid detection of ochratoxin A in *Astragalus membranceus*. *Journal of chromatography. B, Analytical Technologies in the Biomedical and Life Sciences*, **1022:** 102−108.

Zhu, C., Zhao, Y., Yan, M., Huang, Y., Yan, J., Bai, W. and Chen, A. (2016). A sandwich dipstick assay for ATP detection based on split aptamer fragments. *Analytical and Bioanalytical Chemistry*, **408:** 4151–4158.

Zhu, G., Lübbecke, M., Walter, JG., Stahl, F., Scheper, T. (2011). Characterization of Optimal Aptamer-Microarray Binding Chemistry and Spacer Design. *Chemical Engineering and Technology*, **34:** 2022–2028.

Zimbone, M., Baeri. P., Calcagno, L., Musumeci P., Contino, A. Barcellona, M.L and Bonaventura G. (2014). Dynamic light scattering on bioconjugated laser generated gold nanoparticles. *PLoS One*, **9**(3): e89048.

APPENDIX A: MULTIPLE SECONDARY STRUCTURES OF RBA-1

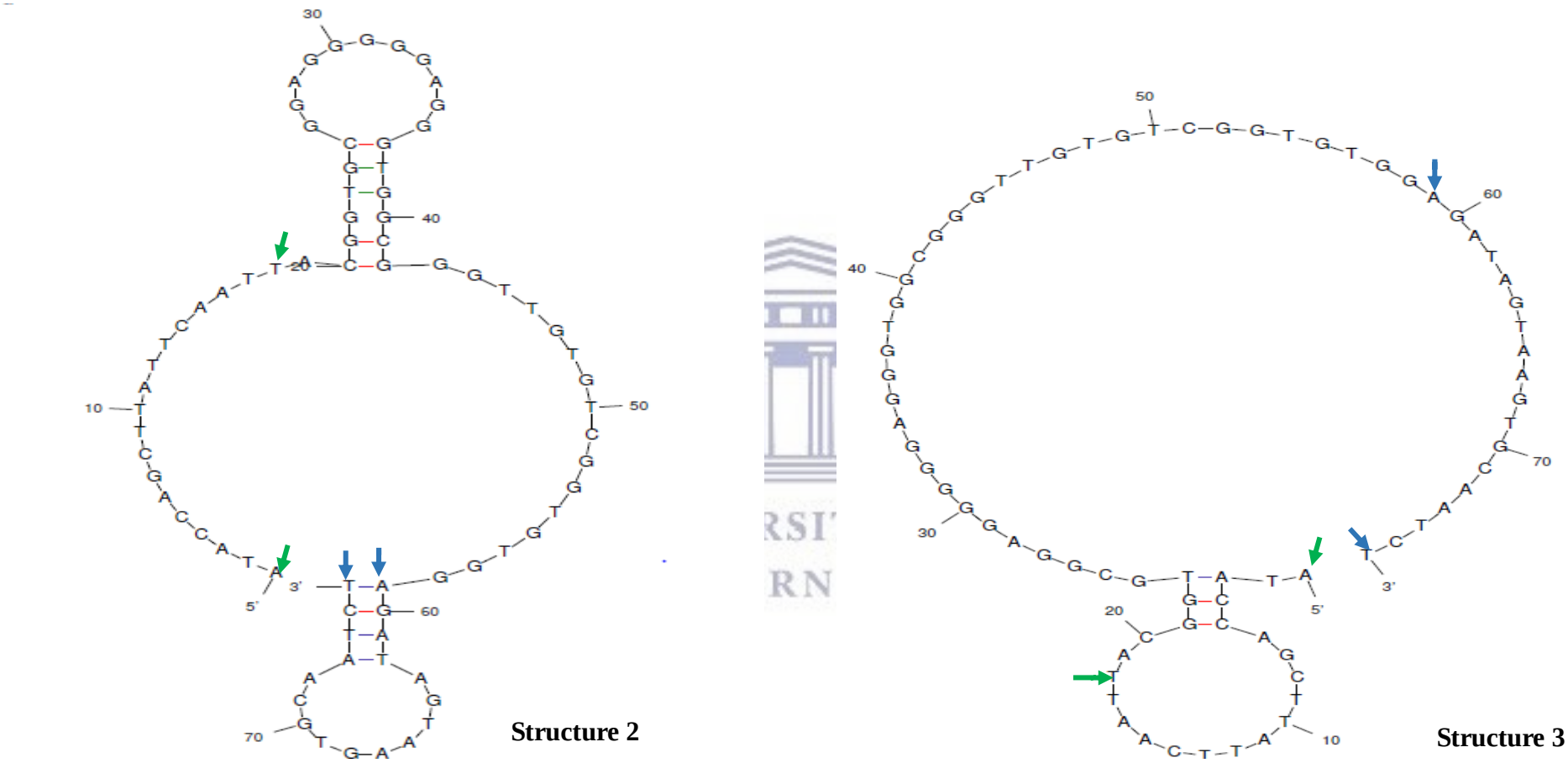

Figure A.1: Secondary structure prediction of RBA-1: (2) (ΔG= -0.18 kJ mol^{-1}) and (3) (ΔG= -0.06 kJ mol^{-1}) as predicted by the M-fold program. The ΔG represents the minimum free energy of each aptamer. The forward primer sequence (base 1-18) is shown by the green colour and the reverse primer (base 59-76) are shown by the blue colour.

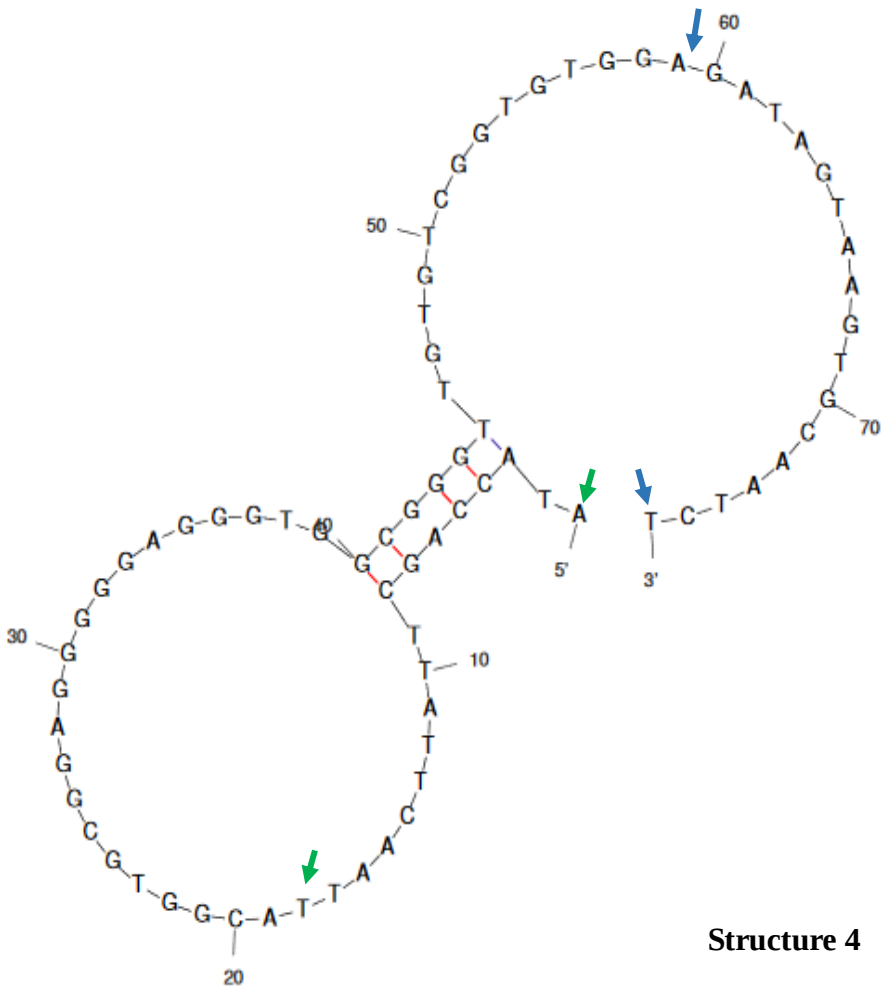

Structure 4

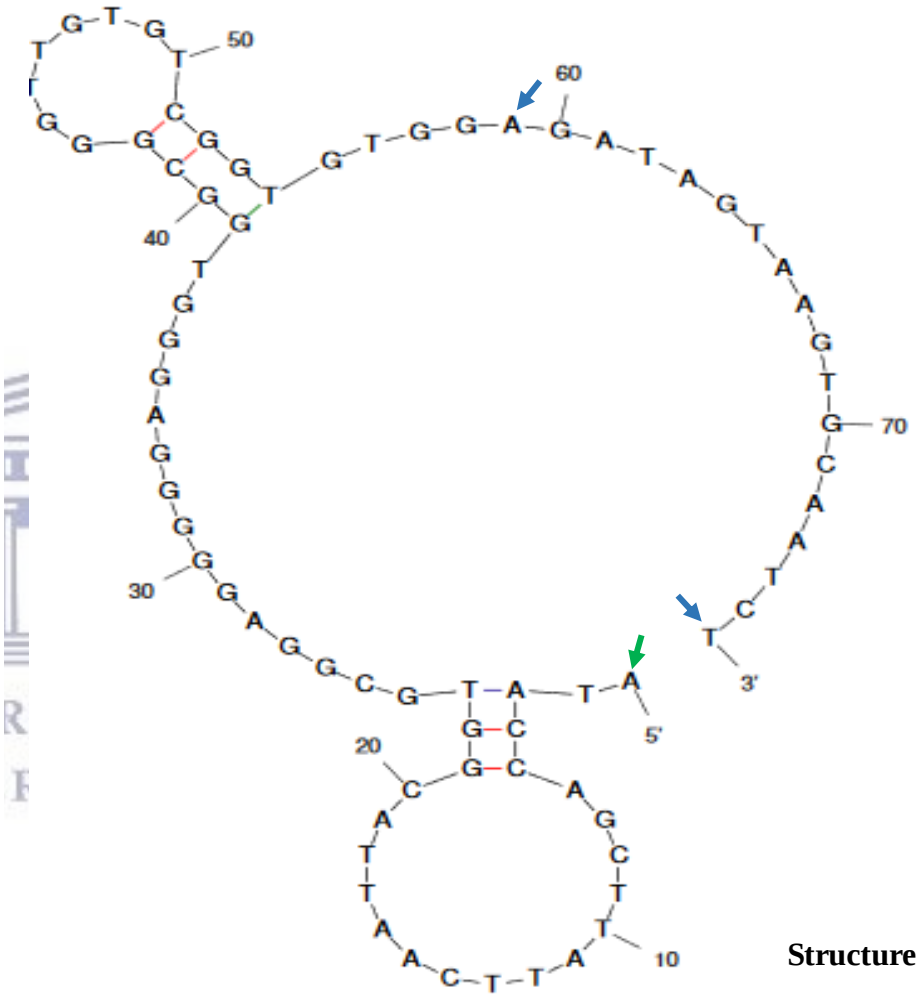

Structure 5

Figure A.2: Secondary structure prediction of RBA-1: (4) (ΔG= -0.04 kJ mol^{-1}) and (5) (ΔG= -0.43 kJ mol^{-1}) as predicted by the M-fold program. The ΔG represents the minimum free energy of each aptamer. The forward primer sequence (base 1-18) is shown by the green colour and the reverse primer (base 59-76) are shown by the blue colour.

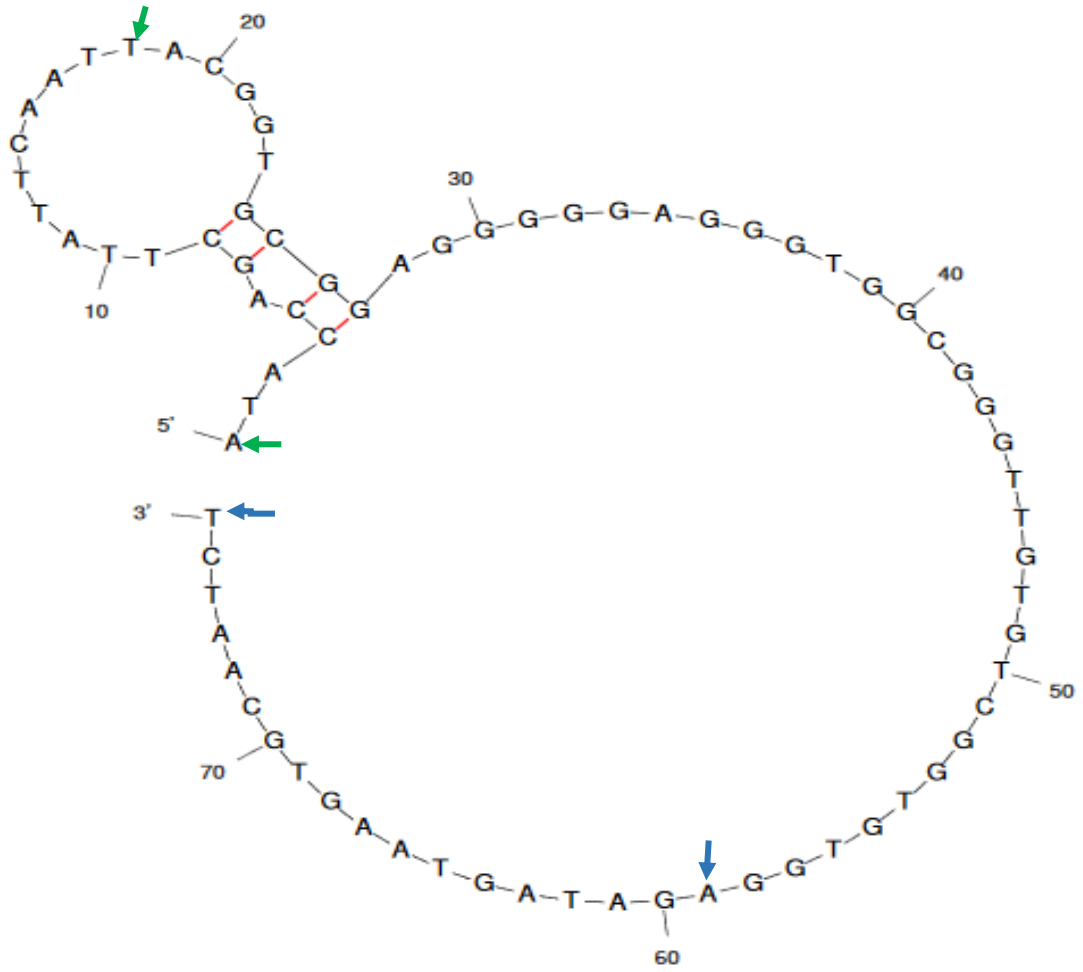

Structure 6

Figure A.3:Secondary structure prediction of RBA-1: (5) (ΔG= -0.55 kJ mol^{-1}) as predicted by the M-fold program. The ΔG represents the minimum free energy of each aptamer. The forward primer sequence (base 1-18) is shown by the green colour and the reverse primer (base 59-76) are shown by the blue colour.